EXTREMUM SEEKING CONTROL OF GRINDING MILL CIRCUITS BASED ON GRIND CURVES

by

Lukasz Ziolkowski

Submitted in partial fulfillment of the requirements for the degree
Master of Engineering (Electrical Engineering)

in the

Department of Electrical, Electronic and Computer Engineering
Faculty of Engineering, Built Environment and Information Technology

UNIVERSITY OF PRETORIA

May 2023

SUMMARY

EXTREMUM SEEKING CONTROL OF GRINDING MILL CIRCUITS BASED ON GRIND CURVES

by

Lukasz Ziolkowski

Supervisor:	Prof. J. D. le Roux
Co-supervisor:	Prof. I. K. Craig
Department:	Electrical, Electronic and Computer Engineering
University:	University of Pretoria
Degree:	Master of Engineering (Electrical Engineering)
Keywords:	Comminution, extremum seeking, grind curves, grinding mill circuit, optimization, process control

Mineral processing plants include several operations to liberate the valuable minerals within raw ore material to produce a concentrate, which is processed into a usable product by a metallurgical refinery. A mineral processing plant consists of a comminution and a separation stage. During the comminution stage, the raw ore material is processed through a grinding mill circuit to liberate the valuable minerals by grinding the ore to fine particles. The product from the comminution stage is then processed at a separation stage, which separates the valuable minerals (concentrate) from the waste material (tailings).

The comminution stage plays a crucial role in the mineral processing industry. It significantly impacts the net revenue generated by a mineral processing plant due to the high operating costs associated with liberating the valuable minerals from the ore material. A grinding stage operates efficiently if it is processing the ore material at its maximum capacity, minimizing power consumption while reducing the amount of valuables lost to the tailings stream. Therefore, the ore material should be sufficiently ground for effective separation in subsequent downstream processes. Ideally, the separation stage requires a consistent stream of fine particles for effective separation.

It is challenging for plant operators to manually achieve the above-mentioned operational objectives, which motivates the need to adopt a suitable control framework and ensure an efficiently run process. The performance of a grinding mill circuit is measured by its throughput and grind quality. These performance indicators are inversely related operational objectives. The challenge in controlling the grinding mill circuit arises in determining the optimal operating conditions to maximize the net revenue generated by the plant.

The optimal operating conditions vary with different ore types and unknown disturbances, such as varying ore hardness, which can result in the comminution stage to operate at sub-optimal operating conditions. Furthermore, grinding mills rely on the cascading motion of the ore material and grinding media to accelerate ore breakage. The cascading motion is a function of the fraction of the mill volume filled with ore and the mill rotating speed, which influences the breakage forces that occur between rocks. Therefore, selecting optimal operating conditions is a difficult task requiring frequent adjustments as the operating conditions vary. Grind curves are a valuable tool that establishes the relationship between the mill load filling and rotational speed to the grinding mill throughput, grind quality and power consumption for a given ore type. Generally, the curves show parabolic features and the peaks vary with changes in the ore characteristics.

A model-free adaptive control strategy is proposed for optimizing the performance of a semi-autogenous grinding (SAG) mill based on grind curves to improve throughput or grind quality. The controller explores an unknown map in search of the extremum of the performance indicators along the grind curves. A perturbation-based (PESC), a time-varying parameter estimation-based (TESC), and a Nelder-Mead simplex-based (SESC) extremum seeking control method are considered to optimize the grinding mill performance.

Several optimization strategies are investigated for an open grinding mill configuration and a closed grinding mill circuit, where the closed circuit is equipped with a screen or with a hydrocyclone classifier to recirculate oversized ore material for additional grinding. The challenge lies in implementing an efficient optimization model-free control framework that will effectively maximize the performance measures of the complex, non-linear behaviour of the grinding mill circuit.

ACKNOWLEDGMENT

I would like to sincerely thank Prof. Ian Craig and Prof. Derik le Roux for all their continuous support. I appreciate the knowledge they have shared with me, and it was a privilege to learn from them. I am truly grateful for the opportunity to have completed my research under their guidance.

I would like to thank my loving parents, Zofia and Boguslaw, and my brothers, Mateusz and Szymon. I appreciate your patience, support and encouragement. I am blessed to have you in my life.

To my friends and those I have met along the way, thank you for being a part of my journey, you have played an essential role in shaping who I am today, and I am grateful for that.

Lastly, I would like to thank the South African National Research Foundation for its financial support during my post-graduate studies.

LIST OF ABBREVIATIONS

ESC	Extremum seeking control
MIMO	Multiple-input, multiple-output
MISO	Multiple-input, single-output
MPC	Model predictive control
PESC	Perturbation-based extremum seeking control
SAG	Semi-autogenous grinding
SESC	Simplex extremum seeking control
SISO	Single-input, single-output
TESC	Time-varying parameter estimation extremum seeking control

TABLE OF CONTENTS

CHAPTER 1 INTRODUCTION

1.1 PROBLEM STATEMENT

1.1.1 Context of the problem

Mineral processing consists of several operations to liberate and concentrate the valuable minerals within ore material for further metallurgical extraction processes to produce a usable product. Comminution is the primary operation within mineral processing plants where the run-of-mine ore material is reduced to fine particles to liberate the valuable minerals within the ore. In run-of-mine mineral processing plants, the feed ore composition is regularly changing and the feed ore characteristics such as hardness and size distribution vary, affecting the throughput and grind quality (Maritz et al. 2019). Manually operating a grinding mill requires frequent monitoring and setpoint adjustments to compensate for these disturbances and maintain the process at suitable operating conditions to maximize the net economic benefit. A significant source of economic loss in process plants is typically attributed to poorly chosen operating conditions, and further losses are due to deviations from the chosen operating conditions (Hodouin 2011). Grinding mill circuits are challenging to operate manually and to run at optimal operating conditions due to the complex process behaviour, various unknown process disturbances and strongly-coupled variables (Zhou et al. 2016). In the absence of a high-level supervisory controller, the plant operator is often responsible for choosing suitable operating conditions for the grinding mill. However, insufficient knowledge of the process behaviour, in addition to the unknown time-varying factors such as the feed ore variation, results in the sub-optimal operation of the grinding mill.

There is an incentive to employ a real-time supervisory controller that ensures the process is continuously tracking the optimal operating conditions that satisfy the operational objectives. As a result, the optimizer would operate in a region nearer to the optimal operating region compared to the periodic setpoint choices of a plant operator as illustrated in Fig. 1.1.

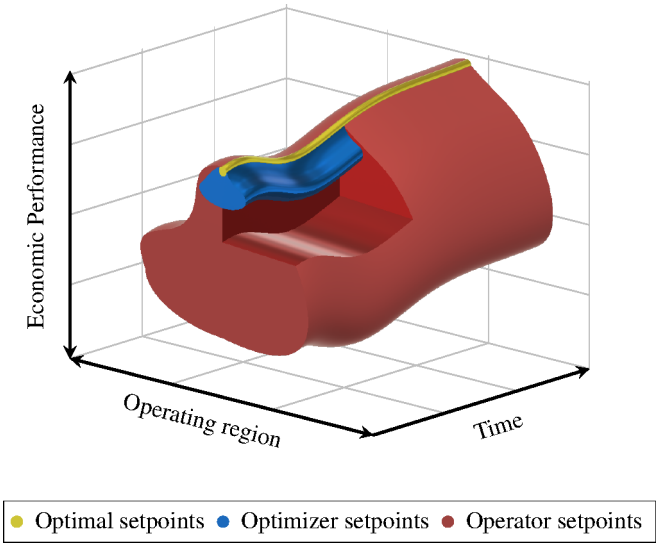

Figure 1.1. Economic performance of a grinding mill as a function of the operating conditions.

1.1.2 Research gap

Two surveys published in 2009 and 2017 (Wei & Craig 2009*b*, Olivier & Craig 2017*b*), highlight the necessity to push for automated control systems within the mineral processing industry. About 30% of the respondents indicated that an operator action occurs at least every 10 minutes and about 20% indicated that the operators are constantly busy ensuring a safe, continuously running and profitable operation (Olivier & Craig 2017*b*). Most of the operator actions (∼50%) consist of changes in the process operating conditions, resulting in frequent process transients. The survey indicates that about 13.6 actions are made per hour by an operator to manage the transients compared to about 4.4 actions during steady-state operation. These frequent actions can satisfy the operator's target objectives over a short term. However, it is not guaranteed that these actions are maximizing grinding mill circuit performance over the long term. Therefore, there is an incentive to employ an adaptive real-time optimization controller. The controller would ensure that the process tracks the optimal operating conditions while satisfying the operational objectives. The optimizer would ideally operate in a region nearer to the optimal operating region compared to the periodic setpoint choices of a plant operator as illustrated in Fig. 1.1.

Grind curves are useful as they indicate where the extremum exists for the throughput, grind or power consumption and are parabolic Powell et al. (2001), van der Westhuizen & Powell (2006), Powell et al. (2009). The significance of grind curves is well understood in industry, but their use as part of an extremum seeking control (ESC) strategy is yet to be formalized. A suitable framework

can be developed to adopt ESC for a general plant and it can prove to be beneficial to the industry since it is a model-free strategy. Therefore, developing grind curves for an individual grinding mill would not be necessary. Instead, the ESC can implicitly optimize the operational objectives, such as maximizing the throughput or grind quality. Additionally, there are challenges in controlling the inherently multivariable, non-linear and complex behaviour of grinding mill circuits, which further motivates the need for a suitable control framework to be implemented.

Following the control framework for a grinding mill circuit presented in (le Roux & Craig 2019), a typical process control system would consist of an economic optimizer operating at the highest level, followed by a supervisory control layer and lastly, a regulatory control layer. The need for developing the optimization control layer is indicated by the lack of advanced control technologies implemented in industry (Olivier & Craig 2017*b*). Most processing plants primarily use proportional-integral-derivative (PID) control ($\sim$90%) and less than 40% of the plants have expanded to implementing advanced control methods, such as model predictive control (MPC) (Olivier & Craig 2017*b*). A significant amount of research for controlling grinding mill circuits is specifically focused on using MPC (Cortinovis et al. 2013, Steyn & Sandrock 2013, le Roux et al. 2014, 2016, Botha et al. 2018). The development of the supervisory and regulatory control layers for grinding mill circuits have received considerable attention, but there is limited research work with regards to the development of the optimization control layer (Zhou et al. 2016). Therefore, the ESC could operate on the optimization layer and steer the process variables such as the mill filling or speed towards a neighbourhood of the steady-state optimum, since these operating conditions are generally manually set by a plant operator.

1.2 RESEARCH OBJECTIVE AND QUESTIONS

The proposed research work aims to investigate an effective control strategy using a model-free real-time optimization method to optimize the grinding mill circuit performance. The performance of the grinding mill circuit will be optimized by utilizing an extremum seeking controller that searches along the unknown grind curve map to steer the process towards an unknown optimum. Grind curves map the essential performance measures of a grinding mill to the mill load and rotational speed. The research questions to be addressed in this study are:

- How to minimize the setpoint deviation in the controlled variables while maintaining extremum seeking functionality?
- If the role of an optimization layer is to introduce variation in the output and the role of a regulatory control layer is to minimize variation, how will the conflicting layers interact during

the transient response?

- Will the convergence speed of an extremum seeking controller be sufficient to track a time-varying optimum?
- Can the process be steered toward optimal operating conditions from several initial conditions?
- Is there an economic benefit in employing an extremum seeking controller as opposed to manually choosing the operating conditions?

1.3 HYPOTHESIS AND APPROACH

Grind curves show that a global maximum for the performance measures (throughput and grind quality) exists. The hypothesis is that the extremum seeking controller will continuously drive the system toward the unknown optimal operating conditions when subject to slow time-varying changes or disturbances. Although the rate of convergence of the model-free perturbation-based scheme is slower relative to model-based schemes, it is expected to be sufficiently fast to track the time-varying optimum. If the feed-ore composition remains relatively consistent for a considerable period, it is expected that the perturbation-based extremum seeking controller will maintain near optimal steady-state conditions with noticeable oscillations in the outputs. However, since the dynamics of the system are relatively slow, the effects of the oscillations will be negligible to the overall process. The following approach will be followed to investigate the hypothesis:

1. A thorough literature study will be conducted on extremum seeking control and the general operating philosophy of grinding mill circuits to understand the process behaviour and how to interpret the outcomes.
2. A suitable plant model of an open grinding mill circuit and a closed grinding mill circuit will be identified and incorporated into a framework for simulating the system with an extremum seeking controller.
3. The optimization and regulatory control layers will be developed for controlling the grinding mill circuit. The optimization layer will aim to maximize the performance measures (throughput or grind quality) and track the optimal steady-state conditions. The regulatory controller will aim to minimize deviations in the controlled variables and maintain process stability.
4. The extremum seeking controller will be applied in simulation to a grinding mill circuit. The simulations will include no disturbances to verify it can reach the unknown optimum and maintain steady-state conditions in an ideal scenario and in the presence of measurement noise. Afterwards, the process will be simulated with disturbances to verify that the control framework

can track the unknown optimum and maintain process stability. Two configurations will be considered for optimizing the grinding stage:

(a) An open grinding mill circuit configuration. A single input or multiple inputs will be manipulated by the extremum seeking controller to optimize a single output or multiple outputs.

(b) A closed grinding mill circuit with a screen or hydrocyclone classifier configuration. A single input will be manipulated by the extremum seeking controller to optimize a single output.

5. A brief analysis of the results will be given and the extremum seeking control framework will be evaluated to determine the potential benefit that could be achieved from implementing a model-free optimization strategy to control a grinding mill circuit.

1.4 RESEARCH GOALS

The research goals of the study are:

1. Identify a suitable plant model to simulate the behaviour of an open grinding mill circuit and a closed grinding mill circuit.
2. Develop and implement an ESC framework to maximize a formulated objective function to optimize the grinding performance (throughput or grind quality) to track the steady-state optimal operating conditions.
3. Demonstrate the effectiveness of an extremum seeking controller subject to common practical issues within mineral processing such as measurement noise and disturbances.
4. Apply the ESC framework to optimize an open grinding mill circuit, and a closed grinding mill circuit with a screen or hydrocyclone classifier to demonstrate the value of grind curves paired with ESC to improve grinding performance.
5. Demonstrate the application of ESC by manipulating a single input or multiple inputs to optimize a single output or multiple outputs.

1.5 RESEARCH CONTRIBUTION

Lu et al. (2021) illustrates how ESC can be applied to optimize grinding mill performance, albeit not with the use of grind curves. The contribution of the work is to implement model-free extremum seeking methods, which will eliminate the process of developing an accurate plant model that is required for model-based control and demonstrate the value of grind curves combined with ESC to maximize the performance of a grinding mill. In contrast to Lu et al. (2021), this dissertation will

investigate several optimization strategies that will aim to satisfy the operational objectives for a grinding mill circuit and steer the process toward optimal operating conditions.

The value of grind curves combined with ESC will be demonstrated to optimize the performance of a grinding mill. For mineral processing plants that do not use a relatively consistent stockpile of ore material, the optimum is time-varying due to feed ore variation. Continuously optimizing the throughput, grind or both can be achieved with ESC by directly using the manipulated variables related to the performance indicators of grind curves.

The study differs from the optimization strategy described in (Pauw et al. 1985) and (Craig et al. 1992) where the optimizer uses the power consumption measurements to indirectly maximize throughput. This strategy does not guarantee that the optimal throughput is achieved when the mill speed varies. For different mill speeds, the difference between the peak power consumption and throughput does not vary linearly with the mill load (Powell et al. 2009). Therefore, tracking the maximum throughput based on power consumption measurements can result in sub-optimal operating conditions if the mill speed varies. Additionally, the mill speed is used as a manipulated variable to optimize the mill performance in comparison to the optimization strategies described in Pauw et al. (1985), Craig et al. (1992), Lu et al. (2021) which only use the mill load.

The dissertation explores several ESC optimization strategies using either the mill load, mill rotational speed or both, as single-input and multiple-input cases, to maximize the throughput, grind or a combination of the two with a weighted objective function, as single output and multiple-output cases. Three extremum seeking optimization methods are considered: a classical perturbation-based method and a time-varying parameter estimation method, which are gradient-based methods, and a non-gradient based Nelder-Mead simplex method.

1.6 RESEARCH OUTPUTS

The following publications resulted from this study, of which the main results are reported in Chapter 5:

- Ziolkowski, L., le Roux, J. D., Craig, I. K., Optimizing grinding mill performance using extremum seeking control, IFAC-PapersOnLine, Volume 54, Issue 11, 2021, pp. 43-48
- Ziolkowski, L., le Roux, J. D., Craig, I. K. (2022). Extremum seeking control for optimization of an open-loop grinding mill using grind curves, *Journal of Process Control*, 114, 54-70.

The results of Chapter 6 are to be submitted as:

- Ziolkowski, L., le Roux, J. D., Craig, I. K. (2022). Extremum seeking control for optimization of a closed grinding mill circuit, To be submitted to *Journal of Process Control*.

1.7 OVERVIEW OF STUDY

The dissertation is organized as follows. Chapter 2 presents the literature review of the knowledge relating to the grinding process of the comminution stage. The chapter provides a brief description of the grinding process and the general operation of a grinding mill circuit. Grind curves and the potential benefits of adopting a model-free ESC framework for a grinding mill circuit are discussed in this chapter. Chapter 3 provides the non-linear process model used to simulate the behaviour of an open grinding mill circuit. The model is then integrated with the addition of a sump module and a screen or hydrocyclone classification module to simulate a closed grinding mill circuit. Chapter 4 outlines the extremum seeking methods used in this study to optimize the performance of the grinding mill circuit. The extremum seeking controllers are employed on the optimization layer to optimize an objective function and track the steady-state optimal operating conditions of the non-linear model described in Chapter 3. The chapter concludes with an example of maximizing a static objective function. Chapter 5 presents the simulated optimization scenarios for an open grinding mill circuit. Chapter 6 presents the simulated optimization scenarios for a closed grinding mill circuit with a screen or hydrocyclone classifier. Chapter 7 concludes the work presented in this dissertation. The chapter highlights the advantages and potential disadvantages of employing ESC to optimize grinding performance.

CHAPTER 2 LITERATURE STUDY

2.1 CHAPTER OVERVIEW

This chapter discusses the operation and the objective of the comminution stage within a mineral processing plant. Section 2.2 describes the grinding process. Section 2.3 describes the concept and use of grind curves. Section 2.4 discusses the state of control in grinding mill circuits and the application of ESC to optimize the grinding performance. Section 2.5 concludes the chapter.

2.2 COMMINUTION

Run-of-mine (ROM) ore material is raw mined ore which is extracted from a mining operation such as an open pit or underground mine. ROM ore is typically unprocessed and has not undergone any prior mineral grading or size classification. Mineral processing is a chain of operations used to liberate and separate the valuable minerals within ore material. The different stages to produce a usable product from the raw ore material are illustrated in Fig. 2.1. During comminution, crushing and grinding is used to expose and liberate the valuable minerals within the ore material. Subsequently, a flotation circuit and thickener are typically used to separate the minerals from the waste material through chemical or physical treatment. Further metallurgical extraction processes such as smelting and refining are then used to produce a usable product.

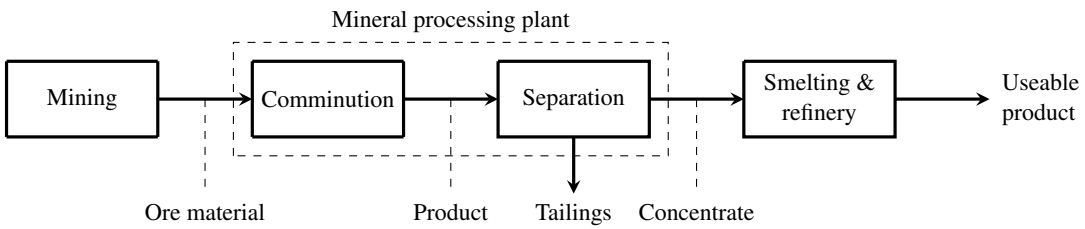

Figure 2.1. Mineral processing operations.

Liberating the valuable minerals from the undesired waste material is necessary so that the mineral can be easily parted from the waste material in the separation stage. Comminution is a crucial stage that influences the effectiveness of the subsequent downstream operations, and hence the economic value of the concentrate product that is sold to a smelter (Napier-Munn et al. 2005, Wills & Finch 2015, Gupta & Yan 2016).

2.2.1 Operating objectives

There are three operational objectives that the plant operator aims to satisfy during the comminution stage. Firstly, to maximize the throughput[1] by processing as much of the ore material as possible. Secondly, to improve the grind[2] quality by ensuring that the ground ore is reduced to a specific and consistent particle size by reducing the variation in the output product stream. Lastly, to minimize unnecessary power consumption by operating the mill efficiently.

Ore material that is not sufficiently ground will result in the valuable minerals being trapped within the ore material. However, over-grinding produces a product that may be too fine for effective separation. It reduces the throughput due to the additional grinding and time that the ore material is resident in the mill. Over-grinding also increases the energy consumption required to achieve a finer grind. Consequently, the poorer recovery rate, increased energy consumption or decreased throughput contributes to diminishing economic gains (le Roux & Craig 2019).

Together these operational objectives affect the net revenue generated by the mineral processing plant due to the comminution stage. However, the objectives are inversely related. An increase in the throughput is typically achieved with a coarser grind or vice-versa. The plant operator would generally aim to maximize the throughput and maintain a minimum acceptable grind quality. However, in a market with high demand and low supply of the mineral, maximizing the grind quality would achieve a greater net economic return if there is a shortage of the ore type. Therefore, an operator would aim to improve the grind quality at the cost of reduced throughput.

The net revenue generated from an increased throughput is often perceived to exceed the economic value that could be generated from the losses incurred in the separation process due to the decreased grind quality. However, it could also be beneficial to maintain a set throughput and minimize the product particle size variation to increase recovery rates (Cramer 2008, Bouffard 2015, le Roux & Craig

[1] The throughput is defined as the volume of solids exiting the grinding mill circuit.

[2] The grind is defined as the fraction of particles exiting the grinding mill circuit that are below a specification size.

2019). From the perspective of a smelter, it is cheaper to smelt a product with a higher concentrate grade due to the lower quantity of impurities, but this is at the expense of a decreased yield due to the lower availability of a high-grade concentrate product (le Roux & Craig 2019). In addition, a higher grade concentrate requires additional processing effort to produce and from the perspective of a grinding mill operator, this is at the expense of reduced throughput and increased energy consumption.

The plant operator must aim to run the comminution stage efficiently to reduce operating costs. In open pit and underground mining, milling on average contributes to about 49% and 34% to the mineral processing plant operating costs, respectively (Curry et al. 2014). Further, it is estimated that about 30% to 80% of the energy used by mineral processing operations is consumed during the comminution stage (Wang et al. 2013, Nadolski et al. 2014). A further breakdown between crushing and grinding operations indicates that about 97% of the energy consumed during comminution is associated with grinding (Ballantyne et al. 2012). A circuit operating near the peak energy consumption to maximize throughput or the high energy consumption required to produce a finely ground product is the primary contributor to the energy-related operating costs. Additionally, up to 40-45% of the comminution costs are due to the mill liner wear and grinding media consumption (Moema et al. 2009). The remaining operating costs are usually negligible in comparison to these costs.

Grinding mill circuits have high capital costs and running costs and the operation of grinding mills is largely an economic optimization problem. Grinding mill circuits are controlled to meet economic objectives and the net return value from liberation should outweigh the expenses involved with the capital and operation costs by either maximizing the revenue generated or minimizing the operational costs. Furthermore, the concentrate grade and the recovery rate of metals in the downstream separation process are influenced by the comminution stage. Therefore, effective recovery of the final product in the separation circuits can be attributed to the effective liberation and decreased variation of the product particle size during grinding.

A balance between the acceptable liberation and operation costs associated with grinding mills has to be considered when deciding on how the grinding mill circuit should be controlled (Hodouin 2011). The economic optimization problem consists of determining the best operating points that increase throughput, improves grind quality and recovery while also reducing operating costs, such as power consumption. Simultaneously achieving all the objectives mentioned is not practically achievable. Therefore, there is a trade-off between each of the objectives. The operator should decide based on

satisfying the operational objectives which will maximize the net return value of running the grinding mill circuit.

These control objectives are derived from the economic objective of optimizing the mineral processing plant from a plant-wide perspective. The plant economic optimization objective can be described by (Herbst & Lo 1996),

$$\text{Profit} = \text{Revenue} - \text{Operating Costs}. \tag{2.1}$$

The revenue is based on the sale contract of the concentrate sold to the smelter. The comminution stage has a key role in preparing the product that will eventually be separated to produce the concentrate. Therefore, the grinding stage has a large influence on the revenue generated and also the operating costs.

2.2.2 Process description

Initially, mined ore material is processed through the comminution stage, where a grinding mill circuit is used to grind the ore to fine particles to liberate the valuable minerals from the ore. Next, a separation stage separates the valuable minerals from the waste through chemical or physical treatments. The separated valuable minerals form the concentrate, and the waste material is referred to as the tailings. Ideally, the separation stage expects a consistent stream of fine particles for effective separation. Therefore, the comminution stage plays a crucial role that affects the end product of the process, as significant variations in the ground product reduce the amount of valuable minerals that are recovered from the ore material.

A grinding circuit can be configured as an open grinding circuit (Fig. 2.2) or as a closed grinding circuit (Figs. 2.3 and 2.4). Further, an open or closed grinding mill circuit may be operated in either open-loop control or closed-loop control. In this dissertation, the prefix terms "open" or "closed" are used to define the grinding circuit configuration and indicate if the ore material is recirculated through the circuit. The terms "open-loop" or "closed-loop" describe the control system for the process variables within the grinding circuit.

In an open grinding mill circuit, the raw ore material is processed through the mill until the ore material is small enough to exit the mill through the discharge grate. The grind or throughput is open-loop controlled by manipulating the feed rate or rotational speed of the mill. No ore is recirculated for further regrinding once it is discharged. The grind is controlled in an open-loop by increasing or

decreasing the time the ore is resident in the mill by grinding slower or faster. An open grinding mill circuit does not guarantee that the desired grind is consistent or meets the target size specification. A closed grinding mill circuit can be used to achieve a more consistent grind. A classifier separates the discharge from the mill between oversized and undersized particles. Any oversized ore material that does not meet the target size specification is recirculated through to the grinding mill and the grinding effort is focused on the oversized ore material. The undersized ore that is below the target size specification is removed from the circuit. The material can be processed through the mill faster and minimize the time that any ore within the desired target size remains in the grinding mill circuit.

The comminution stage of a mineral processing plant consists of a grinding mill that usually forms part of a closed grinding mill circuit. The common grinding mill circuit configurations found in mineral processing plants are a single-stage closed grinding mill circuit or a two-stage grinding mill circuit (Wei & Craig 2009*b*). In a two-stage grinding mill circuit, the first stage is an open grinding mill primarily used to process the bulk content of the ore. The second stage is a closed grinding mill circuit aimed at controlling the final product grind. A single-stage grinding mill circuit configuration is favourable due to the reduced initial capital investment, reduced operating costs and to reduce the control complexity that is involved with multi-stage circuits.

Several types of grinding mills are used in mineral processing such as ball mills, rod mills, autogenous grinding (AG) mills, and semi-autogenous grinding (SAG) mills. Ball and rod mills use steel balls or rods, respectively, as the grinding media to grind ore material. About 80% of the charge of the mill (fraction of the volume of the mill filled with ore, water and grinding media) is predominantly occupied by the grinding media (Wills & Finch 2015). Therefore, a significant portion of the power consumption of the mill, volume and grinding characteristics is associated with the grinding media and not largely affected by the variation in feed ore material. In AG or SAG mills, the ore material makes up a larger component of the grinding media (only ore material is used as grinding media in AG mills). Since SAG mills also use the ore as grinding media, it reduces the media consumption. The drawback is that variation in the feed ore size or hardness significantly influences the grinding performance of the mill, which can be compensated for by manipulating the feed rate of the ore material.

Ball and SAG mills are popular in grinding mill circuits, but SAG mills have become increasingly more common (Wei & Craig 2009*b*). SAG mills are physically much larger, maintain a higher throughput and can handle large fluctuations in the feed (Salazar et al. 2009). Furthermore, SAG mills operate at

reduced operating costs as they are more energy efficient (40%) compared to ball mills (30%) (Musa & Morrison 2009).

A SAG mill is illustrated in Fig. 2.2. The nomenclature is shown in Table 2.1. The mill receives three streams: raw mined ore (u_{MFO}), water (u_{MFW}), and steel balls (u_{MFB}). The mill charge is a mixture of grinding media and slurry. Grinding media refers to the steel balls and rocks which break the ore and slurry refers to the mixture of solids and water. The fraction of the mill filled with charge is denoted by y_{J_T}.

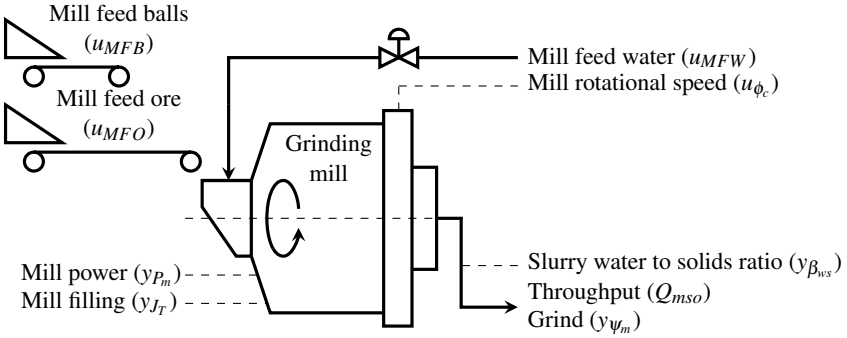

Figure 2.2. An open grinding mill circuit.

Grinding mills are large cylindrical drums that rotate along their longitudinal axis. The inner walls are fit with liners, which lift the grinding media and protect the mill shell. The mill rotational speed is expressed as a fraction of the critical mill speed u_{ϕ_c}. The critical mill speed is defined as the rotational speed where the centrifugal forces acting on the mill charge particles are equal to the gravitational force. At the critical mill speed, the mill charge travels along the mill shell instead of cascading inside the mill. At sub-critical mill speeds, the rotating shell of the mill lifts the grinding media and creates a cascading motion of charge inside the mill, which causes the ore to break through impact breakage, abrasion, and attrition. The repeated tumbling of the cascading grinding media results in the valuable minerals trapped within the ore to be liberated. The ground ore in the mill mixes with water to create a slurry which discharges through an end-discharge grate. Ore too large to pass through the end-discharge grate is referred to as *rocks* and must be broken further. All ore small enough to pass through the end-discharge grate is referred to as *solids*. The flow-rate of solids and water discharging from the mill is given by Q_{mso} and Q_{mwo}, respectively.

The purpose of the grinding mill is to grind the ore to below a specification size, e.g., 150 μm. The mill grind (y_{ψ_m}) is the volume fraction of material in the discharge of the mill below the specification

Table 2.1. Description of comminution circuit variables.

Variable	Unit	Description
u_{MFB}	$(\mathrm{t/h})$	Mill feed rate of steel balls
u_{MFO}	$(\mathrm{t/h})$	Mill feed rate of ore
u_{MFW}	$(\mathrm{m^3/h})$	Mill inlet water flow-rate
u_{SFW}	$(\mathrm{m^3/h})$	Sump feed water
u_{CFF}	$(\mathrm{m^3/h})$	Classifier feed flow-rate
u_{CFW}	$(\mathrm{m^3/h})$	Classifier inlet water flow-rate
Q_{mso}	$(\mathrm{m^3/h})$	Mill solids discharge flow-rate
y_{ψ_m}	$(-)$	Mill grind (e.g. volume fraction of particles in discharge $< 150\ \mu$m)
y_{P_m}	(kW)	Mill power draw
y_{J_T}	$(-)$	Fraction of mill volume filled with charge
u_{ϕ_c}	$(-)$	Fraction of critical mill speed
y_{SVOL}	$(\mathrm{m^3})$	Volume of slurry in sump
y_{CFD}	$(\mathrm{t/m^3})$	Classifier feed density
Q_{csus}	$(\mathrm{m^3/h})$	Circuit throughput (classifier undersize solids discharge flow-rate)
y_{ψ_c}	$(-)$	Circuit grind (e.g. volume fraction of particles in discharge $< 75\mu$m).

size. The broken ore below the specification size is referred to as *fines*. Note, whereas solids refer to all ore small enough to discharge from the mill, fines refer to the portion of solids smaller than the specification size. The discharge flow-rate of fines from the mill is given by Q_{mfo}.

The mill charge is primarily controlled to achieve the desired throughput by manipulating u_{MFO} and u_{MFW}. However, in situations where the feed ore hardness or size varies and the mill charge cannot be effectively controlled to compensate for the disturbances, manipulating u_{ϕ_c} adds an additional degree of freedom to control Q_{mso} or y_{ψ_m} (le Roux et al. 2016).

2.2.3 Classification

As part of the mineral liberation process, particle size classification is required to ensure effective separation in the subsequent downstream processes. Classification is used to achieve a product within the target size specification and to reduce variation in the product particle size.

An open grinding mill circuit consists of no classification equipment (besides for the mill discharge grate) to separate the fine ore from the coarse ore that would need regrinding. The ore material is passed through the grinding mill circuit once, at a rate to maintain a desired throughput. However, it is not guaranteed that the discharge of the grinding mill produces a product of fines within the target size specification, particularly if the feed characteristics vary in size and hardness. A discharge grate is fitted at the end of the mill, but its purpose is to hold back larger rocks or grinding balls rather than to separate the fines from the coarse ore. In an open grinding mill circuit, coarse ore is present in the discharge of the mill due to insufficient grinding and lack of particle size classification. To ensure that the amount of coarse product in the discharge is minimized, the ore material might be ground for a longer duration, but this results in increased energy consumption and throughput reduction. The grinding rate is limited and the throughput cannot be maximized without impacting the grind quality.

A closed grinding mill circuit is realized with the addition of a particle size classifier, such as a screen or a hydrocyclone as illustrated in Figs. 2.3 and 2.4. A sump is placed between the discharge of the mill and the classifier, which is useful in a closed circuit with a hydrocyclone classifier. The sump acts as a buffer and allows the discharged slurry density to be controlled with the addition of a water stream. A hydrocyclone operates effectively when the density of the feed is regulated to achieve the desired split between the coarse and fine ore material. As the mill discharge rate varies, disturbances that would occur in the hydrocyclone feed flow-rate and density can be reduced with the aid of the buffer.

The role of the classifier is to separate the discharged material from the grinding mill into two separate streams containing coarse and fine ore. Coarse ore consists of ore particles larger than the target particle size. The coarse ore is recirculated to the grinding mill for regrinding and the fine ore is removed from the grinding mill circuit. Therefore, adding a classifier is beneficial to reduce the variation in the product particle size and no additional grinding effort is unnecessarily wasted on ore particles that are smaller than the target particle size.

2.2.3.1 Vibrating screen

A screen separates larger particles from smaller particles based on whether the particles can pass through the apertures in the screen mesh. The screen receives the discharged slurry from the grinding mill and the slurry travels across the surface of the screen, as shown in Fig. 2.3. Material that is smaller

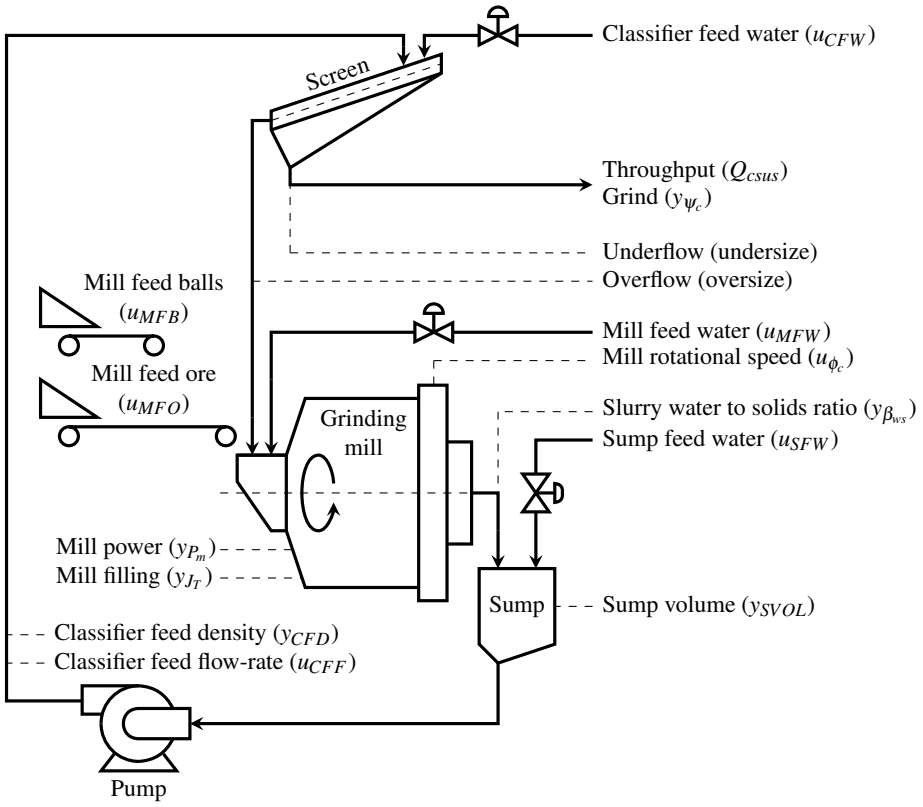

Figure 2.3. Single-stage closed grinding mill circuit with a screen classifier.

than the screen aperture size passes through the aperture of the screen and forms part of the undersized stream. Material too large to pass through the apertures continues to travel across the surface of the screen and is recirculated back for regrinding. Water is used to wash the screen and improve the separation in a dry or dense slurry. A screen can also be angled and the greater the degree of the angle, the narrower the aperture appears from the perspective of the particles, but it eases the travel across the screen surface. Screening is effective for separating larger ore material from 300mm to 40 µm, but reduces in efficiency for a finer target particle size (Wills & Finch 2015). Achieving a fine product with a screen would require a fine mesh that will likely cause a bottleneck in the mineral processing plant.

2.2.3.2 Hydrocyclone

Hydrocyclones are used to separate finer particles compared to what is practically feasible with a screen mesh. The separation principle for hydrocyclones depends on the density of the particles being classified, whereas the classification for a screen depends on the shape and size of the material (Frausto et al. 2021). The hydrocyclone separates the fine and coarse ore of the mill discharge depending on the desired cut size, which is dependent on the feed rate of the incoming material. Hydrocyclones are

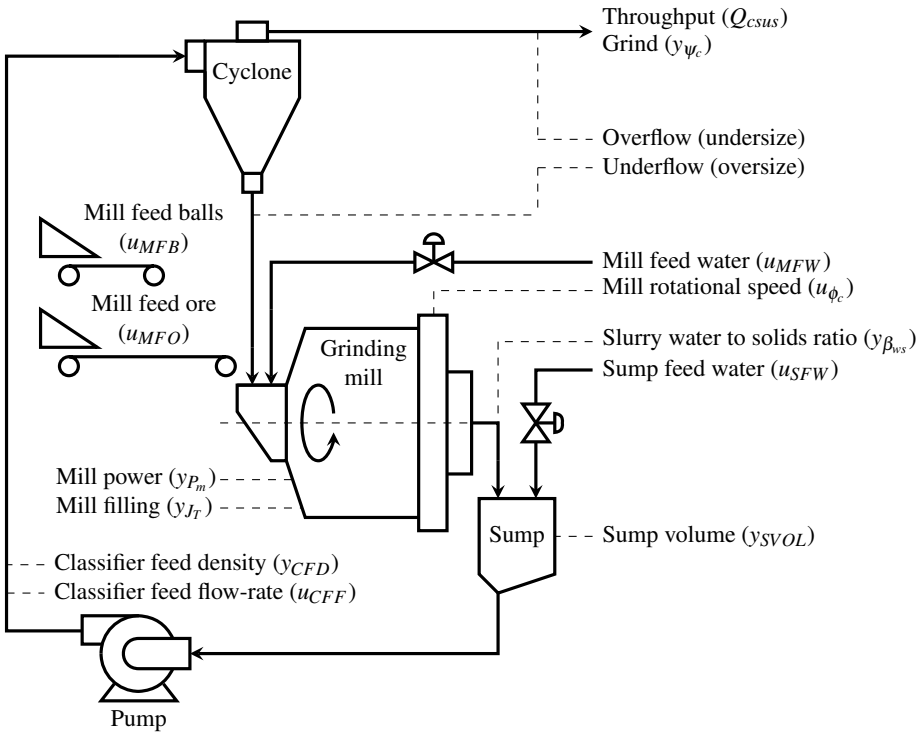

Figure 2.4. Single-stage closed grinding mill circuit with a hydrocyclone classifier.

conically shaped and the incoming material is tangentially fed into the hydrocyclone. This forces the material to travel in a spiral and swirl within the hydrocyclone and creates an upward travelling vortex in the centre of the hydrocyclone. The denser particles from the incoming stream travel downwards along the inner walls of the hydrocyclone, while the less dense particles are carried upward by the vortex, splitting the slurry from the grinding mill into two separate streams of coarse and fine particles, as shown in Fig. 2.4.

2.3 GRIND CURVES

Grinding mills rely on the cascading motion of the ore material and grinding media to accelerate ore breakage. The cascading motion is a function of the fraction of the mill volume filled with ore and the mill rotational speed, which affects the breakage forces occurring between rocks. The selection of optimal operating conditions is a difficult task that requires frequent adjustments as the mill performance varies due to varying feed ore characteristics, the mill load and the mill speed.

The performance indicators of a grinding mill are throughput, grind quality and power consumption. Grind curves describe the relationships between these performance indicators as a function of the mill filling and mill rotational speed (van der Westhuizen & Powell 2006). A notable characteristic of

grind curves is that the curves are parabolic and indicate the optimal operating conditions (mill filling and speed) where the peaks of the performance indicators would occur. Furthermore, as the feed ore characteristics such as hardness vary, the peaks of the performance indicators shift, but the parabolic trend is retained for different ore types (Powell et al. 2001, Viklund et al. 2006).

If a mineral processing plant process receives ore from a similar stockpile, establishing a set of grind curves can prove to be beneficial for determining the optimal operating conditions for a certain ore type as grind curves can be used to (Powell et al. 2001):

1. act as a reference for operating the grinding mill circuit;
2. identify the optimum mill filling for the given mill rotational speed to meet the operational objectives for throughput or grind, and;
3. operate the mill at a stable region.

However, if the feed ore is not relatively consistent, then the issue with using grind curves as a reference for operating the mill is twofold. Firstly, manually operating the grinding mill based on grind curves would require that for each ore type, a set of grind curves has already been established. This is impractical as grind curves are obtained by progressively stepping through a range of operating conditions and allowing the mill to reach a steady-state for each step. Establishing a set of grind curves can be a costly and time-consuming task as the process can take at least a day to establish for an ore type (Powell & Mainza 2006, Powell et al. 2009).

Secondly, if the feed ore characteristic varies, the operator must be aware of the change and make the necessary adjustments to ensure that the mill is operating at the new optimum as the extremum shifts. It can be beneficial if an adaptive control system is implemented that searches along the grind curves in real-time to locate the unknown peak. Therefore, such a control system would implicitly steer the grinding mill toward an optimum mill filling, rotational speed, or both, based on the convex features of grind curves. In addition, the parabolic characteristics of grind curves are desirable as it would ensure that the control system would track the global optimum.

Grind curve data from an industrial open SAG mill is presented in van der Westhuizen & Powell (2006). Although each grinding mill is unique, similar grind curve trends are shown across various grinding mills, which can be transferred to a general plant (Powell et al. 2009). The peaks of the grind curves in van der Westhuizen & Powell (2006) are provided in Table 2.2 and are used to fit

Table 2.2. Performance indicator peaks from van der Westhuizen & Powell (2006) as illustrated in Fig. 2.5(a).

Mill speed	Throughput		Grind		Power	
u_{ϕ_c} $(-)$	y_{J_T} $(-)$	Q_{mso} $(\mathrm{m}^3/\mathrm{h})$	y_{J_T} $(-)$	y_{ψ_m} $(-)$	y_{J_T} $(-)$	y_{P_m} (kW)
0.75	0.35	157.0	0.33	0.56	0.39	4037
0.70	0.31	120.7	0.37	0.69	0.47	4028
0.65	0.23	93.3	0.58	0.94	0.55	3931
0.60	0.18	96.7	0.63	1.00	0.54	3603

the performance indicators as quadratic polynomials in terms of y_{J_T} for each u_{ϕ_c}. Subsequently, the performance indicators are fit as cubic polynomials in terms of u_{ϕ_c} (le Roux et al. 2020).

Fig. 2.5(a) illustrates the grind curves of van der Westhuizen & Powell (2006) and indicates where the curves are extrapolated outside the measured range of the industrial mill. The 3-D surface maps of the grind curves in Fig. 2.5(a) are shown Fig. 2.5(b). Interestingly, the optimal Q_{mso} and y_{ψ_m} occur at similar values of y_{J_T} when $u_{\phi_c} = 0.75$. However, this is not the case for lower values of u_{ϕ_c}. In the context of operating the grinding mill, the surface maps of the grind curves clearly indicate the trade-off that has to be made when optimizing either Q_{mso} or y_{ψ_m}. Assuming that y_{J_T} is kept constant, an increase in Q_{mso} can be achieved by increasing u_{ϕ_c} at the cost of a decrease in y_{ψ_m}, and vice-versa. Alternatively, by maintaining u_{ϕ_c} constant, Q_{mso} is maximized by increasing y_{J_T} up to an extremum, after which Q_{mso} begins to decrease. If the mill charge accumulates, less breakage occurs and Q_{mso} is reduced. Maximizing y_{ψ_m} is usually not as beneficial as there is a maximum acceptable grind quality, after which the product is too fine for the separation process to perform optimally (le Roux & Craig 2019). In addition, because over-grinding wastes energy, it is common for the operational objectives of a grinding mill circuit to maximize Q_{mso} until the minimum acceptable y_{ψ_m} is achieved. The acceptable grind size is usually chosen based on the grain size of the valuable minerals which minimizes the grinding effort required to liberate the minerals from the gangue (Wills & Finch 2015).

The limited range of data available does not illustrate the effects of increasing the mill speed further than $u_{\phi_c} > 0.75$. However, it is expected that as the mill speed increases, a peak will be reached and beyond a certain mill speed, the throughput will begin to decrease. This is due to the mill rotating

sufficiently fast such that centrifugal forces acting on the mill charge overcomes the effects of gravity. The ore is pushed outwards toward the mill shell and reduces the impact of the cascading motion, and consequently reducing the throughput.

The grind curves in Figs. 2.5(a) and 2.5(b) show the performance indicator trends of an open SAG mill, but these parabolic trends are also observed in closed grinding mill circuits (Powell et al. 2009). A grinding mill circuit closed with a hydrocyclone classifier requires that the hydrocyclone feed rate (u_{CFF}) range is not narrowly limited and that the hydrocyclone would not exceed its capacity. These conditions enable the hydrocyclone to maintain its cut-size and water recovery, which impact the performance indicators of grind curves (le Roux & Craig 2019). The circuit throughput (Q_{csus}) and grind (y_{ψ_c}) can, therefore, be related to the mill performance indicators (Q_{mso}, y_{ψ_m}), which are dependent on the mill load (y_{J_T}) and the mill rotational speed (u_{ϕ_c}).

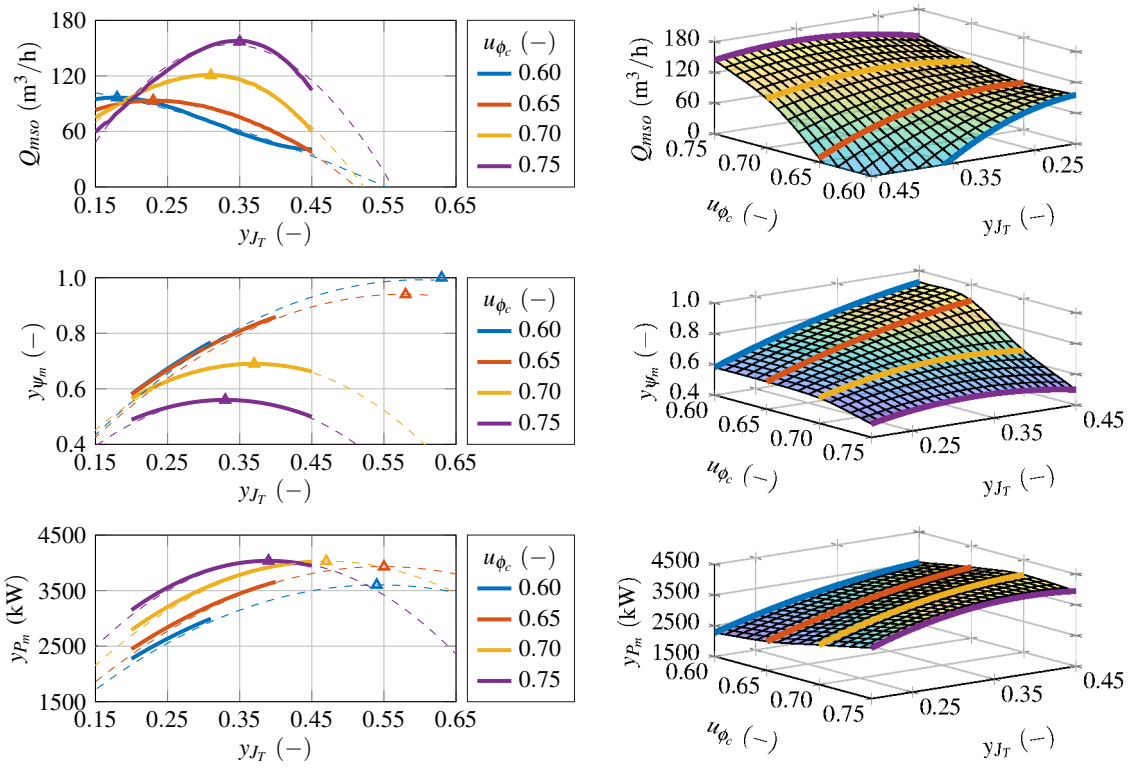

(a) Grind curves.

(b) Grind curve surface maps.

Figure 2.5. Grind curves for mill discharge (Q_{mso}), grind (y_{ψ_m}), and power (y_{P_m}) reproduced from the data in Table 2.2. The dashed lines show the extrapolated grind curves and the △ data markers indicate the peaks at each mill speed (u_{ϕ_c}).

2.4 GRINDING MILL CIRCUIT CONTROL

A significant effort has been invested in the mineral processing industry to reduce the wasted resources and operating expenses while maximizing the net profit of a plant through the implementation of sophisticated control systems. An adequate control system for grinding mill circuits is necessary to ensure stability, reject undesired disturbances or optimize an economic objective to maximize the net profit. Automated control systems are implemented to automating these tasks and minimizing operator errors. In light of the discussion in Section 1.1.2, the frequent actions of the operators can satisfy the target objectives over a short term, but do not guarantee that these actions are maximizing grinding mill circuit performance over the longer term.

In the context of a grinding mill circuit, stability is achieved in the mill by preventing the mill from overfilling or being run empty. Overfilling the mill prevents the charge from breaking and would require the mill to be manually emptied. Underfilling the mill exposes the mill shell to the impact of the ore material causing damage to the equipment. Furthermore, for a circuit closed with a hydrocyclone classifier to perform effectively, the sump should not run dry or overfill and maintain a constant feed rate to the hydrocyclone.

Once stability is achieved, the grinding mill circuit performance can be controlled to optimize the process and maximize the revenue generated. To improve the grinding mill circuit performance, these control objectives are generally formulated to (Craig & MacLeod 1995):

1. maximize the throughput;
2. improve the quality of the product by increasing the fineness of the grind and reducing the product size variation;
3. reduce the power consumption of the mill circuit, and;
4. minimize the consumption of grinding media.

However, the challenge in achieving these control objectives is the trade-off that has to be made. As illustrated by the grind curves in Fig. 2.5, the throughput and grind quality are inversely related (Bauer & Craig 2008). Furthermore, maximum throughput is achieved near peak power consumption. Grinding mill circuits are energy intensive and power consumption can be reduced by focusing the breaking energy on larger ore instead of regrinding ore within the target size specification. The general operating philosophy is to maximize the throughput and control the grind to a target setpoint. Increasing the fineness of the grind does maximize the amount of valuable minerals that are liberated,

but at the cost of increased energy consumption and also introduces difficulty in the separation process (Hodouin et al. 2001). If the ore is not sufficiently ground, the grade of the concentrate sold to the smelter is decreased. Furthermore, variations in the grind reduce the amount of minerals that are recovered.

2.4.1 State of control

Grinding mill circuit control systems range from single-loop regulatory controllers to high-level advanced control systems. Single-loop regulatory controllers are required to stabilize the mill load and sump level. However, regulatory controllers are only sufficient to maintain the process at chosen operating conditions. The need for a higher level, sophisticated control system is driven by the need for rejecting disturbances, reducing variations in key process variables and maximizing the process performance while subject to the process constraints (Zhou et al. 2016). A source of economic loss in process plants is attributed to deviations from the chosen operating conditions. However, a higher source of economic loss is due to poorly chosen operating conditions (Hodouin 2011). It is common for an operator to be responsible for choosing suitable operating conditions and maximizing the process performance in the absence of advanced control systems. Advanced control systems are not readily available for every process plant and simple regulatory control tends to dominate the control technologies used in mineral processing (Wei & Craig 2009*b*, Olivier & Craig 2017*b*). The decisions of the operators are influenced by their knowledge of the process dynamics, the information available to them and the targets that should be satisfied. Advanced control systems are beneficial for reducing the workload required from an operator and steering the process toward achieving the operational objectives.

A generalized process control system can be structured into three hierarchical layers, namely;

1. the regulatory layer;
2. the supervisory layer, and;
3. the optimization layer.

The optimization layer operates on the slowest time-scale and determines an optimum reference for the supervisory layer which can be based on a plant-wide economic objective. The supervisory layer determines the setpoints for the regulatory layer and operates over a shorter time period compared to the optimization layer. The supervisory layer chooses lower-level operating conditions that ensure the plant operates within its operating limits and maintains stability. The role of the regulatory layer is

to maintain the process at the chosen operating conditions and minimize deviations due to process disturbances (Skogestad 2004).

2.4.1.1 Regulatory control

The regulatory control layer is typically approached by either implementing multiple decentralized single-input, single-output controllers or multivariable controllers (Pomerleau et al. 2000). Single-loop control is commonly used in the regulatory layer in grinding mill circuit control, where a single manipulated variable is paired to control one of the process variables. Traditionally, the decentralized single-loop controllers are implemented as a simple on-off (bang-bang) controller or a PID controller, which is widely used in mineral processing (Wei & Craig 2009*b*, Olivier & Craig 2017*b*). A PID controller is simple to implement and does not require an advanced skill set for tuning. PID controllers perform well when processes do not deviate far from the operating conditions the controller was initially tuned on. However, setpoint changes or large disturbances can upset the process and result in a long settling time or undesired oscillations if the controller is poorly tuned.

Fractional order proportional-integral (FOPI) controllers present an improved alternative to using PID controllers in multiple-input, multiple-output (MIMO) systems. FOPI controllers are simple to implement and provide robust independent control (Aguila-Camacho et al. 2017, 2020). The controller demonstrated better or at least comparable performance to a linear model predictive controller (LMPC), which is an advanced controller.

Single-loop control is favoured for its simplicity and can provide satisfactory performance if the correct input-output pairing is chosen. However, grinding mill circuits exhibit non-linear behaviour, have large time delays and variables that are strongly coupled to one another (Zhou et al. 2016). A single-loop controller is typically not capable of achieving multiple control objectives on a process with multiple controlled outputs that are strongly coupled. Multiple single-loop PID controllers can be used to regulate the system about these setpoints. However, it would require conservative tuning to reduce the interactions between the multiple single-loop controllers of the circuit, which can result in poor performance. Therefore, there is a desire to achieve decoupled control of the key process variables in the multivariable grinding mill circuit.

Multivariable controllers have shown significant performance improvements in grinding mill circuits, such as increased throughput, reduced power consumption or improved grind quality without requiring

a large trade-off (Hulbert et al. 1990, Craig et al. 1992, Craig & MacLeod 1995, Pomerleau et al. 2000, Matthews & Craig 2013). These minor improvements over a long term operation can significantly increase the generated revenue and reduce operating costs. However, the multivariate nature of a grinding mill circuit often results in undesired interactions when manipulating variables. Achieving independent control in a multivariate system would allow for multiple objectives to be achieved without requiring a significant compromise in performance. The fundamental idea behind a multivariable regulatory controller is to develop a compensator that decouples the interactions between the controlled variables. The compensator paired with a single-loop controller such as PID control, can be used to achieve independent control. In Hulbert et al. (1990), a compensator was developed from the modelled process dynamics using the Inverse Nyquist Array method. The controller improved the product particle size while maintaining the throughput (Hulbert et al. 1990).

Another proposed multivariable control approach is a multivariable decision-making system. The control actions are decided on an "IF-THEN" rule which is the basis of a fuzzy logic control system. A fuzzy expert control system (FECS) was implemented as a supervisory controller in a grinding mill circuit using a rule-based strategy to maximize the throughput and minimize power consumption (Chen, Zhai, Li & Fei 2007, Laiji et al. 2012, Hadizadeh et al. 2017). The control actions are decided on an "IF-THEN" rule which is the basis of a fuzzy logic control system. The FECS is set to handle all the expected operating conditions to stabilize and optimize the grinding mill circuit performance. An FECS aims to eliminate the need for operators to be present within the control room. The significant drawback of the system is that it requires an experienced grinding mill operator to determine these rules. There is no formal way for the rule criteria to be assigned. For example, a rule is described as "if (SUMP LEVEL is HIGH) and (PUMP SPEED is LOW) then (PUMP SPEED is INCREASE)" (Hadizadeh et al. 2017). Although the method is simple and flexible to implement, it does not control the grinding mill circuit optimally.

2.4.1.2 Supervisory control

Regulatory control tends to dominate the process control systems used as advanced control systems can be complex and difficult to maintain once implemented if there is a lack of expert knowledge on the control technology. The lack of expertise in understanding the process dynamics and control systems for grinding mill circuits prevents advanced controllers from being adopted (Wei & Craig 2009*b*). However, process performance can be significantly improved with supervisory control. The role of the supervisory layer is to provide the setpoints that the regulatory layer will track. In addition,

it ensures that the process operates within its limitations and can reduce the workload of the plant operator. It is common for the supervisory layer to be combined with the regulatory layer (le Roux & Craig 2019)

A significant contribution to control technologies used in industrial process control is model-predictive control (MPC) (Qin & Badgwell 2003). MPC performs well in constrained MIMO systems with large time delays and non-linearities, making them suitable to be adopted in grinding mill circuit control as a supervisory controller. A model of the process and the online measurements are used to predict the output of the plant over a horizon and compute the set of operating conditions that would minimize an objective function. The objective function can be weighted among several objectives such as:

1. penalizing setpoint deviation;
2. penalizing the rate of change in the manipulated variables;
3. penalizing controlled variables that exceed soft limits, and;
4. maximizing the performance of a controlled variable.

It is an iterative technique, where for each iteration, a new set of optimal control moves are computed that would minimize the objective function using the prediction model (Rawlings 2000). The control strategy uses a receding horizon approach, where only the first set of control moves of the iteration is used and the prediction horizon is shifted forward.

Several variations of model predictive controllers have been developed for improving grinding mill circuit performance, such as traditional MPC, non-linear MPC, robust non-linear MPC and hybrid non-linear MPC (Ramasamy et al. 2005, Wei & Craig 2009*a*, Coetzee et al. 2010, le Roux et al. 2016, Botha et al. 2018). Other improvements using optimization strategies with MPC such as load shifting, have achieved decreased power consumption while maintaining a consistent monthly throughput (Matthews & Craig 2013). MPC has been shown to improve the performance of grinding mill circuits compared to traditional PID controllers (Ramasamy et al. 2005, Wei & Craig 2009*a*). Model-based controllers show robust performance on a supervisory level, can effectively track setpoint changes and reject external disturbances.

One of two drawbacks of MPC is that the control technique can be computationally intensive due to the complex models used and the number of parameters that need to be solved per iteration (Coetzee et al. 2010). An alternative approach to consider could be to divide the grinding mill controller into

two controllers to handle the fast and slow dynamics of a grinding mill circuit separately. In le Roux et al. (2016), the non-linear MPC is responsible for the plant-wide control of the slow dynamics and a dynamic inversion controller is used for controlling the fast dynamics of the sump slurry volume. A model predictive static programming technique is used in le Roux et al. (2014) to improve convergence time and achieve comparable performance to a non-linear MPC. However, the increased computation power that is readily available today is not necessarily a limiting factor. The second drawback of MPC is that the required measurements for state feedback are not always available due to the lack of instrumentation or faulty equipment. Therefore, additional effort is necessary to develop tools such as observers for state and parameter estimation (le Roux & Craig 2019).

The effectiveness of model-based controllers, such as MPC is dependent on the accuracy of the process model used. Generally, linearisation and simplifications of the process behaviour are used to decrease the computational effort necessary for control and optimization. The simplified models tend to only accurately describe non-linear process behaviour over a narrow operating region and do not capture the process dynamics across the full operating range of the circuit. If the optimal operating region is outside of the modelled operating range due to external disturbances, the system cannot be controlled optimally and the controller can perform poorly. Grinding mill circuit models are generally modelled with fixed parameters (Craig & MacLeod 1995, Chen, Zhai, Li & Li 2007, le Roux, Craig, Hulbert & Hinde 2013). However, this does not always accurately represent the system due to its time-varying behaviour. The feed characteristics change, circuit configuration changes or equipment damage such as mill liner wear result in a model that no longer accurately describes the system. Any mismatch between the models and the plant needs to be compensated for through recalibration, remodelling or retuning (Olivier & Craig 2015).

Optimizing run-of-mine grinding mill circuits with model-free methods is driven by the need to eliminate the process of developing an accurate plant model of the complex grinding mill behaviour. In ROM mineral processing plants, the feed ore composition is regularly changing and the feed ore characteristics such as the ore hardness and size distribution vary (Tessier et al. 2007, Maritz et al. 2019). Furthermore, changes in the feed ore characteristics affect the breakage rate of the ore which influences the performance of the grinding mill (Morrell et al. 1996).

Grind curves demonstrate that there exists an unknown peak for each of the grinding mill performance indicators. A model-free extremum seeking method would be beneficial to optimize grinding

mill performance. Since the most common objectives of grinding mill circuits are maximizing the throughput, minimizing the power draw and minimizing the variation in the product grind, the grind curves described in Section 2.3 can be used to determine the optimal operating conditions that would maximize the grinding mill circuit performance. Although each grinding mill is unique, the general trends of the grind curves are common to all SAG mills and the idea can, therefore, be transferred to a general grinding mill circuit.

2.4.2 Adaptive Control

Adaptive control is a technique aimed at controlling processes with uncertain or time-varying parameters to achieve desired process performance and stability. An adaptive control law is used to estimate key parameters identified in the design stage that is crucial to achieving the desired control performance. The principle of adaptation is based on measurable performance errors, where the online measurements are used as feedback to update and converge the estimates of the uncertain parameters towards their true values (Tao 2014).

Adaptive control can be separated into model-based, partially model-based or model-free methods and is useful in applications where there are variations in process dynamics, parameter uncertainties, disturbances or to improve and optimize processes (Åström & Wittenmark 2013, Benosman 2016). Model-based methods are efficient for optimization as the information of the plant behaviour is exploited and used to maximize the performance of the controller. The knowledge of the process behaviour can significantly improve transient performance compared to model-free methods. Modelling process behaviour and pairing it with a simulation environment can be useful to provide insight into the process and reproduce unique scenarios that can be costly to experiment on the physical process. For example, a model describing the slow grinding process can be used to quickly simulate multiple scenarios without interrupting the process itself. However, developing an accurate model for the complex, non-linear behaviour of a grinding mill can be difficult, time-consuming, and requires measured plant data for validation. Furthermore, the accuracy of the model is dependent on the complexity and effort invested into recreating a "digital twin" of the model.

Complex models are computationally expensive to execute, whereas, simplified models poorly predict the behaviour of the process over a broad operating region. Grinding mill circuits are typically modelled with fixed parameters which do not accurately represent the model due to its time-varying behaviour. Over time the model drifts from its initial representation due to equipment wear and changes in

operating conditions. Therefore, model-based optimization can determine optimal results for the model, but not necessarily the process itself due to plant-model mismatches, unmodelled uncertainties and undesired disturbances.

In contrast, model-free adaptive control methods do not use any explicit knowledge of the process dynamics. Instead, the method is data-driven from online process measurements and an adaptive control law steers the process to optimize an objective function. However, the lack of knowledge of the process behaviour suggests that model-free methods are perhaps better suited for use as optimization controllers that compensate for slowly varying process parameters.

2.4.2.1 Extremum Seeking Control

ESC is a class of adaptive control techniques used to search for the unknown optimal inputs of a process to maximize (or minimize) an objective function. It is a model-free optimization method and the need for accurate models to optimize a complex process with uncertainty can be eliminated. The concept of extremum seeking is to sufficiently excite and observe the process response through a measurable objective function to be optimized. The change in the measured objective function due to the excitation is used as feedback to control the process toward an unknown extremum as illustrated in Fig. 2.6. In Fig. 2.6, u is a manipulated variable and J is the corresponding value of the objective function, which is described by $f(u)$. The search begins with the initial conditions, $J_0 = f(u_0)$. The extremum seeking method progressively manipulates u in the direction toward the extremum of J, located at $J^* = f(u^*)$. The manner in which the extremum seeking method approaches the extremum is dependent on the extremum seeking algorithm. The functional value of an objective function is iteratively evaluated and the algorithm aims to progressively step toward the optimal solution. In another approach, if the objective function gradient information is available, then the extremum seeking method aims to find the solution that results in a zero gradient.

ESC is separated into deterministic and stochastic control methods which can be classified by the probing signal used. Deterministic extremum seeking uses a periodic excitation signal to perturb the system to extract information, whereas stochastic methods utilize a zero-mean random-noise perturbation signal (Liu & Krstić 2016). Stochastic control methods are preferable for systems where the periodic perturbation would be unnatural such as biological systems, as it introduces predictability (Manzie & Krstić 2007). In deterministic extremum seeking methods, the choice of the periodic perturbation signal is important to consider and can influence the rate of convergence toward the

extremum (Nešić et al. 2006).

The history and development of extremum seeking as an adaptive control technique is well described in Tan et al. (2010), which highlights key ESC literature and the application of the classical perturbation extremum seeking technique. Many extremum seeking methods have been proposed to optimize processes such as perturbation-based ESC (Krstić & Wang 1997), sliding mode ESC (Korovin & Utkin 1974, Pan et al. 2003, Fu & Ümit Özgüner 2011), Newton-based ESC (Moase et al. 2009, Ghaffari et al. 2012), numerical optimization ESC (Zhang & Ordóñez 2012), estimation-based ESC (Guay & Dochain 2015), proportional-integral (PI) ESC (Guay & Dochain 2017) and least-squares ESC (Hunnekens et al. 2014, Chioua et al. 2016). The application of ESC has extended to various industrial fields such as automotive applications, process control, controller design and optimization, and energy conversion (Zhang & Ordóñez 2012). The advancement of the ESC techniques has shown to improve upon the challenges associated with model-free methods such as the slow convergence rate to the optimum.

Examples of extremum seeking applied to optimize grinding mill circuits in the mineral processing industry are illustrated in Pauw et al. (1985), Craig et al. (1992), Lu et al. (2021). A perturbation-based ESC being used on an input-constrained closed grinding mill circuit is illustrated in Lu et al. (2021). The work considers both the problems associated with regulation for setpoint tracking and throughput optimization by maximizing the feed rate of ore material, and also proves the stability of multivariable ESC. Other implementations of extremum seeking techniques, referred to as peak seeking methods, have also been employed to optimize grinding mill circuit performance (Pauw et al. 1985, Craig et al. 1992). The idea is based on the assumption that the maximum throughput of a grinding mill is achieved at maximum power consumption Pauw et al. (1985). Therefore, the throughput is maximized with

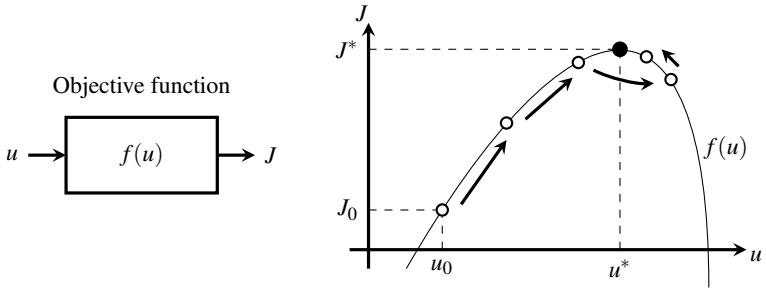

Figure 2.6. Concept of extremum seeking.

a peak-seeking optimizer to manipulate the mill load filling up to the point where the grinding mill operates at maximum power consumption. However, as later observed in Craig et al. (1992), the maximum throughput of the mill is generally achieved below the peak power consumption. Therefore, the peak seeking algorithm was improved by manipulating the mill load filling to a point before the peak power consumption is achieved, and the grinding mill would operate closer to the throughput peak.

Grind curves are useful for ESC as they establish the relationships that are observed between the throughput, grind, and power consumption of a mill to the mill filling and rotational speed. Grind curves furthermore indicate where the extremum exists for these performance variables and are parabolic (Powell et al. 2001, van der Westhuizen & Powell 2006, Powell et al. 2009). The significance of grind curves is well understood in industry, but their use as part of an ESC strategy is yet to be formalized. A suitable ESC framework can be developed for a general grinding mill circuit that can optimise operational objectives, such as maximizing the throughput or grind quality. It would not be necessary to develop explicit grind curves for the mill as the ESC strategy is model-free and only relies on the fact that an extremum exists.

Following the control framework for a grinding mill circuit presented in (le Roux & Craig 2019), a typical process control system would consist of an economic optimizer operating at the highest level, followed by a supervisory control layer and lastly, a regulatory control layer. The need for developing the optimization control layer is indicated by the lack of advanced control technologies implemented in industry. Most processing plants primarily use PID control ($\sim$90%) and less than 40% of the plants have expanded to implementing advanced control methods, such as MPC (Olivier & Craig 2017*b*). A significant amount of research for controlling grinding mill circuits is specifically focused on using MPC as a supervisory controller (Cortinovis et al. 2013, Steyn & Sandrock 2013, le Roux et al. 2014, 2016, Botha et al. 2018). However, there is limited research that addresses the development of the optimization control layer (Zhou et al. 2016).

In (Pauw et al. 1985) and (Craig et al. 1992), extremum seeking is used to optimize grinding performance with the mill load based on the measured power consumption to indirectly maximize the throughput. However, this strategy does not guarantee that the optimal throughput is achieved when the mill speed varies. For example, for different mill speeds, the difference between the peak power consumption and throughput does not vary linearly with the mill load (Powell et al. 2009). There-

fore, tracking the maximum throughput based on power consumption measurements can result in sub-optimal operating conditions if both the mill load and speed are manipulated.

The application of extremum seeking to optimize process performance is not without certain requirements that can be undesirable from the operating perspective. Extremum seeking is effective if the technique can extract useful information to drive the process towards an extremum. It is important to consider the effects of the persistent excitation required to maintain the process at an extremum. Ideally, an operator would aim to maintain the process at near steady-state conditions once the process has converged toward the optimal operating conditions. However, without continuously perturbing and observing the process, it cannot be guaranteed that the operating conditions will remain optimal if there are time-varying disturbances in the process. The perturbation frequency is also a key parameter to consider. If the perturbations occur at a rate significantly faster than the process dynamics, the extremum seeking method will be unable to differentiate the effects of the excitations on the optimized objective function from the process dynamics. Therefore, the perturbations must occur on a time-scale slower than the process dynamics. Additionally, for a process with slow dynamics, the required time-scale separation between the perturbation frequency and process dynamics can result in long convergence times.

On a single-input, single-output process, extremum seeking can effectively drive the process based on the input-output relationship. However, for a multivariable process with multiple inputs being perturbed, it is important to isolate the influence of each perturbed input on the measured objective function by means of perturbing at different frequencies. Additionally, the magnitude of the perturbations should overpower the noise levels on the measured outputs. Otherwise, the ESC will steer the process in the direction of the noise without a distinct direction. However, the perturbations should not be so large that the effects of the persistent perturbations contribute to a greater loss than finding the near-optimal steady-state operating conditions.

This dissertation aims to explore several ESC optimization strategies combined with grind curves to demonstrate the value of ESC as an optimizer. In this work, the ESC uses the mill load, mill rotational speed or both, as single-input and multiple-input cases, to maximize the throughput, grind or a combination of the two with a weighted objective function. These operating conditions are currently mostly set manually and the ESC would steer the mill filling or speed towards a neighbourhood of the steady-state optimum.

2.5 CHAPTER SUMMARY

Comminution is an expensive and crucial stage in the chain of mineral processing operations. It is energy intensive and the net revenue generated by the mineral processing plant is affected by the quality and volume of the processed ore material through the grinding stage.

Grinding mill circuits are complex, multivariable and there are time-varying parameters to consider that make manually determining the optimal operating conditions difficult. Insufficient knowledge of the process behaviour can often lead to sub-optimal operation during the grinding stage. Advanced control methods have shown considerable process performance improvements that ensure the grinding mill operates about a set of chosen operating conditions without significant deviations. However, there is limited literature that considers optimizing the operating conditions. These operating conditions are generally manually set by a plant operator. They are often sub-optimal due to external disturbances unknown to the operator, such as the lack of information about the feed ore to the mill. Market demand of the ore material also plays an important role in whether throughput or grind quality should be optimized to maximize the revenue generated by a mineral processing plant.

Grind curves show that there exists an extremum for each of the performance indicators that can be useful to a plant operator. However, grind curves can be time-consuming to establish for different ore types. Several advanced control methods are currently used to optimize the grinding process, but these methods require accurate models, sufficient measurements and can be computationally expensive. The dependency on requiring models can be eliminated by utilizing control strategies that do not necessarily rely on the dynamics of the system, such as ESC. Therefore, there is an incentive to employ an adaptive real-time optimization controller. The controller would ensure that the process is tracking the optimal operating conditions while satisfying the operational objectives. The optimizer would ideally operate in a region nearer to the optimal operating region compared to the periodic setpoint choices of a plant operator. Additionally, employing an extremum seeking controller as an optimizer would reduce the workload of a plant operator.

ESC is used in several applications such as combustion engines, windmills, braking systems and chemical reactors. The successful application of ESC in these non-linear systems with uncertainty suggests that ESC would be suitable for optimizing grinding mill circuit performance.

CHAPTER 3 MODEL OF A SINGLE-STAGE GRINDING MILL CIRCUIT

3.1 CHAPTER OVERVIEW

This chapter describes the dynamic non-linear model of a SAG mill which is fit to measured grind curve data. The grinding mill model is then extended to form a model of a single-stage closed SAG mill circuit. The grinding mill circuit is closed with either a screen or a hydrocyclone classifier used to separate the undersize and oversize material, where the oversize material is recirculated for regrinding as illustrated in Fig. 3.1. The closed SAG mill circuit dynamic behaviour is modelled by three separate modules:

1. the SAG mill;
2. the sump, and;
3. the classifier (screen or hydrocyclone).

Section 3.2 provides a description of the grinding mill model. Section 3.3 describes the sump, and Section 3.4 describes the screen and hydrocyclone classifier used to close the grinding mill circuit. Table 3.1 provides a description of the lower case subscripts for the model flow-rates, Q $(\mathrm{m}^3/\mathrm{h})$ and the model states, x (m^3). The first subscript indicates the circuit unit (mill, sump, classifier) and the second subscript specifies the model state (rocks, solids, coarse, fines, or water). For flow-rates the third subscript indicates an inflow, outflow, oversize or undersize stream. The variables of the grinding mill circuit model are summarized in Table 3.2 and the description of the parameters used in the circuit are provided in Table 3.3.

Table 3.1. Description of the state and flow-rate subscript nomenclature.

Variable	Unit	Subscript description
$x_{\square\triangle}$	(m^3)	$\square$: m-mill; s-sump; c-classifier $\triangle$: w-water; s-solids; c-coarse; f-fines; r-rocks; b-balls
$Q_{\square\triangle\bigcirc}$	$(\mathrm{m}^3/\mathrm{h})$	$\bigcirc$: i-inflow; o-outflow; os-oversize; us-undersize

Table 3.2. Description of the grinding mill circuit variables.

Variable	Unit	Description
		Manipulated variables
u_{MFO}	(t/h)	Feed rate of ore to the mill
u_{MFW}	$(\mathrm{m}^3/\mathrm{h})$	Flow-rate of water to the mill
u_{ϕ_c}	$(-)$	Fraction of critical mill speed
u_{SFW}	$(\mathrm{m}^3/\mathrm{h})$	Flow-rate of water to the sump
u_{CFF}	$(\mathrm{m}^3/\mathrm{h})$	Feed rate to the classifier
u_{CFW}	$(\mathrm{m}^3/\mathrm{h})$	Flow-rate of water to the screen
		Controlled variables
Q_{mso}	$(\mathrm{m}^3/\mathrm{h})$	Grinding mill solids discharge
y_{ψ_m}	$(-)$	Mill grind (e.g. volume fraction of particles in discharge $< 150\ \mu$m)
y_{J_T}	$(-)$	Fraction of mill volume filled with charge
$y_{\beta_{ws}}$	$(-)$	Mill discharge water to solids ratio
y_{P_m}	(kW)	Mill power draw
Q_{csus}	$(\mathrm{m}^3/\mathrm{h})$	Circuit throughput
y_{ψ_c}	$(-)$	Circuit grind (e.g. volume fraction of particles in discharge $< 75\mu$m).
y_{SVOL}	(m^3)	Volume of slurry in sump
y_{CFD}	$(\mathrm{t}/\mathrm{m}^3)$	Classifier feed density

Table 3.3. Description of the grinding mill circuit parameters.

Variable	Unit	Description
		Grinding mill
α_f	$(-)$	Fraction of fines in u_{MFO}
α_r	$(-)$	Fraction of rocks in u_{MFO}
ρ_o	$(\mathrm{t/m^3})$	Ore density
ρ_w	$(\mathrm{t/m^3})$	Water density
d_q	$(1/\mathrm{h})$	Discharge rate constant
x_{mb}	$(\mathrm{m^3})$	Volumetric filling of balls in mill
V_{mill}	$(\mathrm{m^3})$	Total mill volume
δ_v	$(-)$	Power change parameter for the volume of mill filled
δ_s	$(-)$	Power change parameter for volume fraction of solids in the slurry
φ_N	$(-)$	Rheology normalization factor
ε_0	$(-)$	Maximum fraction of solids by volume of slurry at zero slurry flow
		Screen
D_1	$(-)$	Fraction of the water flow-rate that forms part of the circulating load carrying the solids parameter
D_2	$(-)$	Fraction of solids in the slurry that are larger than the target specification size and form part of the circulating load parameter
D_3	$(-)$	Final product particle size fitting parameter
		Hydrocyclone
α_{su}	$(-)$	Fraction of solids in the underflow parameter
ε_c	$(\mathrm{m^3/h})$	Coarse split parameter
C_1	$(-)$	Fitting parameter
C_2	$(-)$	Fitting parameter
C_3	$(-)$	Fitting parameter
C_4	$(-)$	Fitting parameter
C_5	$(-)$	Fitting parameter

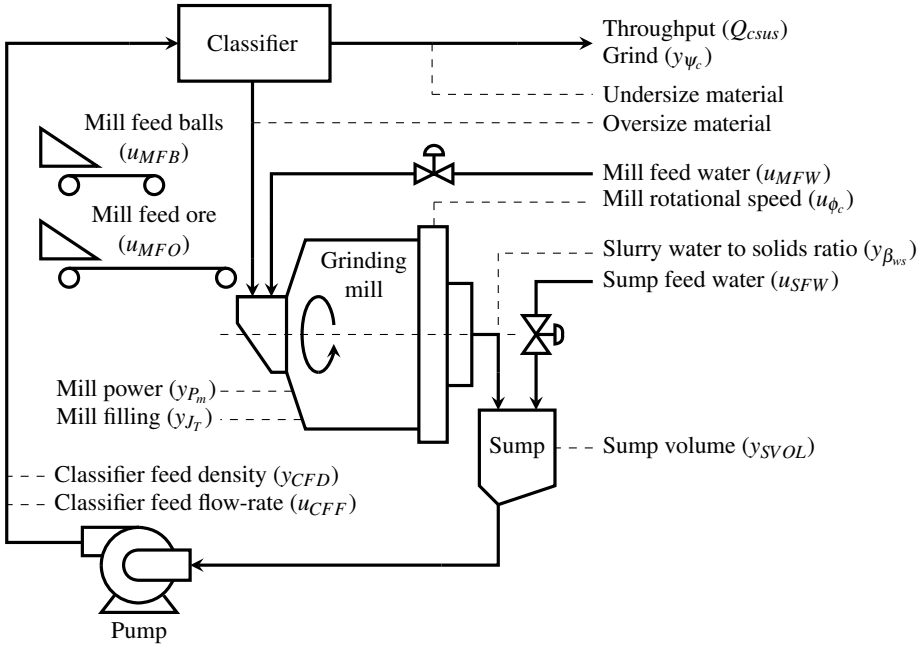

Figure 3.1. Single-stage closed grinding mill circuit.

3.2 GRINDING MILL

The SAG mill model is based on the dynamic non-linear model as given in le Roux, Craig, Hulbert & Hinde (2013). The grinding mill model is fit to the grind curve data from van der Westhuizen & Powell (2006) using the step-wise procedure described in le Roux et al. (2020). The model produces a realistic dynamic and steady-state response over a wide range of operating conditions which is suitable for testing an ESC in search of an unknown optimum. A summary of the model as in le Roux et al. (2020) is provided in the following section.

The modelled grinding mill dynamics are described by a population volume balance around the mill. Fig. 3.2 illustrates the feed flow-rates, discharge flow-rates and the model states associated with the

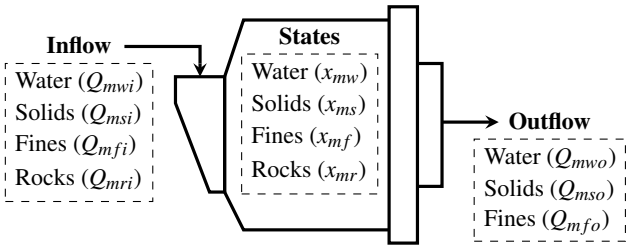

Figure 3.2. Grinding mill.

grinding mill module. The accumulation of the constituents inside the mill are determined by the difference of the feed rate of particles into the mill and the discharge rate of the particles out of the mill,

$$\dot{x}_{mw} = Q_{mwi} - Q_{mwo}, \tag{3.1a}$$

$$\dot{x}_{ms} = Q_{msi} - Q_{mso} + Q_{RC}, \tag{3.1b}$$

$$\dot{x}_{mf} = Q_{mfi} - Q_{mfo} + Q_{FP}, \tag{3.1c}$$

$$\dot{x}_{mr} = Q_{mri} - Q_{RC}, \tag{3.1d}$$

where x_{mw}, x_{ms}, x_{mf} and x_{mr} (m^3) represent the volume of water, solids, fines and rocks in the grinding mill, respectively. Q_{mwi}, Q_{msi}, Q_{mfi} and Q_{mri} $(\mathrm{m}^3/\mathrm{h})$ is the mill feed flow-rate of water, solids, fines and rocks, respectively. Q_{mwo}, Q_{mso} and Q_{mfo} $(\mathrm{m}^3/\mathrm{h})$ is the mill discharge flow-rate of water, solids and fines, respectively. Q_{RC} and Q_{FP} $(\mathrm{m}^3/\mathrm{h})$ are the rock consumption and fine production terms. The feed rate of steel balls $(Q_{mbi} = u_{MFB})$ into the mill is not dynamically modelled and a constant feed rate of steel balls is assumed. The mill feed flow-rates are described by,

$$Q_{mwi} = u_{MFW} + Q_{cwos}, \tag{3.2a}$$

$$Q_{msi} = \frac{u_{MFO}}{\rho_o}(1-\alpha_r) + Q_{csos}, \tag{3.2b}$$

$$Q_{mfi} = \frac{u_{MFO}}{\rho_o}(\alpha_f) + Q_{cfos}, \tag{3.2c}$$

$$Q_{mri} = \frac{u_{MFO}}{\rho_o}(\alpha_r), \tag{3.2d}$$

where ρ_o $(\mathrm{t}/\mathrm{m}^3)$ is the ore density, and α_f and α_r denote the fraction of fines and rocks in u_{MFO}, respectively. Q_{cwos}, Q_{csos} and Q_{cfos} $(\mathrm{m}^3/\mathrm{h})$ are the classifier discharge flow-rates of water, solids and fines that are larger than the target set specification size, respectively. The terms representing the oversize streams from the classifier are included as part of a closed circuit configuration. The oversize material is returned to the mill for further grinding. If an open grinding mill circuit configuration is used, these terms are zero $(Q_{cwos} = Q_{csos} = Q_{cfos} = 0\ \mathrm{m}^3/\mathrm{h})$. The mill discharge flow-rates are described by,

$$Q_{mwo} = d_q \varphi x_{mw}\left(\frac{x_{mw}}{x_{mw}+x_{ms}}\right), \tag{3.3a}$$

$$Q_{mso} = d_q \varphi x_{mw}\left(\frac{x_{ms}}{x_{mw}+x_{ms}}\right), \tag{3.3b}$$

$$Q_{mfo} = d_q \varphi x_{mw}\left(\frac{x_{mf}}{x_{mw}+x_{ms}}\right), \tag{3.3c}$$

where d_q $(1/\mathrm{h})$ is the discharge rate constant and φ is the empirical rheology factor. A discharge grate is fitted at the end of the mill with a large aperture that is used to prevent large ore and steel balls from

exiting the mill. The volume of the water to solids ratio in the discharged slurry is denoted by $y_{\beta_{ws}}$. It is used in le Roux et al. (2020) in a feedback loop to maintain a constant slurry density and from (3.3a) and (3.3b) it is equivalent to,

$$y_{\beta_{ws}} = \frac{Q_{mwo}}{Q_{mso}}. \tag{3.4}$$

A ratio equal to $y_{\beta_{ws}} = 1.5$ indicates that the slurry consists only of water and if $y_{\beta_{ws}} = 0$, the slurry is a non-flowing mud. The fraction of the total mill filled with charge is,

$$y_{J_T} = \frac{x_{mw} + x_{ms} + x_{mf} + x_{mb}}{V_{mill}}, \tag{3.5}$$

where V_{mill} (m^3) is the total internal volume of the mill and x_{mb} (m^3) represents the volume of steel balls in the grinding mill.

The mill power consumption is modelled as a function of y_{J_T} and u_{ϕ_c},

$$y_{P_m}(y_{J_T}, u_{\phi_c}) = P_{max}(u_{\phi_c}) \left(1 - \delta_s \left(\frac{\varphi}{\varphi_N} - 1\right)^2 - \delta_v \left(\frac{y_{J_T}}{J_{T,P_{max}}(u_{\phi_c})} - 1\right)^2\right), \tag{3.6}$$

where δ_v and δ_s are the power change parameter for the volume of mill filled and for the volume fraction of solids in the slurry, respectively, and φ_N is a normalization factor. $J_{T,P_{max}}(u_{\phi_c})$ is a parametrized function of the fraction of the mill filled at maximum power draw given by,

$$J_{T,P_{max}}(u_{\phi_c}) = -7.52u_{\phi_c}^2 + 9.06u_{\phi_c} - 2.18, \tag{3.7}$$

and $P_{max}(u_{\phi_c})$ (kW) is a parametrized function of the maximum mill power consumption given by,

$$P_{max}(u_{\phi_c}) = \left(-2.70u_{\phi_c}^2 + 3.92u_{\phi_c} - 1.02\right) \times 10^4. \tag{3.8}$$

The empirical rheology factor (φ) is given by,

$$\varphi = \begin{cases} \sqrt{1 - \frac{x_{ms}}{x_{mw}}\left(\varepsilon_0^{-1} - 1\right)} & , \text{if } \frac{x_{ms}}{x_{mw}} \leq \left(\varepsilon_0^{-1} - 1\right)^{-1} \\ 0 & , \text{if } \frac{x_{ms}}{x_{mw}} > \left(\varepsilon_0^{-1} - 1\right)^{-1}, \end{cases} \tag{3.9}$$

where ε_0 is the maximum fraction of solids by volume of slurry at zero slurry flow. The rock consumption and fine production terms in (3.1) are described by,

$$Q_{RC} = \frac{y_{P_m}}{\rho_o K_{RC}(y_{J_T},\, u_{\phi_c})}, \tag{3.10a}$$

$$Q_{FP} = \frac{y_{P_m}}{\rho_o K_{FP}(y_{J_T},\, u_{\phi_c})}. \tag{3.10b}$$

where $K_{RC}(y_{J_T},\, u_{\phi_c})$ and $K_{FP}(y_{J_T},\, u_{\phi_c})$ are functions which indicate the energy required per tonne of rocks consumed and fines produced, respectively,

$$\begin{aligned} K_{RC}(y_{J_T},\, u_{\phi_c}) = \big(&(-0.478u_{\phi_c}^3 - 3.06u_{\phi_c}^2 + 1.55u_{\phi_c} - 0.183)y_{J_T}^3 \\ &+ (2.68u_{\phi_c}^3 + 5.13u_{\phi_c}^2 - 2.92u_{\phi_c} + 0.355)y_{J_T}^2 \\ &+ (-3.15u_{\phi_c}^3 - 2.61u_{\phi_c}^2 + 1.78u_{\phi_c} - 0.226)y_{J_T} \\ &+ (1.05u_{\phi_c}^3 + 0.361u_{\phi_c}^2 - 0.352u_{\phi_c} + 0.0472)\big) \times 10^6, \end{aligned} \tag{3.11a}$$

$$\begin{aligned} K_{FP}(y_{J_T},\, u_{\phi_c}) = \big(&(-3.73u_{\phi_c}^3 + 0.602u_{\phi_c}^2 + 0.301u_{\phi_c} - 0.0487)y_{J_T}^3 \\ &+ (8.76u_{\phi_c}^3 - 1.97u_{\phi_c}^2 - 0.453u_{\phi_c} + 0.0877)y_{J_T}^2 \\ &+ (-6.82u_{\phi_c}^3 + 1.91u_{\phi_c}^2 + 0.180u_{\phi_c} - 0.0501)y_{J_T} \\ &+ (1.77u_{\phi_c}^3 - 0.581u_{\phi_c}^2 - 0.00728u_{\phi_c} + 0.00882)\big) \times 10^6. \end{aligned} \tag{3.11b}$$

The grind of the mill is defined as a ratio of the discharged flow-rate of the mill fines to the solids,

$$y_{\psi_m} = \frac{Q_{mfo}}{Q_{mso}}. \tag{3.12}$$

3.3 SUMP

The sump receives the discharged slurry from the grinding mill, which is pumped to the classifier. Fig. 3.3 illustrates the feed flow-rates, discharge flow-rates and the model states associated with the sump module. The sump volume (y_{SVOL}) should not exceed the total available volume to prevent spillage. Additionally, the sump should not run dry. Manipulating the feed rate of the slurry to the classifier (u_{CFF}) or adding water to the sump (u_{SFW}) can be used to control y_{SVOL}. However, the addition of u_{SFW} reduces the slurry density (y_{CFD}).

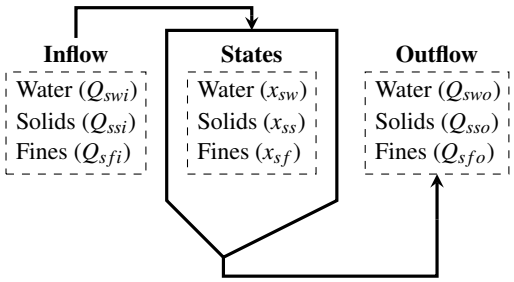

Figure 3.3. Sump.

It is assumed that the water, solids and fines within the sump are perfectly mixed. As a result of the mill discharge grate, it is also assumed that none of the rocks (x_{ms}) or steel balls (x_{mb}) from the mill

are discharged into the sump. The dynamic equations that represent the sump are,

$$\dot{x}_{sw} = Q_{swi} - Q_{swo}, \tag{3.13a}$$

$$\dot{x}_{ss} = Q_{ssi} - Q_{sso}, \tag{3.13b}$$

$$\dot{x}_{sf} = Q_{sfi} - Q_{sfo}, \tag{3.13c}$$

where x_{sw}, x_{ss} and x_{sf} (m^3) represent the volume of water, solids and fines in the sump, respectively. Q_{swi}, Q_{ssi} and Q_{sfi} $(\mathrm{m}^3/\mathrm{h})$ are the sump feed flow-rates of water, solids and fines, respectively. Q_{swo}, Q_{sso} and Q_{sfo} $(\mathrm{m}^3/\mathrm{h})$ are the sump discharge flow-rates of water, solids and fines, respectively. The sump feed flow-rates are described by,

$$Q_{swi} = Q_{mwo} + u_{SFW}, \tag{3.14a}$$

$$Q_{ssi} = Q_{mso}, \tag{3.14b}$$

$$Q_{sfi} = Q_{mfo}. \tag{3.14c}$$

The sump discharge flow-rates are described by,

$$Q_{swo} = u_{CFF}\left(\frac{x_{sw}}{x_{sw}+x_{ss}}\right), \tag{3.15a}$$

$$Q_{sso} = u_{CFF}\left(\frac{x_{ss}}{x_{sw}+x_{ss}}\right), \tag{3.15b}$$

$$Q_{sfo} = u_{CFF}\left(\frac{x_{sf}}{x_{sw}+x_{ss}}\right). \tag{3.15c}$$

The volume of slurry in the sump is given by,

$$y_{SVOL} = x_{sw} + x_{ss}. \tag{3.16}$$

The density of the slurry stream received by the classifier is given by,

$$y_{CFD} = \frac{x_{sw}\rho_w + x_{ss}\rho_o}{x_{sw}+x_{ss}}. \tag{3.17}$$

where ρ_w $(\mathrm{t}/\mathrm{m}^3)$ is the density of water.

3.4 CLASSIFIER

A classifier is used to split the feed from the sump into separate streams of oversized or undersized material based on a classification size required for downstream operations. Material that is larger than the specification size is recirculated for further grinding and the fine material is processed downstream. The classifier considered in this study is either a screen (Section 3.4.1) or a hydrocyclone (Section 3.4.2).

The classifier feed flow-rates are described by,

$$Q_{cwi} = Q_{swo}, \tag{3.18a}$$

$$Q_{csi} = Q_{sso}, \tag{3.18b}$$

$$Q_{cfi} = Q_{sfo}. \tag{3.18c}$$

where Q_{cwi}, Q_{csi} and Q_{cfi} $(\mathrm{m}^3/\mathrm{h})$ are the feed flow-rates of water, solids and fines into the classifier, respectively.

3.4.1 Screen

Fig. 3.4 illustrates the feed flow-rates and discharge flow-rates associated with the screen classifier module. The undersized material from the screen module forms part of the underflow stream and the oversized material forms part of the overflow stream. A detailed dynamic model for a screen is described in Meyer & Craig (2010). However, the dynamics of the screen are much faster compared to the dynamics of the grinding mill and the sump (le Roux, Craig & Padhi 2013). Therefore, the screen is represented with algebraic equations. The flow-rates of the oversize material from the screen are,

$$Q_{cwos} = D_1 Q_{cwi}, \tag{3.19a}$$

$$Q_{csos} = D_2 Q_{csi}, \tag{3.19b}$$

$$Q_{cfos} = 0, \tag{3.19c}$$

where Q_{cwos}, Q_{csos} and Q_{cfos} $(\mathrm{m}^3/\mathrm{h})$ are the discharge flow-rates of water, solids and fines that are larger than the desired target particle size, respectively. D_1 is the fraction of the water flow-rate that forms part of the circulating load carrying the solids and D_2 is the fraction of solids in the slurry that are larger than the target specification size, which forms part of the circulating load. It is assumed that the flow-rate of the discharged fines in the circulating load is negligible. The flow-rates of the

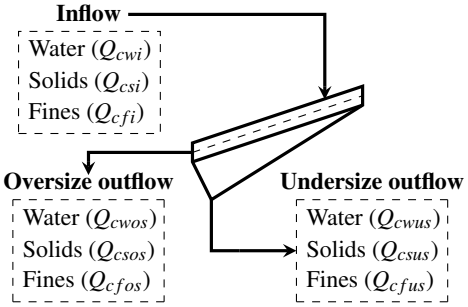

Figure 3.4. Screen classifier.

undersize material from the screen are,

$$Q_{cwus} = (1 - D_1)\, Q_{swo} + u_{CFW}, \tag{3.20a}$$

$$Q_{csus} = (1 - D_2)\, Q_{sso}, \tag{3.20b}$$

$$Q_{cfus} = Q_{sfo}, \tag{3.20c}$$

where Q_{cwus}, Q_{csus} and Q_{cfus} $(\mathrm{m}^3/\mathrm{h})$ are the discharge flow-rates of water, solids and fines that are smaller than the desired target particle size, respectively. The throughput of the circuit closed with a screen classifier is denoted by the flow-rate of undersized solids, Q_{csus}. The addition of water (u_{CFW}) is used to wash the screen and aid the slurry to propagate over, or through the screen mesh. The circuit grind is described by the final product particle size estimate given by,

$$y_{\psi_c} = D_3 - \frac{Q_{cfus}}{Q_{csus}}, \tag{3.21}$$

where D_3 is a fitting parameter.

3.4.2 Hydrocyclone

The hydrocyclone classifier can be implemented as a single hydrocyclone module or a cluster of hydrocyclones (Botha et al. 2018). This study considers a single hydrocyclone module (le Roux, Craig, Hulbert & Hinde 2013). Fig. 3.5 illustrates the feed flow-rates and discharge flow-rates associated with the hydrocyclone module. The undersized material from the hydrocyclone module forms part of the overflow stream and the oversized material forms part of the underflow stream. Similarly, the dynamics of a hydrocyclone are neglected as they are significantly faster relative to the grinding mill circuit. Therefore, the hydrocyclone is represented by algebraic equations. The oversize coarse material that forms part of the hydrocyclone underflow is given by,

$$Q_{ccos} = (Q_{csi} - Q_{cfi}) \left(1 - C_1 \exp\left(-\frac{u_{CFF}}{\varepsilon_c}\right)\right) \left(1 - \left(\frac{F_i}{C_2}\right)^{C_3}\right) \left(1 - P_i^{C_4}\right) \tag{3.22}$$

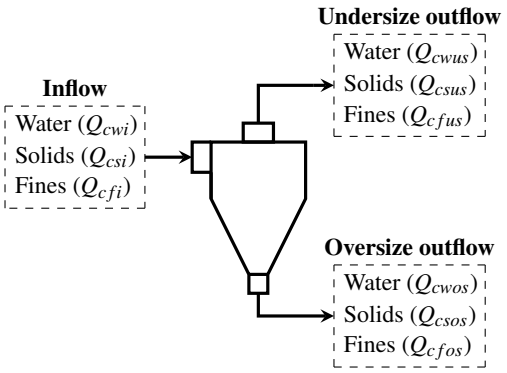

Figure 3.5. Hydrocyclone classifier.

where the fraction of solids in the hydrocyclone feed (F_i) is given by,

$$F_i = \frac{Q_{csi}}{u_{CFF}}, \tag{3.23}$$

where u_{CFF} is the hydrocyclone feed rate. The fraction of fines (P_i) in the hydrocyclone feed is given by,

$$P_i = \frac{Q_{cfi}}{Q_{csi}}. \tag{3.24}$$

The fraction of solids in the underflow is,

$$F_u = C_5 - (C_5 - F_i)\exp\left(-\frac{Q_{ccos}}{\alpha_{su}\varepsilon_c}\right). \tag{3.25}$$

The flow-rates of the oversize particles from the hydrocyclone are,

$$Q_{cwos} = \frac{Q_{cwi}\,(Q_{ccos} - F_u Q_{ccos})}{F_u Q_{cwi} + F_u Q_{cfi} - Q_{cfi}}, \tag{3.26a}$$

$$Q_{csos} = \frac{Q_{cfi}\,(Q_{ccos} - F_u - Q_{ccos})}{F_u Q_{cwi} + F_u Q_{cfi} - Q_{cfi}} + Q_{ccos}, \tag{3.26b}$$

$$Q_{cfos} = \frac{Q_{cfi}\,(Q_{ccos} - F_u - Q_{ccos})}{F_u Q_{cwi} + F_u Q_{cfi} - Q_{cfi}}. \tag{3.26c}$$

The flow-rates of the undersized particles can be determined from a flow balance around the hyrdocyclone module,

$$Q_{cwus} = Q_{cwi} - Q_{cwos}, \tag{3.27a}$$

$$Q_{csus} = Q_{csi} - Q_{csos}, \tag{3.27b}$$

$$Q_{cfus} = Q_{csi} - Q_{csos}. \tag{3.27c}$$

where the throughput of the circuit closed with a hydrocyclone classifier is denoted by the flow-rate of undersized solids, Q_{csus}. The circuit grind is described by the final product particle size estimate given by,

$$y_{\psi_c} = \frac{Q_{cfus}}{Q_{csus}}. \tag{3.28}$$

3.5 GRINDING MILL CIRCUIT

A state-space model of the grinding mill circuit can be formulated as,

$$\dot{\mathbf{x}} = \mathbf{f}(t, \mathbf{x}, \mathbf{u}), \tag{3.29a}$$

$$\mathbf{y} = \mathbf{h}(t, \mathbf{x}, \mathbf{u}). \tag{3.29b}$$

For the open grinding mill circuit, the vectors of the state-space model are,

$$\mathbf{x} = \left[x_{mw},\ x_{ms},\ x_{mr},\ x_{mf}\right]^T, \tag{3.30a}$$

$$\mathbf{u} = \left[u_{MFW},\ u_{MFO},\ u_{\phi_c}\right]^T, \tag{3.30b}$$

$$\mathbf{y} = \left[Q_{mso},\ y_{\beta_{ws}},\ y_{J_T},\ y_{P_m},\ y_{\psi_m}\right]^T, \tag{3.30c}$$

where function $\mathbf{f}(\cdot)$ is given by (3.1) and function $\mathbf{h}(\cdot)$ is given by (3.3b), (3.4), (3.5), (3.6) and (3.12).

The single-stage closed grinding mill circuit consists of the grinding mill, the sump and the classifier module. For the grinding mill circuit closed with a screen classifier, the vectors of the state-space model are,

$$\mathbf{x} = [x_{mw},\ x_{ms},\ x_{mr},\ x_{mf},\ x_{sw},\ x_{ss},\ x_{sf}]^T, \tag{3.31a}$$

$$\mathbf{u} = \left[u_{MFW},\ u_{MFO},\ u_{\phi_c},\ u_{SFW},\ u_{CFF},\ u_{CFW}\right]^T, \tag{3.31b}$$

$$\mathbf{y} = \left[y_{\beta_{ws}},\ y_{J_T},\ y_{P_m},\ y_{SVOL},\ y_{CFD},\ Q_{csus},\ y_{\psi_c}\right]^T, \tag{3.31c}$$

where function $\mathbf{f}(\cdot)$ is given by (3.1) and (3.13) and function $\mathbf{h}(\cdot)$ is given by (3.4), (3.5), (3.6), (3.16), (3.17), (3.20b) and (3.21). For the grinding mill circuit closed with a hydrocyclone classifier, the vectors of the state-space model are,

$$\mathbf{x} = [x_{mw},\ x_{ms},\ x_{mr},\ x_{mf},\ x_{sw},\ x_{ss},\ x_{sf}]^T, \tag{3.32a}$$

$$\mathbf{u} = \left[u_{MFW},\ u_{MFO},\ u_{\phi_c},\ u_{SFW},\ u_{CFF}\right]^T, \tag{3.32b}$$

$$\mathbf{y} = \left[y_{\beta_{ws}},\ y_{J_T},\ y_{P_m},\ y_{SVOL},\ y_{CFD},\ Q_{csus},\ y_{\psi_c}\right]^T, \tag{3.32c}$$

where function $\mathbf{f}(\cdot)$ is given by (3.1) and (3.13) and function $\mathbf{h}(\cdot)$ is given by (3.4), (3.5), (3.6), (3.16), (3.17), (3.27b) and (3.28).

3.6 MODEL SIMULATION

3.6.1 Dynamic step response of the open grinding mill circuit model

A dynamic step response of the open grinding mill circuit (Fig. 2.2) is shown in Fig. 3.6 to demonstrate the plant dynamics and the interactions. Each manipulated variable is stepped up by 2% from its initial value for a period of 4 hours and each output is left uncontrolled. An integrating response is clearly seen in y_{J_T} when u_{MFO} is manipulated. The increased ore feed rate results in the mill load as the ore begins to accumulate inside the mill. Increasing the mill speed results in a decreasing trend in the mill load due to the increased rate of ore breakage, and for a limited period, there is an increased throughput (Q_{mso}). However, if the ore feed rate is not increased while the mill speed is increased, Q_{mso} will begin to decrease. Manipulating u_{ϕ_c} has the largest effect on Q_{mso} and y_{ψ_m} and has the longest settling time compared to u_{MFO} and u_{MFW}. Increasing u_{ϕ_c} results in y_{ψ_m} to decrease as the ore material is processed through the mill at a faster rate. Consequently, there is a higher volume of solids discharged from the mill that are coarse, whereas, decreasing u_{ϕ_c} would increase the volume of fines in the discharged solids.

3.6.2 Dynamic step response of the closed grinding mill circuit model with a screen

A dynamic step response of the closed grinding mill circuit with a screen (Fig. 2.3) is shown in Fig. 3.7 to demonstrate the plant dynamics and the interactions. Each manipulated variable is stepped up by 2% from its initial value for a period of 4 hours and each output is left uncontrolled. It can be seen that u_{CFW} has no influence on any of the controlled variables. It is assumed that all of the water added at the screen is passed through to the underflow of the screen and does not recirculate to the grinding mill. A direct relationship exists between Q_{csus} and y_{CFD}, since the grinding mill circuit throughput is measured by the volumetric flow rate of solids in the under size stream. Therefore, Q_{csus} can be increased by decreasing u_{SFW} (this would result in a non-flowing slurry) or by increasing the solids discharge rate from the mill (Q_{mso}) as discussed in Section 3.6.1.

3.6.3 Dynamic step response of the closed grinding mill circuit model with a hydrocyclone

A dynamic step response of the closed grinding mill circuit with a hydrocyclone (Fig. 2.4) is shown in Fig. 3.8 to demonstrate the plant dynamics and the interactions. Each manipulated variable is stepped up by 2% from its initial value for a period of 2 hours and each output is left uncontrolled. A step period of 2 hours is used to avoid the sump state variables ($x_{sw}, x_{ss} and x_{sf}$ from reaching a value of zero, i.e. the sump runs dry. In the dynamic step response of closed grinding circuit models with a screen or a hydrocyclone (Figs. 3.7 and 3.8), an integrating response is seen in y_{SVOL} when u_{SFW} or u_{CFF} is manipulated. In Fig. 3.8, y_{ψ_c} tends to follow the trend of y_{J_T}, whereas, in Fig. 3.7, there is an inverse relationship between y_{ψ_c} and y_{J_T}.

3.7 CHAPTER SUMMARY

A non-linear model for a SAG mill is presented in this chapter, which is fit to measured grind curve data. The grinding mill model is extended to form part of a single stage grinding mill circuit model, closed with either a screen or hydrocyclone classifier. The dynamic behaviour of a sump is included between the grinding mill and the classifier.

A dynamic response of the open grinding mill circuit, the closed grinding mill circuit with a screen and the closed grinding mill circuit with a hydrocyclone are presented to demonstrate the interactions that exist between the manipulated and controlled process variables.

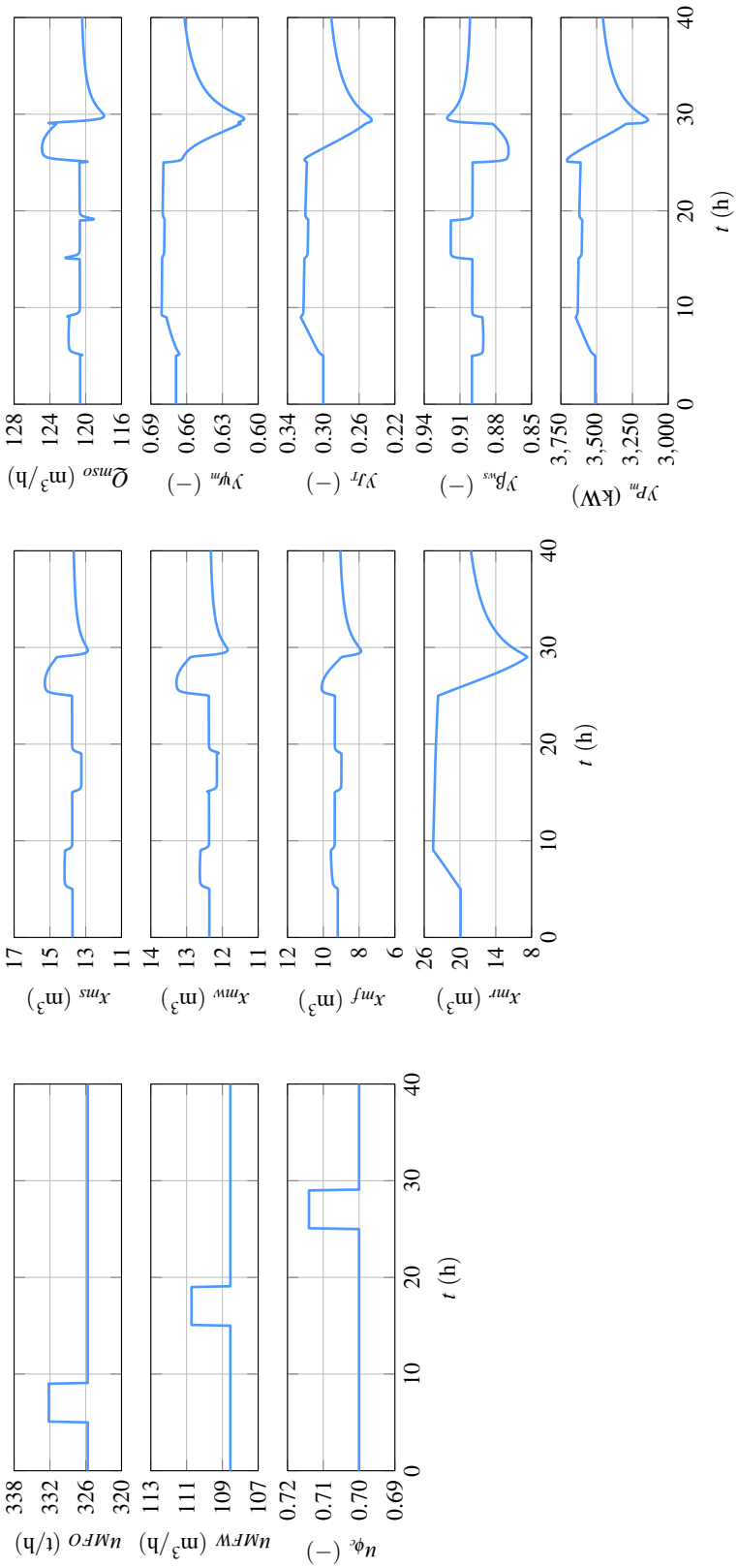

Figure 3.6. Dynamic step response of the open grinding mill circuit model.

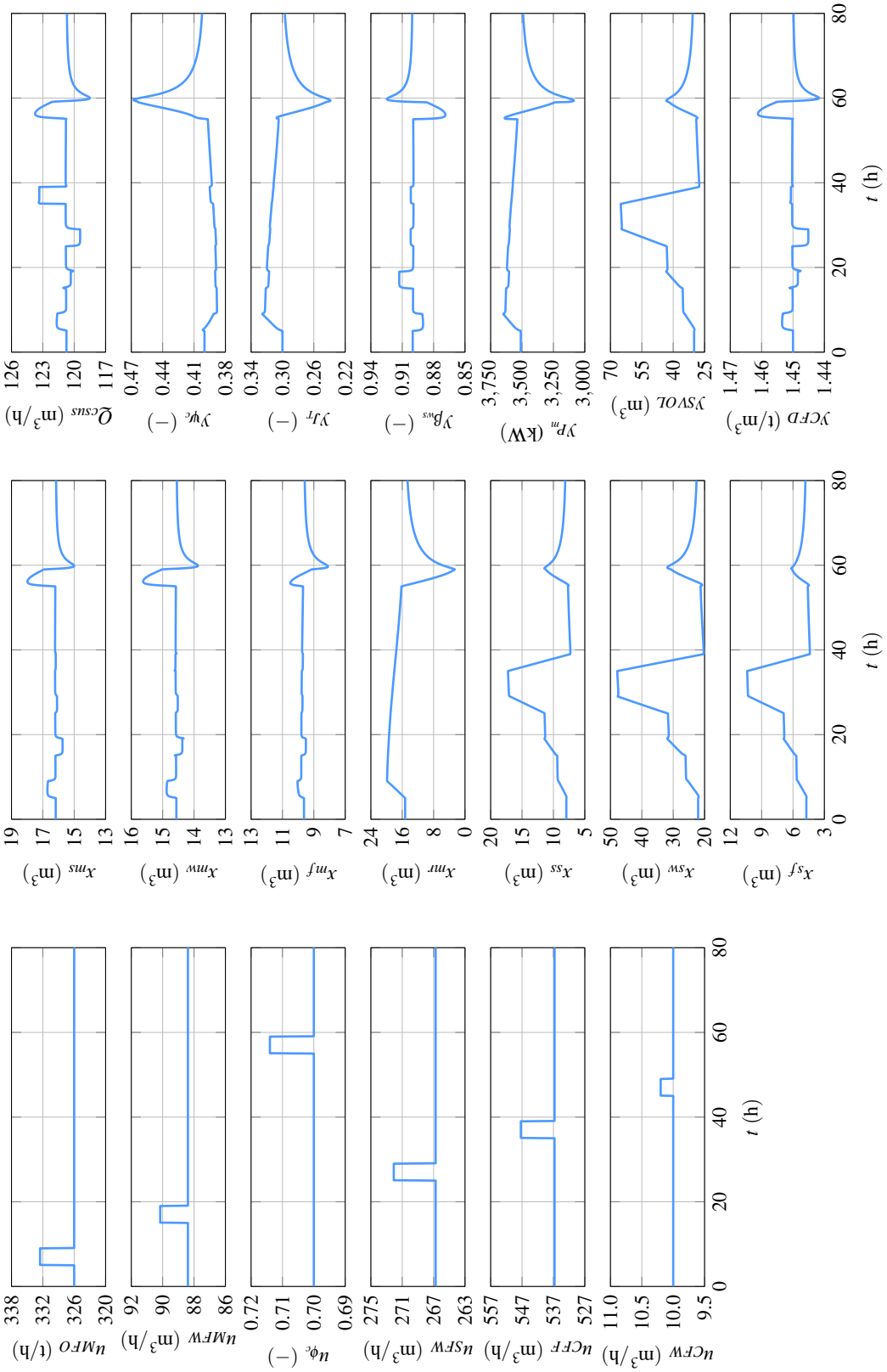

Figure 3.7. Dynamic step response of the closed grinding mill circuit model with a screen.

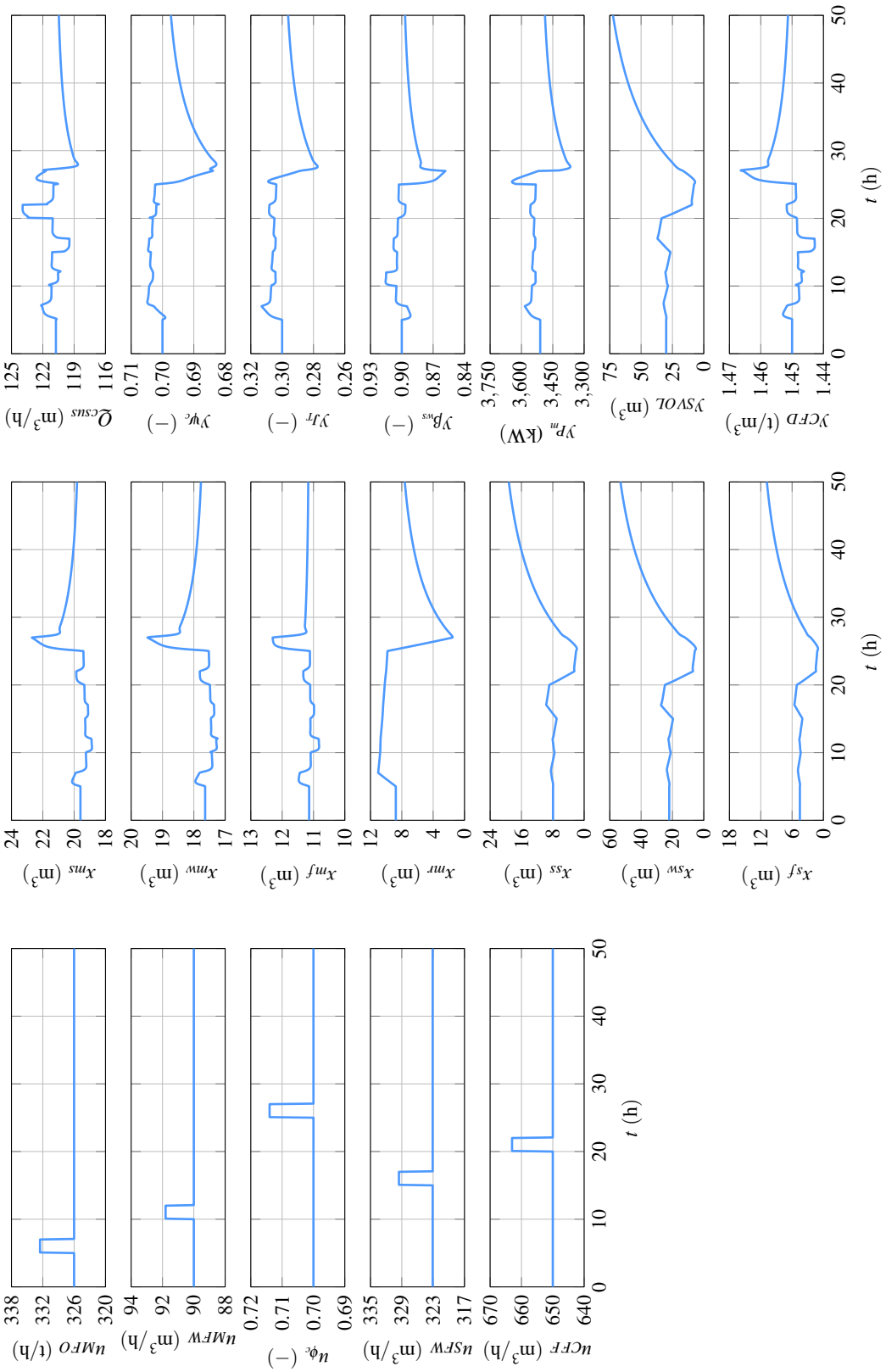

Figure 3.8. Dynamic step response of the closed grinding mill circuit model with a hydrocyclone.

CHAPTER 4 EXTREMUM SEEKING CONTROL

4.1 CHAPTER OVERVIEW

In this chapter, model-free extremum seeking methods are presented. ESC is an optimization technique that maximizes an objective function by exploring an unknown static map and steering the system toward the optimal operating condition.

The motive behind choosing an extremum seeking method is based on either the ease of tuning or the desired optimization performance. A controller with more tuning parameters can be more difficult to tune, but it is more likely to achieve the desired performance. The performance indicators of an extremum seeking controller to consider are (Nešić et al. 2006),

- **Speed of convergence:** the convergence rate at which the optimization method evolves toward an extremum.
- **Domain of convergence:** the larger the domain of convergence, the more likely the ESC is to converge toward a global extremum. In contrast, a smaller domain of convergence might lead to the ESC converging towards a local extremum.
- **Accuracy:** the size of the neighbourhood to which the optimized variable converges to.

4.2 PERTURBATION-BASED EXTREMUM SEEKING

Perturbation-based extremum seeking (PESC) is a gradient-search method that is dependent on a measurable, convex objective function and does not rely on the explicit knowledge of the process behaviour. PESC employs a periodic excitation or dither signal added to the input of the system, which is used to obtain the gradient information of the objective function. The PESC scheme is shown in Fig. 4.1 and the closed-loop system dynamics with ESC are described by (Krstić & Wang 1997),

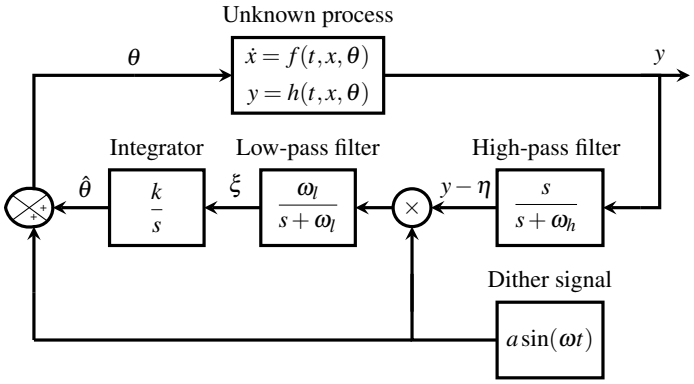

Figure 4.1. Perturbation-based extremum seeking scheme (adapted from Krstić & Wang (1997) © 1997 IEEE).

$$\dot{x} = f(t,x,\theta), \tag{4.1a}$$

$$y = h(t,x,\theta), \tag{4.1b}$$

$$\dot{\hat{\theta}} = k\xi, \tag{4.1c}$$

$$\dot{\xi} = -\omega_l \xi + \omega_l (y-\eta) a\sin(\omega t), \tag{4.1d}$$

$$\dot{\eta} = -\omega_h \eta + \omega_h y, \tag{4.1e}$$

where the unknown process dynamics are described by $\dot{x}$, y is the measurable output, and ω_l and ω_h are the cut-off frequencies for the low-pass and high-pass filters, respectively. The state of the high-pass filter is indicated by η which removes the average value from the perturbed output, resulting in the filtered output, $y-\eta$. A low-pass filter is used to reduce the effects of high-frequency noise and the estimated gradient (ξ) is driven to zero by an integrator with gain, k. The best estimate of the optimal input $(\hat{\theta})$ converges towards the unknown optimal input. The input (θ) to the process consists of the best estimate of the optimal input $(\hat{\theta})$ and the periodic dither signal,

$$\theta = \hat{\theta} + a\sin(\omega t), \tag{4.2}$$

where a and ω is the dither amplitude and frequency respectively.

Applying extremum seeking to a dynamic process requires a sufficient time-scale separation between the perturbation frequency and the process dynamics to enable the optimizer to search through an unknown static map (Krstić & Wang 1997). Therefore, a suitable perturbation frequency is required to be chosen so that the process dynamics operate at the fastest time-scale, followed by the medium

time-scale dynamics of the perturbation signal, and finally, the slowest time-scale for the optimization. A slow perturbation signal is necessary to prevent the process dynamics from interfering with the estimation of the gradient. Therefore, the input-output relationship of the process can be viewed as a static plant. For the case of multiple-input, single-output systems, additional time scale separations are required to separate the effects of each input. Consequently, the range of ω for each input is further limited. Further, the cut-off frequency of the high-pass and low-pass filter should be lower than the chosen perturbation frequency, and k needs to be chosen to be sufficiently small. The amplitude for the dither signal should be chosen to be larger than the expected noise, but small enough to minimize the perturbations that propagate to the output, such that ESC converges to a sufficiently small neighbourhood of the optimum. Due to the required time-scale separations necessary for convergence, PESC has transient performance limitations that are related to the dynamics of the process.

4.3 TIME-VARYING PARAMETER ESTIMATION EXTREMUM SEEKING

The time-varying parameter estimation extremum seeking control (TESC) method proposed in Guay & Dochain (2015) is based on estimating the gradient as a time-varying parameter. The method optimizes an objective function by estimating the unknown time-varying parameter $\hat{\theta}$, which minimizes the objective function. Similar to the perturbation-based method, a dither signal is used to excite the system and extract gradient information. However, it can be omitted to achieve a perturbation-free response if the system dynamics provide sufficient excitation (Guay & Dochain 2015). The advantage of TESC is that it provides additional freedom in tuning the controller, which can achieve improved

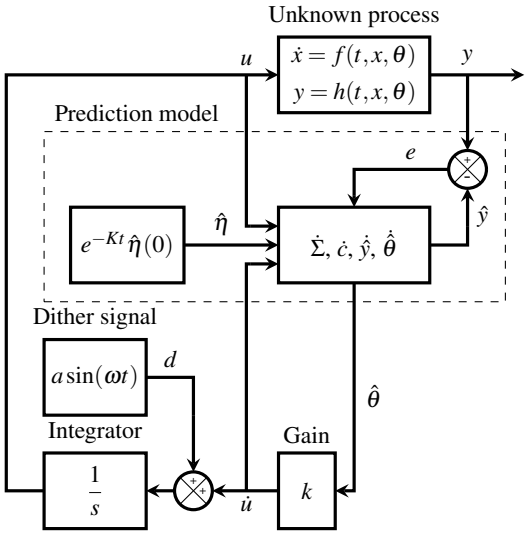

Figure 4.2. Time-varying parameter estimation extremum seeking scheme (adapted from Guay et al. (2015), with permission).

transient performance. As opposed to PESC, the tuning of the controller is not primarily limited to the tuning parameters of the dither signal. The TESC scheme is shown in Fig. 4.2 and the closed-loop system dynamics are given by,

$$\dot{x} = f(t,x,u), \tag{4.3a}$$

$$y = h(t,x,u), \tag{4.3b}$$

$$K = k_{\eta_1} + k_{\eta_2} c^T c, \tag{4.3c}$$

$$\dot{u} = -k\hat{\theta} + d, \tag{4.3d}$$

$$\dot{\hat{\theta}} = \text{Proj}\left\{\Sigma^{-1}(c(e-\hat{\eta}) - \sigma\hat{\theta}), \hat{\theta}\right\}, \tag{4.3e}$$

$$\dot{\hat{y}} = \dot{u}^T\hat{\theta} + Ke + c^T\dot{\hat{\theta}}, \tag{4.3f}$$

$$\dot{c} = -Kc + \dot{u}, \tag{4.3g}$$

$$\dot{\hat{\eta}} = -K\hat{\eta}, \tag{4.3h}$$

$$\dot{\Sigma}^{-1} = -\Sigma^{-1}cc^T\Sigma^{-1} + k_T\Sigma^{-1} - 2\sigma\Sigma^{-2}, \tag{4.3i}$$

where $e = y - \hat{y}$, is the error between the measured and predicted output, $d = a\sin(\omega t)$ is the dither signal, K is a time-varying gain, and $\hat{\eta}$ is the estimation error. The combination of $\hat{y}$, c, $\hat{\eta}$ and Σ form the prediction model for estimating the unknown time-varying parameter. The projection operator, $\text{Proj}\left\{\phi, \hat{\theta}\right\}$ is defined as,

$$\dot{\hat{\theta}} = \begin{cases} \phi, & \text{if } \mathcal{P}(\hat{\theta}) > 0 \text{ or } \nabla_{\hat{\theta}}\mathcal{P}(\hat{\theta})\phi \leq 0 \\ \left(I - \frac{\nabla_{\hat{\theta}}\mathcal{P}(\hat{\theta})^T\nabla_{\hat{\theta}}\mathcal{P}(\hat{\theta})}{\|\nabla_{\hat{\theta}}\mathcal{P}(\hat{\theta})\|^2}\right)\phi, & \text{otherwise,} \end{cases} \tag{4.4}$$

where $\phi = \Sigma^{-1}(c(e-\hat{\eta}) - \sigma\hat{\theta})$ and the function $\mathcal{P}(\hat{\theta})$ is defined as,

$$\mathcal{P}(\hat{\theta}) = ||\hat{\theta}||^2 - z_{\hat{\theta}}^2, \tag{4.5}$$

where $z_{\hat{\theta}}$ is the radius of the uncertainty set. The gradient of $\mathcal{P}(\hat{\theta})$ is given by,

$$\nabla_{\hat{\theta}}\mathcal{P}(\hat{\theta}) = 2\hat{\theta}^T. \tag{4.6}$$

The projection operator limits the transients of the parameter estimate within defined bounds and guarantees that the unknown parameter is within the uncertainty set $\hat{\theta} \in \Pi$, $\forall t > 0$, providing robustness to the prediction model. Therefore, the unknown parameter converges towards its true estimate value within the set boundary. K and k_T are the optimization estimation gains, and, k_{η_1} and k_{η_2} are positive constants to be assigned (Guay & Dochain 2015). The optimization gain affects the speed of the optimization, but it cannot be arbitrarily increased. An increased gain reduces the effects of the dither signal, which in turn affects the estimation routine. If the optimization gains are chosen too large, it

can result in an oscillatory behaviour as the speed of the process dynamics become negligible relative to the ESC dynamics. The tuning parameter, σ, should be chosen as small as possible to guarantee that the parameter estimation routine can effectively track the time-varying gradient. The purpose of σ is to ensure that Σ does not become too small which would impede the estimation routine. Finally, z_θ has to be increased for smaller choices of σ (Guay et al. 2015).

4.4 SIMPLEX EXTREMUM SEEKING

Simplex extremum seeking control (SESC) is based on the Nelder-Mead simplex algorithm. It is an optimization method that minimizes an objective function without utilizing gradient information (Nelder & Mead 1965). Instead, it is an iterative direct search method that evaluates the function values of an objective function at a set of points to form a simplex. In each iteration, the simplex is transformed by means of either four operations: reflection, expansion, contraction about the simplexes centroid or the simplex is shrunk. The coefficients used to influence the effect of each operation should satisfy,

$$\rho > 0,\ \chi > 1,\ 0 < \gamma < 1,\ 0 < \sigma < 1, \tag{4.7}$$

where ρ, χ, γ and σ are the coefficients of reflection, expansion, contraction and shrinkage, respectively. The Nelder-Mead simplex method is described in Algorithm 1. At each step of the iteration a new vertex is computed and the objective function corresponding to the vertex is evaluated and ranked. An operation that produces a lower objective function value is accepted and the new point replaces the worst performing vertex at the end of the iteration. These operations lead the vertices of the simplex to converge toward a solution that minimizes the objective function.

The simplex method is applied to optimize a dynamic process by assigning the values of the simplex vertices to the inputs of the process and allowing a sufficient period (T_s) for the process to reach steady-state before manipulating the inputs again. However, depending on the coefficients chosen, this can lead to undesired plant behaviour such as overshooting if a step size is too large. This is especially important in the case of the grinding mill considered in this paper as it is sensitive to step changes in the mill load or rotational speed (le Roux et al. 2016, 2020). The manipulated variables transition from the previous iteration operating point to the new operating point by interpolating between the points through a straight line function that is described by,

$$x(t) = \left(\frac{x_n - x_p}{t_n - t_p}\right)(t - t_p) + x_p, \tag{4.8}$$

where $x(t)$ is the value of the operating point at time t, x_n and x_p are the new and previous operating points, respectively, and t_n and t_p are the start time and end time, respectively, for which the ramp

Algorithm 1 Nelder-Mead simplex method adapted from Lagarias et al. (1998).

Setup:

$\boldsymbol{\theta}^{(0)} \leftarrow [\theta_1, ..., \theta_n]$ (Initial conditions)

$\rho > 0, \ \chi > 1, \ 0 < \gamma < 1, \ 0 < \sigma < 1$

Initialization:

Form the initial simplex around $\boldsymbol{\theta}^{(0)}$,

$$\mathbf{v}_m^{(0)} = \boldsymbol{\theta}^{(0)} + h\mathbf{j}_m, \ m = 1, ..., n+1$$

where $\mathbf{v}_m$ is a vertex of the simplex, h is a step size and $\mathbf{j}$ is a unit vector in the m-th dimension.

Repeat:

Begin iteration, i and rank the performance of each vertex such that,

$$J(\mathbf{v}_1^{(i)}) < ... < J(\mathbf{v}_n^{(i)}) < J(\mathbf{v}_{n+1}^{(i)})$$

where $\mathbf{v}_1^{(i)}$ is the *best* point and $\mathbf{v}_{n+1}^{(i)}$ is the *worst* point in the set of vertices for the current iteration.

Compute the centroid of the vertices

$$\bar{\mathbf{v}} = \frac{\sum_{k=1}^{n} \mathbf{v}_k^{(i)}}{n}$$

$\mathbf{v}_r = \bar{\mathbf{v}} + \rho(\bar{\mathbf{v}} - \mathbf{v}_{n+1}^{(i)})$ (*reflection*)

if $J(\mathbf{v}_r) < J(\mathbf{v}_1^{(i)})$ **then**

  $\mathbf{v}_e = \mathbf{v}_r + \chi(\mathbf{v}_r - \bar{\mathbf{v}})$ (*expansion*)

  if $J(\mathbf{v}_e < J(\mathbf{v}_r))$ **then**

    $\mathbf{v}_{n+1}^{(i+1)} = \mathbf{v}_e$ (*accept expansion point*)

  else

    $\mathbf{v}_{n+1}^{(i+1)} = \mathbf{v}_r$ (*accept reflection point*)

  end if

else

  if $J(\mathbf{v}_r) < J(\mathbf{v}_n^{(i)})$ **then**

    $\mathbf{v}_{n+1}^{(i+1)} = \mathbf{v}_r$ (*accept reflection point*)

  else

    if $J(\mathbf{v}_r) < J(\mathbf{v}_{n+1}^{(i+1)})$ **then**

      $\mathbf{v}_{co} = \bar{\mathbf{v}} + \gamma(\mathbf{v}_r - \bar{\mathbf{v}})$ (*outside contraction*)

      if $J(\mathbf{v}_{co}) \leq J(\mathbf{v}_r)$ **then**

        $\mathbf{v}_{n+1}^{(i+1)} = \mathbf{v}_{co}$ (*accept outside contraction point*)

      else

        $\mathbf{v}^{(i+1)} = \mathbf{v}_1^{(i)} + \sigma(\mathbf{v}_j^{(i)} - \mathbf{v}_1^{(i)}), \ j = 2, ..., n+1$ (*shrink*)

      end if

    else

      $\mathbf{v}_{ci} = \bar{\mathbf{v}}^{(i)} - \gamma(\bar{\mathbf{v}} - \mathbf{v}_{n+1}^{(i)})$ (*inside contraction*)

      if $J(\mathbf{v}_{ci}) < J(\mathbf{v}_{n+1}^{(i+1)})$ **then**

        $\mathbf{v}_{n+1}^{(i+1)} = \mathbf{v}_{ci}$ (*accept inside contraction point*)

      else

        $\mathbf{v}^{(i+1)} = \mathbf{v}_1^{(i)} + \sigma(\mathbf{v}_j^{(i)} - \mathbf{v}_1^{(i)}), \ j = 2, ..., n+1$ (*shrink*)

      end if

    end if

  end if

end if

Terminate iteration

transition occurs. This reduces the aggressive plant behaviour during the transient response between steps and produces a response without excessive overshoot.

The simplex method only evaluates the objective function itself and not the gradient of the function. Therefore, SESC is robust to the presence of noise or small variations in the objective function. The disadvantage of SESC is that as the method converges toward the optimum the size of the simplex decreases, effectively reducing the magnitude of the perturbations. As the simplex size decreases, the method maintains the operating points at the same conditions. If the optimum varies the method is unable to react accordingly and adjust the simplex to track the new optimum. Therefore, the method has to be reinitialized to begin tracking the new optimum. The challenge is to identify how often this occurs while reducing the number of disturbances that occur due to the method attempting to find the new optimum. Therefore, the method is primarily suitable for optimizing a static objective function. Although it is not considered in this work, the method can be adapted to implement a fixed or variable simplex size to track a time-varying optimum, referred to as the dynamic simplex method (Xiong & Jutan 2003). This is achieved by enforcing a minimum simplex size to ensure that during run time the step size is always sufficiently large to disturb the process and track the optimum.

An additional aspect to consider for SESC is the tuning parameters of the simplex algorithm. For example, if the step size for the mill load is large and the settling time (T_s) is chosen to be sufficiently long, the mill could be unintentionally driven towards an unstable operating condition if a supervisory controller is not implemented. For example, if a high mill load setpoint is assigned by the SESC, the mill can begin to overfill and would need to be manually emptied to resume operation.

4.5 STATIC ESC EXAMPLE

In this section, the extremum seeking methods are applied to optimize a simple static, two-dimensional objective function to illustrate how the methods converge toward the optimal solution. The two-dimensional function is described by,

$$y(u_1,\, u_2) = -u_1^2 - u_1 - u_2^2 - u_2. \tag{4.9}$$

The surface map of the two-dimensional function is shown in Fig. 4.3. The objective function is to maximize (4.9),

$$J = \max_{(u_1,\, u_2)} y(u_1,\, u_2), \tag{4.10}$$

where the solution to the optimization problem is, $y(u_1^*,\, u_2^*) = 0.5$, $u_1^* = -0.5$ and $u_2^* = -0.5$.

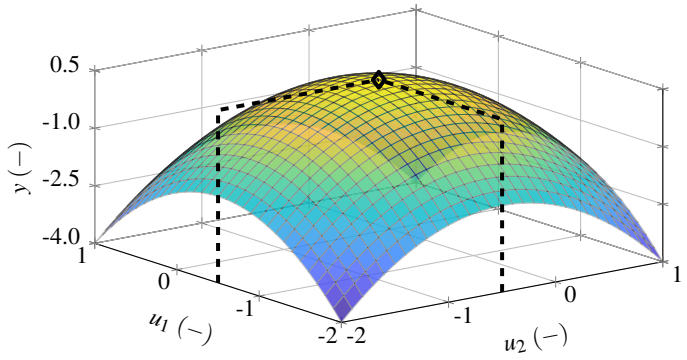

Figure 4.3. 3-D surface map of the optimized function (4.9). The extremum $y(u_1^*,\ u_2^*) = 0.5$ is located at $u_1^* = -0.5$ and $u_2^* = -0.5$.

The tuning parameters for both perturbed inputs of the extremum seeking methods are provided in Table 4.1. The simulations begin with initial conditions, $u_1 = -1$ and $u_2 = 0.5$, where u_1 is lower than u_1^* and u_2 is higher than u_2^*.

4.5.1 Perturbation-based extremum seeking method optimization

The input, output and state trajectories of the perturbation-based extremum seeking method are shown in Figs. 4.4 and 4.5. The ξ state trajectories in Fig. 4.5 indicate the estimated gradient that is driven toward zero to steer the inputs toward their optimal values and maximize the measured objective

Table 4.1. Static objective function ESC tuning parameters.

Method	Variable	Tuning parameter values	Results
PESC	u_1	$k = 10,\ a = 0.2,\ \omega_h = 8$ rad/s, $\omega = 10$ rad/s, $\omega_l = 0.5$ rad/s	Figs. 4.4 and 4.5
	u_2	$k = 10,\ a = 0.2,\ \omega_h = 4$ rad/s, $\omega = 5$ rad/s, $\omega_l = 0.5$ rad/s	
TESC	u_1	$k_T = 10,\ k_{\eta_1} = 5,\ k_{\eta_2} = 2,\ \sigma = 1 \times 10^{-8},\ z_\theta = 0.1,$ $a = 0.01,\ \omega = 5$ rad/s, $k = 2$	Figs. 4.6 and 4.7
	u_2	$k_T = 10,\ k_{\eta_1} = 5,\ k_{\eta_2} = 2,\ \sigma = 1 \times 10^{-8},\ z_\theta = 0.1,$ $a = 0.01,\ \omega = 2$ rad/s, $k = 2$	
SESC	u_1	$\rho = 1, \chi = 2, \gamma = 0.5, \sigma = 0.5$	Figs. 4.8 and 4.9
	u_2	$\rho = 1, \chi = 2, \gamma = 0.5, \sigma = 0.5$	

function. As u_1 is initially lower than u_1^* a positive gradient trajectory is seen for ξ_1, whereas, u_2 is initially higher than u_2^*, and therefore, a negative gradient trajectory is seen in ξ_2. The average component of the perturbed output is shown in the η state trajectories, which can be seen by comparing the state trajectories to the output trajectory (y) in Fig. 4.4. Both perturbed inputs (u_1 and u_2) converge and oscillate about their optimal values and it is important that both inputs are perturbed at different frequencies. As PESC converges toward the neighbourhood of the optimum value, the perturbations from the inputs begins to decay although the amplitude of the perturbations remain the same and achieving a near steady-state output.

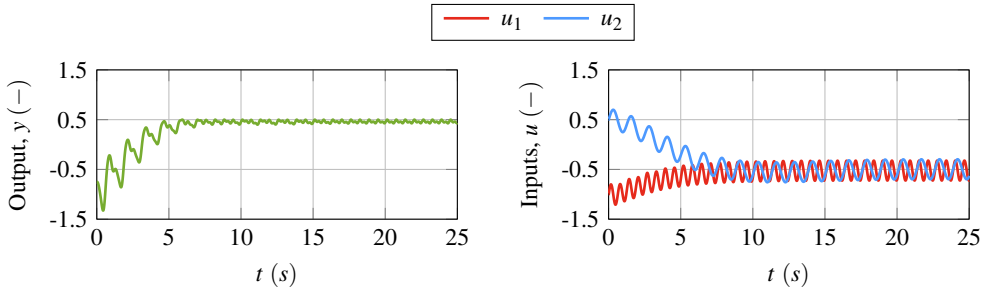

Figure 4.4. PESC input and output trajectories.

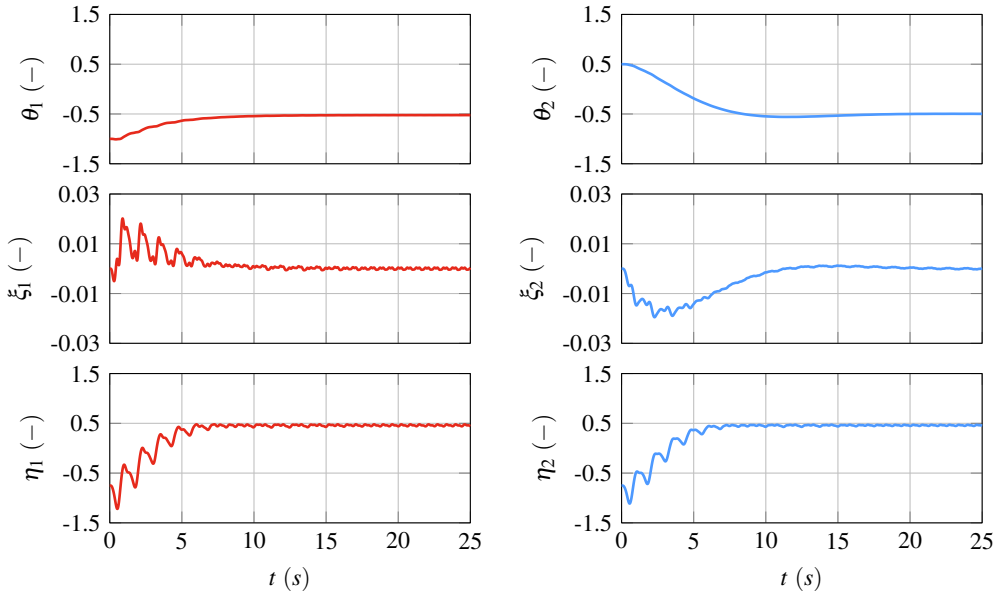

Figure 4.5. PESC state trajectories.

4.5.2 Time-varying parameter estimation extremum seeking method optimization

The input, output and state trajectories of the time-varying parameter estimation extremum seeking method are shown in Figs. 4.6 and 4.7. The advantage of TESC is that a much lower perturbation amplitude can be used to achieve a comparable (or faster) convergence rate than with PESC. The

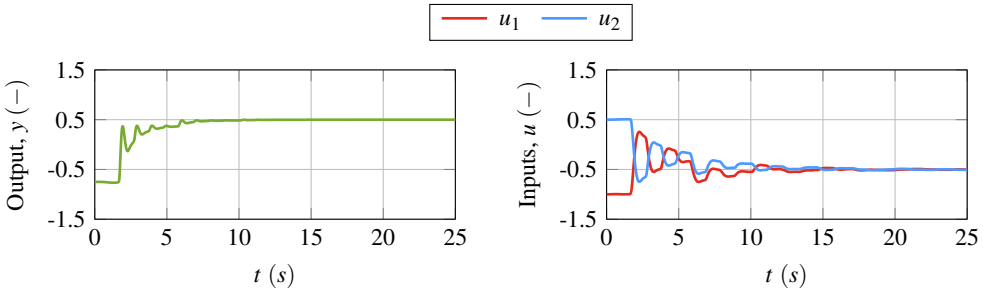

Figure 4.6. TESC input and output trajectories.

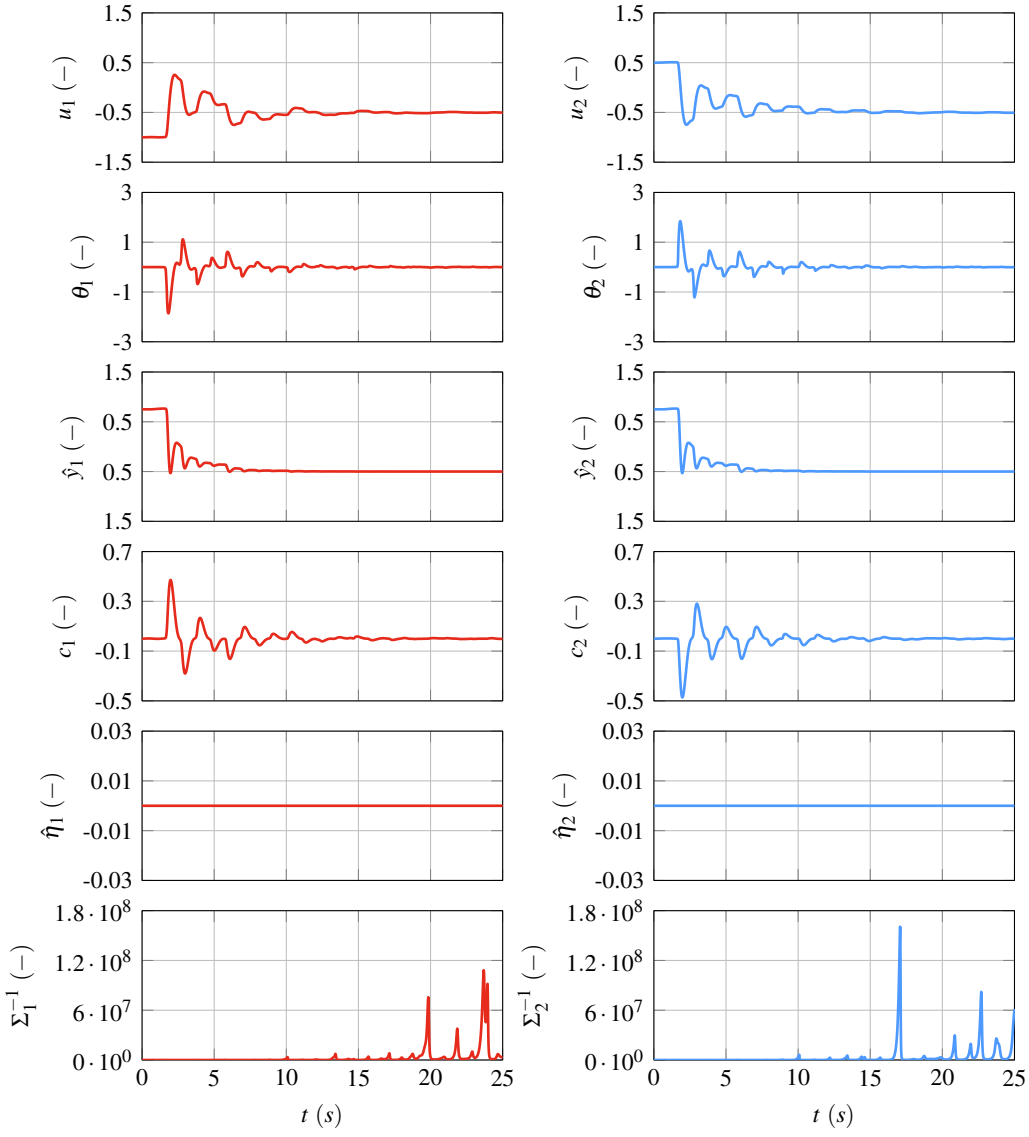

Figure 4.7. TESC state trajectories.

magnitude of the perturbation amplitude used for TESC is an order of magnitude smaller than with PESC. Furthermore, as the perturbed inputs converge toward the optimum, the oscillations from the

perturbations are attenuated. The output (y) is at steady-state for $t > 11$ seconds, as seen in Fig. 4.6. The θ state trajectories in Fig. 4.7 indicate the estimated gradient that is driven toward zero to steer the inputs toward their optimal values and maximize the measured objective function. The trajectories of $\hat{y}$ shows the predicted output (although negative) which is identical to the actual output (y) in Fig. 4.6 since the estimation error trajectories ($\hat{\eta}$) are near zero. The near steady-state output is achieved due to the components of the prediction model ($\hat{y}$, c, $\hat{\eta}$ and Σ). Σ^{-1} can be interpreted as a variable that tracks the level of confidence of the prediction model and shows if the inputs are near their optimal values. Therefore, perturbations with large amplitudes are not required to extract gradient information. Instead, the estimation routine periodically resets, which is seen in the state trajectories of Σ^{-1}. Similarly, since TESC is a gradient-based method, both inputs should be perturbed at different frequencies to achieve effective extremum seeking optimization.

4.5.3 Simplex-based extremum seeking method optimization

The input and output trajectories for SESC are shown in Fig. 4.8. Fig. 4.9 illustrates how the vertices of the simplex converge toward the optimal solution. The advantage of SESC is that the inputs are not continuously perturbed as in the gradient-based methods. Instead, the objective function is repeatedly evaluated at different input values and used to obtain the input-output information. Each function evaluation is ranked and used to steer the inputs toward their optimal values. At each iteration, the vertices of the simplex converge toward the optimal values if the consecutive objective function

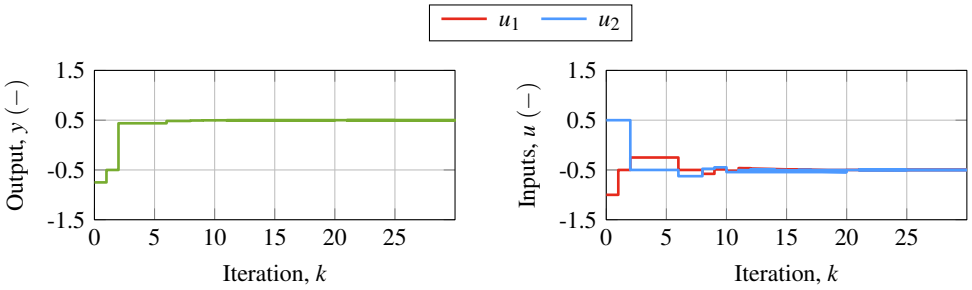

Figure 4.8. SESC input and output trajectories.

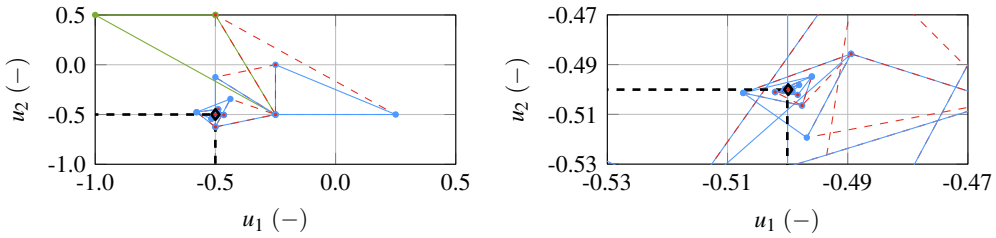

Figure 4.9. SESC input evolution.

evaluation is better than the previous one. This is illustrated by the shrinking simplex in Fig. 4.9. However, the simplex can also expand or reflect if the algorithm results in input values that are away from the optimal values.

4.6 CHAPTER SUMMARY

Three model-free, extremum seeking optimization methods are presented in this chapter: a classical perturbation-based method and a time-varying parameter estimation method, which are gradient-based, and a non-gradient based Nelder-Mead simplex method. These extremum seeking methods only use the available measured information to steer the objective function toward a maximum (or minimum).

The progression of the ESC methods from sub-optimal conditions to optimal conditions is illustrated with an example of the extremum seeking methods applied to optimize a static, two-dimensional objective function.

CHAPTER 5 OPTIMIZING A SINGLE-STAGE OPEN GRINDING MILL CIRCUIT

5.1 CHAPTER OVERVIEW

In this chapter, the model of the open grinding mill circuit described in Section 3.2 of Chapter 3 is simulated and optimized with the extremum seeking methods described in Chapter 4. Several optimization strategies are simulated to improve the grinding mill performance. The performance trajectories of the extremum seeking controlled grinding mill circuit are shown along the surface map of the measured grind curve data. The values of the parameters used for simulating the grinding mill model are provided in Table 5.1.

5.2 SIMULATIONS

5.2.1 Setup

The simulation environment is depicted in Fig. 5.1 and is summarized as follows:

- A sampling period of 60 seconds is used for the simulations.
- White Gaussian noise with a noise level of -10 dB is added to the output Q_{mso}, and a noise level of -50 dB is added to the outputs y_{ψ_m} and y_{J_T} to evaluate the performance of the ESCs subject to measurement noise.
- A PI controller is used to regulate the mill discharge water to solids ratio at $y_{\beta_{ws,sp}} = 0.9$ by manipulating u_{MFW}.
- The ESCs are restricted to explore in a region defined by the grind curves, $y_{J_T} \in [0.20, 0.45]$ and $u_{\phi_c} \in [0.60, 0.75]$ by enforcing hard constraints on both y_{J_T} and u_{ϕ_c}.
- If the ESC optimizes the mill performance by manipulating $y_{J_{T,sp}}$, the ESC perturbations are added to $y_{J_{T,sp}}$ and a PI controller is used to control y_{J_T} to setpoint by manipulating u_{MFO}. In comparison, the ESC can directly perturb u_{ϕ_c}. The configuration in Fig. 5.1 illustrates that

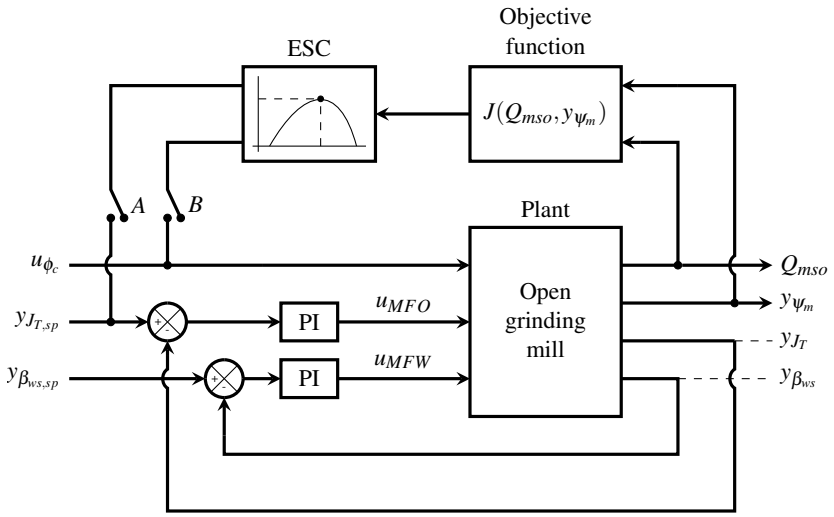

Figure 5.1. Control system diagram of the open grinding mill circuit optimized with ESC.

either $y_{J_{T,sp}}$ or u_{ϕ_c} can be separately manipulated while the other variable is kept constant, or the ESC can simultaneously manipulate both to steer the grinding mill. If either of the manipulated variables are disconnected from the ESC by opening switch A or B in Fig. 5.1, they are set to a constant value.

Table 5.1. Open grinding mill model parameter values.

Variable	Value	Unit	Description
α_f	0.1	$(-)$	Fraction of fines in u_o
α_r	0.5	$(-)$	Fraction of rocks in u_o
ρ_o	2.7	$(\mathrm{t/m^3})$	Ore density
d_q	36.4	$(1/\mathrm{h})$	Discharge rate constant
x_b	16.4	$(\mathrm{m^3})$	Volumetric filling of balls in mill
V_{mill}	208	$(\mathrm{m^3})$	Total mill volume
δ_v	0.923	$(-)$	Power change parameter for the volume of mill filled
δ_s	0.923	$(-)$	Power change parameter for volume fraction of solids in the slurry
φ_N	0.509	$(-)$	Rheology normalization factor
ε_0	0.6	$(-)$	Maximum fraction of solids by volume of slurry at zero slurry flow

5.2.2 Dynamic step response

A stepped sweep response of the open grinding mill circuit model is shown in Fig. 5.2(a). The 3-D surface maps of Q_{mso}, y_{ψ_m} and y_{P_m} are obtained by sweeping $y_{J_{T,sp}}$ over the range $y_{J_{T,sp}} \in [0.20,\ 0.45]$ and u_{ϕ_c} over the range $u_{\phi_c} \in [0.60,\ 0.75]$, with initial conditions $(y_{J_{T,sp}},\ u_{\phi_c}) = (0.20,\ 0.75)$. The discharged solids to water ratio is controlled to setpoint, $y_{\beta_{ws,sp}} = 0.9$.

The grind curves measured at the industrial circuit (van der Westhuizen & Powell 2006) in Fig. 5.2(b) compare well to the simulated grind curves in Fig. 5.2(a). There is a good correlation in the maps for Q_{mso} and y_{P_m}. However, because the model extrapolates the peak positions for y_{ψ_m} at low u_{ϕ_c} past the observed industrial grind curve data, the surface map of the modelled y_{ψ_m} in Fig. 5.2(a) differs slightly from the surface map for y_{ψ_m} in Fig. 5.2(b).

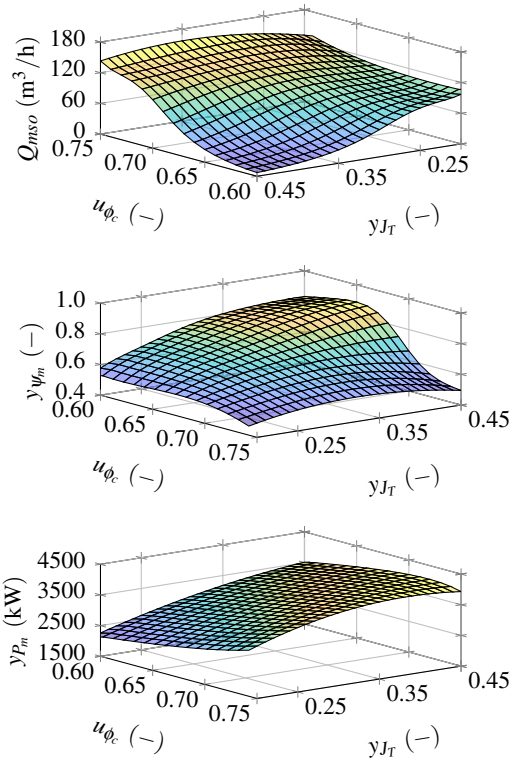

(a) Open grinding mill circuit model response.

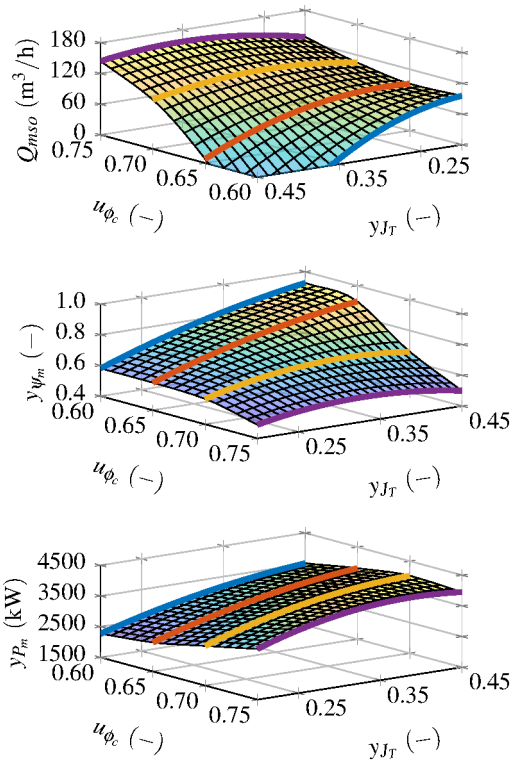

(b) Measured grind curve surface maps (Fig. 2.5(b)).

Figure 5.2. The 3-D surface map of the open grinding mill circuit model dynamic step response compared to the measured industrial circuit data.

5.3 OPTIMIZATION

5.3.1 Objective function

The configuration of the open grinding mill circuit with ESC is illustrated by the block diagram in Fig. 5.1. The objective function for the ESC is to maximize the performance indicators (throughput or grind) using the measured mill outputs,

$$J(Q_{mso},\, y_{\psi_m}) = Q_{mso} \text{ (throughput optimization)}, \tag{5.1a}$$

$$J(Q_{mso},\, y_{\psi_m}) = y_{\psi_m} \quad \text{(grind optimization)}. \tag{5.1b}$$

For the simulation scenario described in Section 5.3.5.1, the objective function consists of a combined weighted contribution between the measured throughput and grind.

There is no formal or systematic approach followed to tune the ESCs to achieve a desired performance criteria. Each of the ESCs were tuned through trial and error to achieve a reasonable balance between the ESC performance indicators discussed in Chapter 4. Specific attention was paid to achieving good transient performance and convergence speed, taking into consideration the process dynamics.

5.3.2 Convergence criteria

The performance of the various ESC algorithms is evaluated and compared according to their convergence rate. The ESC criteria for convergence is chosen as the time it takes for the ESC to reach and settle within a 2% threshold of the final mean value of the objective function. The simulated results are post-processed with a moving average filter with a window size of 20 samples to smoothen the effects of noise. The final mean value is determined by averaging the objective function over the last 5 hour period of the simulation scenario. The earliest instance for which J remains within the 2% threshold

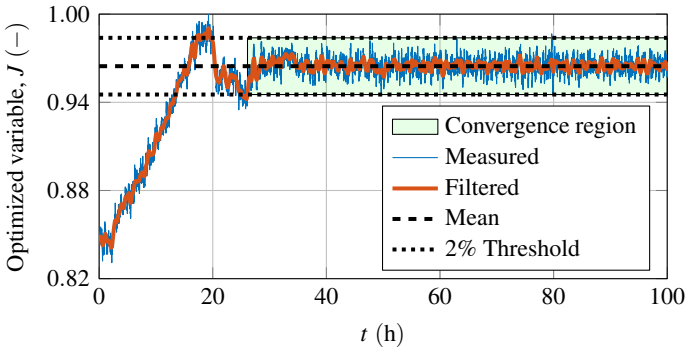

Figure 5.3. Illustration of the convergence criteria.

from the start of the simulation is taken as the convergence rate of the ESC method. The convergence criteria is illustrated in Fig. 5.3.

5.3.3 Effects of noise and disturbances

This section aims to demonstrate the influence of measurement noise and disturbances on the ESC that is common to industrial environments. The results are shown in Figs. 5.4–5.6 and the ESC methods are compared to each other without measurement noise in Fig. 5.7. The ESC tuning parameters used are given in Table 5.2 and the convergence results are summarized in Table 5.3. Once the ESCs have reached the neighbourhood of the optimum, it is important that the ESCs maintain the process near the optimum if the optimum is time-varying, or if the process is subject to disturbances. For simplicity, the rotational speed of the mill (u_{ϕ_c}) is used as a disturbance variable to mimic the effects of varying feed ore hardness. The mill speed is stepped from $u_{\phi_c} = 0.70$ to $u_{\phi_c} = 0.66$ over a 5 hour period, which results in a new maximum throughput to be achieved at a new mill load value.

Figs. 5.4–5.6 show that the ESCs do not stray far from the ideal case and converge toward a neighbourhood near the optimal operating conditions if all three ESCs are adequately tuned. If the noise is random, the ESCs do on average converge with a similar trajectory as the ideal case. However, in certain cases, if the noise is correlated to the measured objective functions, it can for a period deviate in the direction of the noise as seen in Fig. 5.4. When searching along y_{J_T} at $u_{\phi_c} = 0.70$, the grind curves plateau and range between $Q_{mso} \in [120.23, 120.74]$ m^3/h for $y_{J_T} \in [0.28, 0.33]$ as seen in Fig. 2.5(b). There is minimal gradient change in the objective function and the direction of the ESC is influenced by the noise, hence, the variation observed in y_{J_T} within this range. Therefore, it could be attributed to the effects of noise that PESC manipulates the mill load between $y_{J_T} \in (0.26, 0.29)$ for $t = 150$ h due to the measured change in Q_{mso} as a result of the additive noise. For SESC, the

Table 5.2. SISO throughput (Q_{mso}) ESC tuning parameters for disturbance simulations.

Method	Variable	Tuning parameter values	Results
PESC	$y_{J_{T,sp}}$	$k = 25$, $a = 0.002$, $\omega_h = 1.8$ rad/h, $\omega = 2$ rad/h, $\omega_l = 0.1$ rad/h	Figs. 5.4 and 5.7
TESC	$y_{J_{T,sp}}$	$k_T = 2$, $k_{\eta_1} = 0.25$, $k_{\eta_2} = 0.25$, $\sigma = 0.001$, $z_\theta = 1$, $a = 0.0005$, $\omega = 0.5$ rad/h, $k = 0.01$	Figs. 5.5 and 5.7
SESC	$y_{J_{T,sp}}$	$\rho = 0.75$, $\chi = 2$, $\gamma = 0.5$, $\sigma = 0.5$, $T_s = 2$ h	Figs. 5.6 and 5.7

effects of noise are indistinguishable relative to the ideal case as both scenarios produce near identical trajectories (Fig. 5.6). On the other hand, there is an improved performance in TESC for the chosen tuning parameters as there is reduced variation in y_{J_T} in the presence of noise compared to the ideal case once the method is within the neighbourhood of the optimum (Fig. 5.5).

The ESCs could be better tuned to alleviate the issue due to noise, but this would usually be at the cost of transient performance or a trade-off in the operational objectives. For example, the amplitude of the dither signal in PESC and TESC could be chosen to be significantly larger than the noise level, producing a distinct separation between the noise and the perturbations. However, the increased amplitude of the dither signal would produce a larger undesired perturbation in the measured outputs.

To demonstrate the ESCs response subject to disturbances, the noise is removed for the simulations shown in Fig. 5.7. SESC manipulates $y_{J_{T,sp}}$ up to $t = 25$ h hours, after which the ESC has converged toward the peak of $Q_{mso} = 120.4$ m^3/h for $u_{\phi_c} = 0.70$. At $t = 100$ hours, the mill speed is stepped to $u_{\phi_c} = 0.66$. SESC maintains the same mill load setpoint and the throughput achieved is $Q_{mso} = 92.3$ m^3/h, whereas, PESC and TESC both begin to track the new extremum for $u_{\phi_c} = 0.66$ and reach a higher throughput at the new operating conditions. Therefore, if the feed-ore is varying, SESC will tend to drift away from the optimal operating region. The nature of the SESC method relies on adapting a simplex to converge toward the extremum. However, as the method converges, the vertices converge to the same values and any operation, such as reflection, expansion, contraction or shrinkage, has no significant effect to disturb the process sufficiently to locate the new extremum. Therefore, the method fails to track a time-varying extremum. However, this can be prevented by enforcing a minimum simplex size to allow the process to continuously be disturbed and track a time-varying extremum.

PESC and TESC both respond to the disturbance, however, TESC has a delayed response of approximately 40 hours with the chosen tuning parameters. Furthermore, TESC appears to periodically reset its optimization routine as can be seen in Fig. 5.7, which is not as obvious as in the simulations with noise (Fig. 5.5).

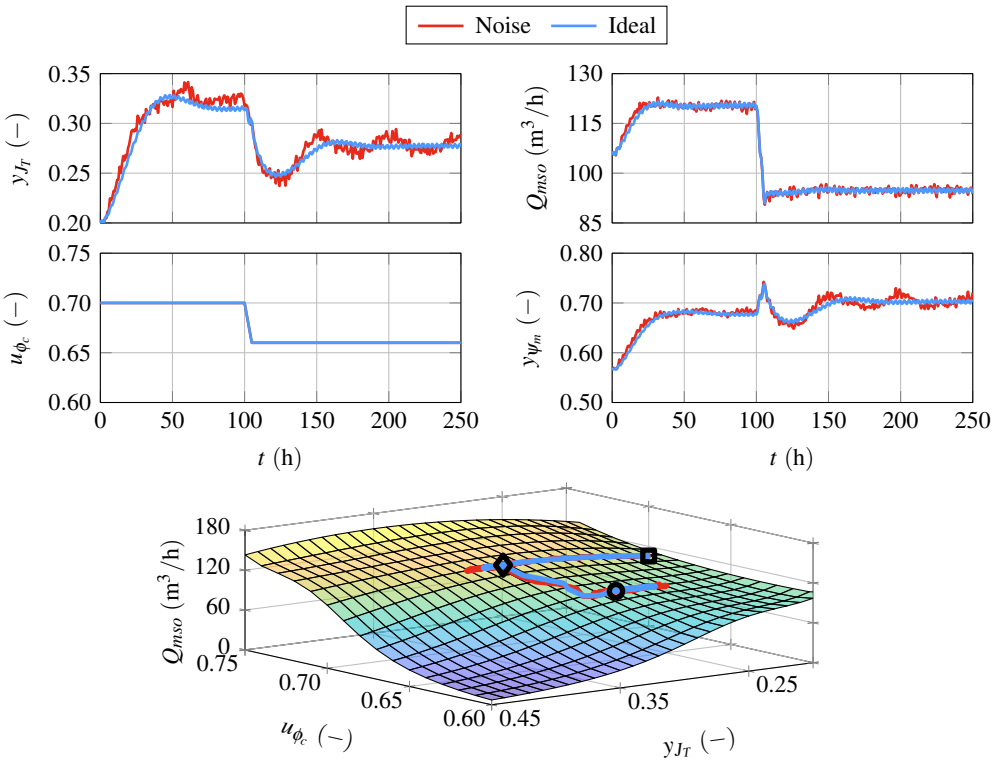

Figure 5.4. PESC throughput (Q_{mso}) optimization with a disturbance. The initial conditions are indicated by the □, the disturbance at $t = 100$ h is indicated by the ♢ and the final time conditions are indicated by the ○.

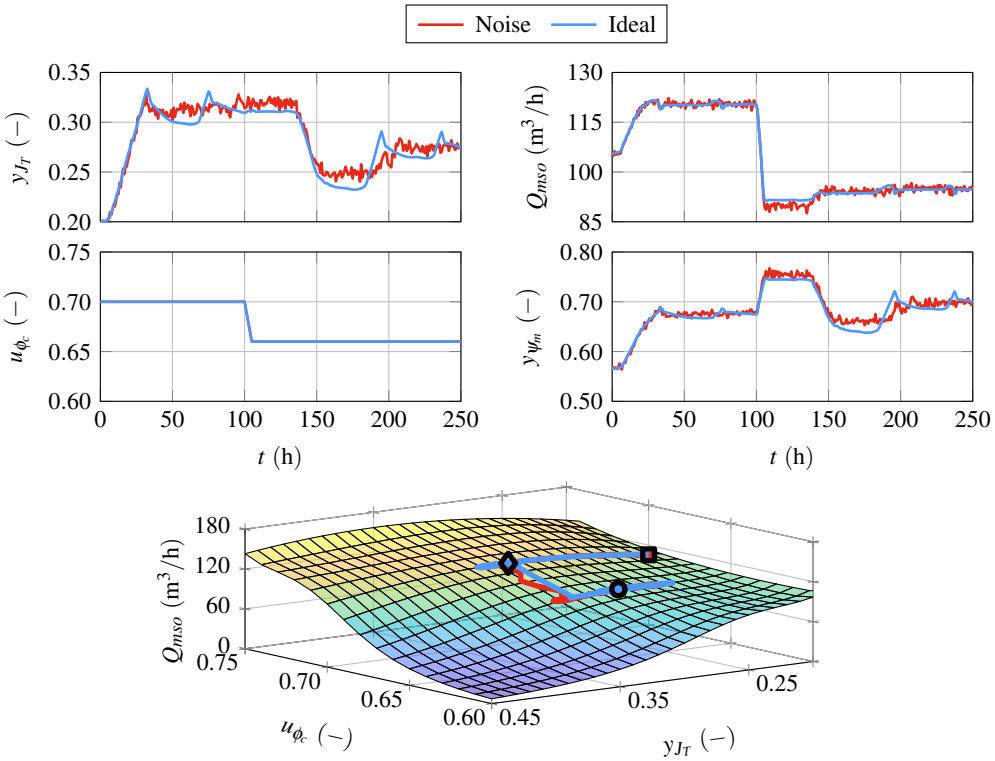

Figure 5.5. TESC throughput (Q_{mso}) optimization with a disturbance. The initial conditions are indicated by the □, the disturbance at $t = 100$ h is indicated by the ♢ and the final time conditions are indicated by the ○.

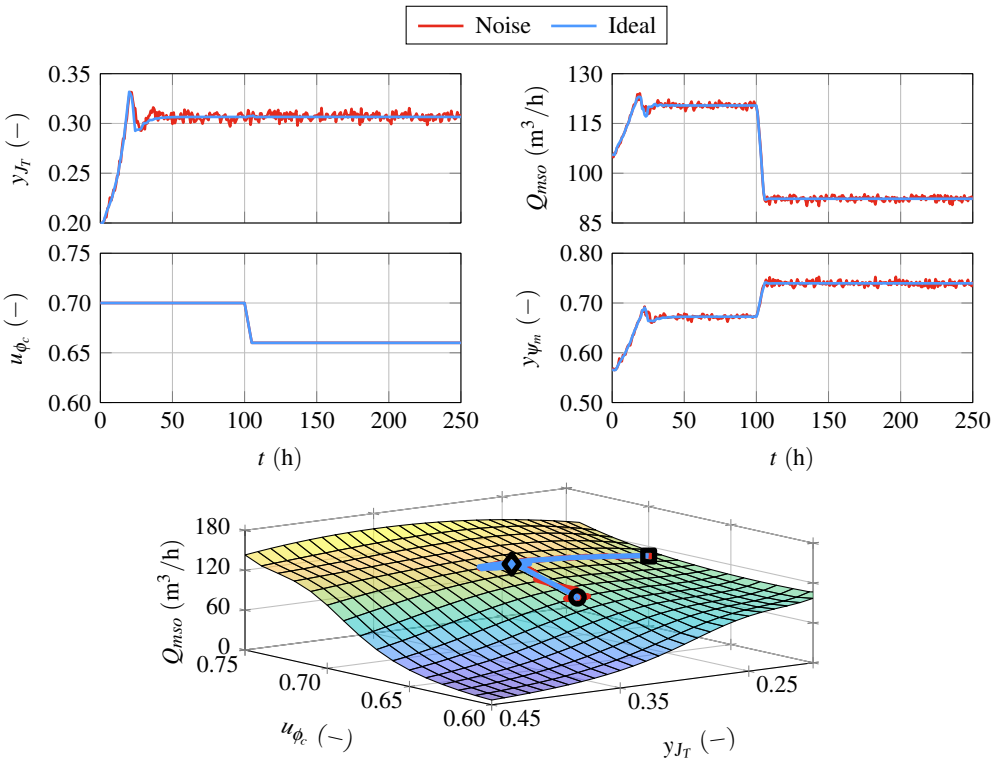

Figure 5.6. SESC throughput (Q_{mso}) optimization with a disturbance. The initial conditions are indicated by the □, the disturbance at $t = 100$ h is indicated by the ♢ and the final time conditions are indicated by the ○.

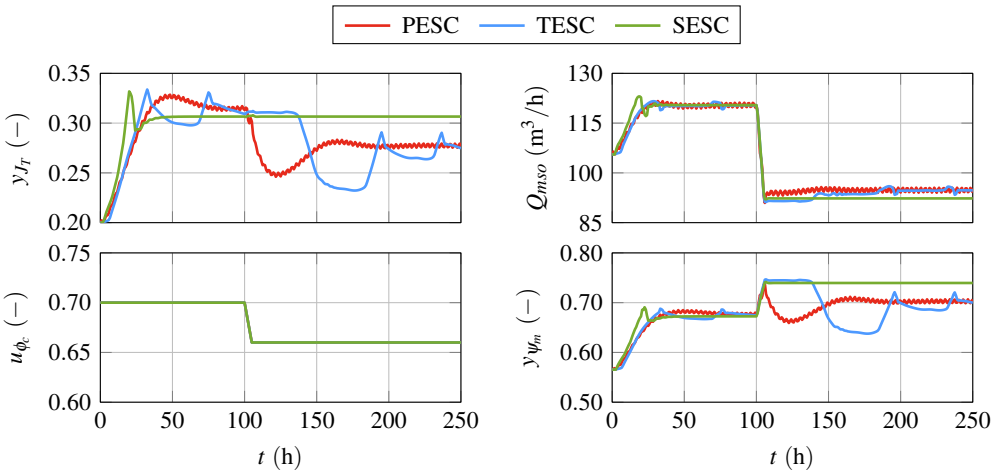

Figure 5.7. ESC Comparison of throughput (Q_{mso}) optimization with disturbance and without measurement noise.

Table 5.3. Throughput (Q_{mso}) optimization results with and without noise for disturbance simulations. $\overline{Q}^1_{mso}$ indicates the average peak reached with $y_{J_{T,sp}}$ before the disturbance and $\overline{Q}^2_{mso}$ indicates the final average peak reached with $y_{J_{T,sp}}$ after the disturbance.

Convergence results without measurement noise			
Method	Average value	Convergence rate	Results
PESC	$\overline{Q}^1_{mso} = 120.34\ \mathrm{m^3/h}$	$t = 21.2$ h	Figs. 5.4 and 5.7
	$\overline{y}^1_{J_{T,sp}} = 0.31\ (-)$		
	$\overline{Q}^2_{mso} = 94.91\ \mathrm{m^3/h}$	$t = 6.4$ h	
	$\overline{y}^2_{J_{T,sp}} = 0.28\ (-)$		
TESC	$\overline{Q}^1_{mso} = 120.37\ \mathrm{m^3/h}$	$t = 18.0$ h	Figs. 5.5 and 5.7
	$\overline{y}^1_{J_{T,sp}} = 0.31\ (-)$		
	$\overline{Q}^2_{mso} = 95.38\ \mathrm{m^3/h}$	$t = 107.2$ h	
	$\overline{y}^2_{J_{T,sp}} = 0.28\ (-)$		
SESC	$\overline{Q}^1_{mso} = 120.42\ \mathrm{m^3/h}$	$t = 24.3$ h	Figs. 5.6 and 5.7
	$\overline{y}^1_{J_{T,sp}} = 0.31\ (-)$		
	$\overline{Q}^2_{mso} = 92.31\ \mathrm{m^3/h}$	$t = 5.0$ h	
	$\overline{y}^2_{J_{T,sp}} = 0.31\ (-)$		
Convergence results with measurement noise			
Method	Average value	Convergence rate	Results
PESC	$\overline{Q}^1_{mso} = 120.07\ \mathrm{m^3/h}$	$t = 17.0$ h	Fig. 5.4
	$\overline{y}^1_{J_{T,sp}} = 0.32\ (-)$		
	$\overline{Q}^2_{mso} = 95.02\ \mathrm{m^3/h}$	$t = 30.7$ h	
	$\overline{y}^2_{J_{T,sp}} = 0.29\ (-)$		
TESC	$\overline{Q}^1_{mso} = 120.05\ \mathrm{m^3/h}$	$t = 18.1$ h	Fig. 5.5
	$\overline{y}^1_{J_{T,sp}} = 0.32\ (-)$		
	$\overline{Q}^2_{mso} = 94.82\ \mathrm{m^3/h}$	$t = 52.2$ h	
	$\overline{y}^2_{J_{T,sp}} = 0.27\ (-)$		
SESC	$\overline{Q}^1_{mso} = 120.38\ \mathrm{m^3/h}$	$t = 26.4$ h	Fig. 5.6
	$\overline{y}^1_{J_{T,sp}} = 0.31\ (-)$		
	$\overline{Q}^2_{mso} = 92.35\ \mathrm{m^3/h}$	$t = 5.0$ h	
	$\overline{y}^2_{J_{T,sp}} = 0.31\ (-)$		

5.3.4 Single plant output optimization

In single-output optimization, only one plant output is optimized by the ESC and the other output is left uncontrolled. The results are shown in Figs. 5.8–5.11. The convergence results and tuning parameters used are summarized in Tables 5.4–5.11.

5.3.4.1 ESC perturbing a single variable (SISO)

In this section, either $y_{J_{T,sp}}$ or u_{ϕ_c} is individually manipulated to optimize Q_{mso} or y_{ψ_m}. It is assumed that switch A or B, as shown in Fig. 5.1, is closed by an operator for the purpose of this section. This configuration is referred to as single-input single-output (SISO) optimization. Switch A is closed initially up until such time as $y_{J_{T,sp}}$ does not change anymore, after which B is closed with A open. For throughput optimization (Fig. 5.8) the switchover from A to B happens at $t = 50$ hours, and for grind optimization (Fig. 5.9) at $t = 100$ hours. Since $y_{J_{T,sp}}$ and u_{ϕ_c} are not simultaneously perturbed, the ESCs do not need distinct tuning parameters between $y_{J_{T,sp}}$ or u_{ϕ_c} to distinguish their effects on the direction of the objective function. The results comparing the ESC methods are shown in Figs. 5.8–5.11.

For throughput (Q_{mso}) optimization (Fig. 5.8), for $t \leq 50$ hours the ESCs steer the process toward the optimum by manipulating $y_{J_{T,sp}}$. The ESC then switches to manipulate u_{ϕ_c} for $t > 50$ hours and $y_{J_{T,sp}}$ is maintained at the current best operating point obtained by the ESC. The final value reached for Q_{mso} for each method varies based on the final value of $y_{J_{T,sp}}$ reached before switching from manipulating $y_{J_{T,sp}}$ to u_{ϕ_c}. Therefore, each method may reach different values of Q_{mso} at the final conditions. All three ESC methods tend to follow the same trajectory in tracking the extremum for Q_{mso} along y_{J_T} and then u_{ϕ_c}. SESC makes relatively large steps in comparison to PESC and TESC. However, the large steps cause the method to temporarily oscillate around the neighbourhood of the optimal y_{J_T}. TESC initially has a delay before it begins to converge and manipulate $y_{J_{T,sp}}$ or u_{ϕ_c} as seen in Fig. 5.8.

For grind (y_{ψ_m}) optimisation (Fig. 5.9), for $t \leq 100$ hours the ESCs steer the process toward the optimum by manipulating $y_{J_{T,sp}}$. The ESC then manipulates u_{ϕ_c} for $t > 100$ hours and $y_{J_{T,sp}}$ is maintained at the current best operating point obtained by the ESC. The final value reached for y_{ψ_m} for each method varies based on the final value of $y_{J_{T,sp}}$ reached. The ESCs have a longer convergence time when optimizing y_{ψ_m} compared to Q_{mso} when perturbing u_{ϕ_c}. Furthermore, as the grind approaches $y_{\psi_m} \to 0.80$ when the mill speed approaches $u_{\phi_c} \to 0.60$, the relationship between u_{ϕ_c} and y_{ψ_m} is relatively flat and the extracted gradient information is primarily due to the measurement noise. SESC converges relatively quickly to the y_{ψ_m} peak as it is robust to measurement noise. However, PESC and TESC take longer to

Table 5.4. SISO throughput (Q_{mso}) ESC tuning parameters.

Method	Variable	Tuning parameter values	Results
PESC	$y_{J_{T,sp}}$	$k = 25$, $a = 0.002$, $\omega_h = 1.8$ rad/h, $\omega = 2$ rad/h, $\omega_l = 0.1$ rad/h	Fig. 5.8
	u_{ϕ_c}	$k = 25$, $a = 0.002$, $\omega_h = 1.8$ rad/h, $\omega = 2$ rad/h, $\omega_l = 0.01$ rad/h	
TESC	$y_{J_{T,sp}}$	$k_T = 2$, $k_{\eta_1} = 0.25$, $k_{\eta_2} = 0.25$, $\sigma = 0.001$, $z_\theta = 1$, $a = 0.0005$, $\omega = 0.5$ rad/h, $k = 0.01$	Fig. 5.8
	u_{ϕ_c}	$k_T = 2$, $k_{\eta_1} = 0.25$, $k_{\eta_2} = 0.25$, $\sigma = 0.001$, $z_\theta = 1$, $a = 0.0005$, $\omega = 0.5$ rad/h, $k = 0.01$	
SESC	$y_{J_{T,sp}}$	$\rho = 0.75$, $\chi = 2$, $\gamma = 0.6$, $\sigma = 0.6$, $T_s = 2$ h	Fig. 5.8
	u_{ϕ_c}	$\rho = 0.75$, $\chi = 2$, $\gamma = 0.6$, $\sigma = 0.6$, $T_s = 2$ h	

Table 5.5. SISO grind (y_{ψ_m}) ESC tuning parameters.

Method	Variable	Tuning parameter values	Results
PESC	$y_{J_{T,sp}}$	$k = 4000$, $a = 0.002$, $\omega_h = 1.8$ rad/h, $\omega = 2$ rad/h, $\omega_l = 0.1$ rad/h	Fig. 5.9
	u_{ϕ_c}	$k = 2000$, $a = 0.001$, $\omega_h = 1.8$ rad/h, $\omega = 2$ rad/h, $\omega_l = 0.1$ rad/h	
TESC	$y_{J_{T,sp}}$	$k_T = 3$, $k_{\eta_1} = 0.25$, $k_{\eta_2} = 0.25$, $\sigma = 1e-05$, $z_\theta = 1$, $a = 0.001$, $\omega = 1$ rad/h, $k = 0.01$	Fig. 5.9
	u_{ϕ_c}	$k_T = 2$, $k_{\eta_1} = 0.5$, $k_{\eta_2} = 0.5$, $\sigma = 1e-05$, $z_\theta = 1$, $a = 0.001$, $\omega = 1$ rad/h, $k = 0.01$	
SESC	$y_{J_{T,sp}}$	$\rho = 0.6$, $\chi = 2$, $\gamma = 0.6$, $\sigma = 0.6$, $T_s = 4$ h	Fig. 5.9
	u_{ϕ_c}	$\rho = 0.6$, $\chi = 2$, $\gamma = 0.6$, $\sigma = 0.6$, $T_s = 4$ h	

converge, which can be attributed to the effects of noise as there is an insignificant gradient change between y_{ψ_m} and u_{ϕ_c}. If u_{ϕ_c} is fixed, each ESC method converges to relatively similar operating conditions to optimize Q_{mso} or y_{ψ_m} as shown in Tables 5.6 and 5.7.

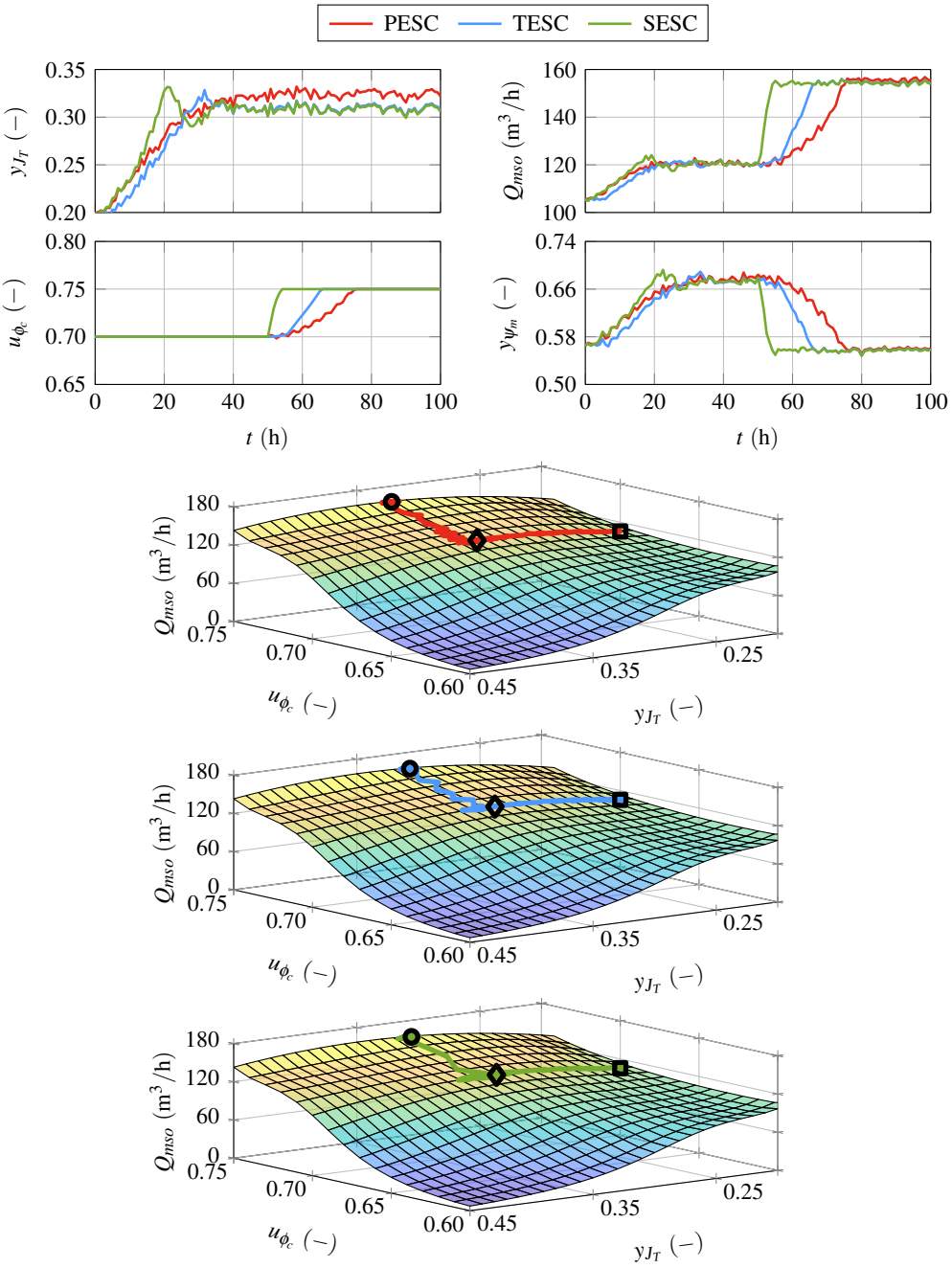

Figure 5.8. Comparison of SISO throughput (Q_{mso}) optimization with $y_{J_{T,sp}}$ for $t \leq 50$ hours and with u_{ϕ_c} for $t > 50$ hours. The initial conditions are indicated by $\square$, the switchover occurring at $t = 50$ h is indicated by $\diamondsuit$, and the final time conditions are indicated by $\bigcirc$.

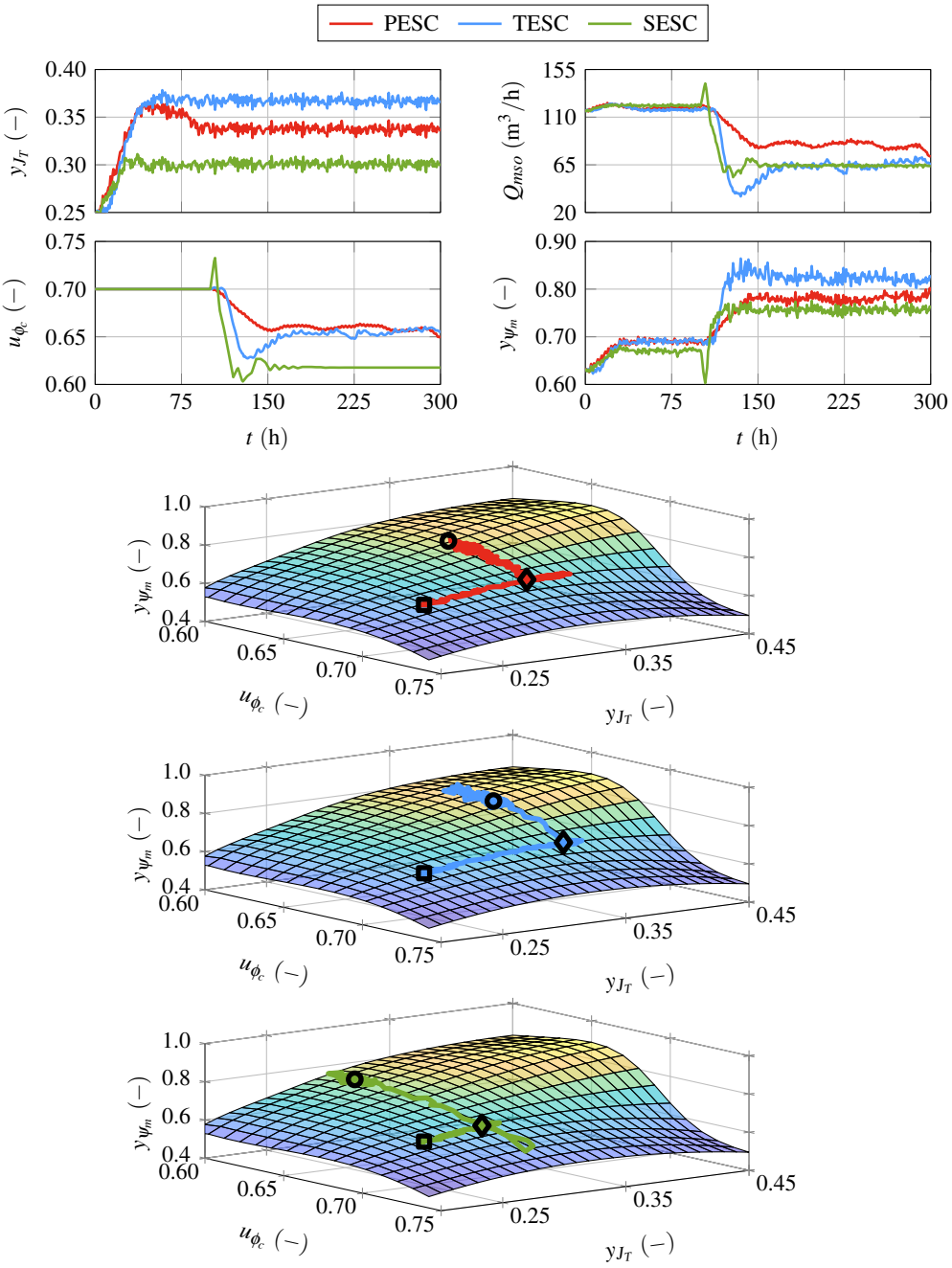

Figure 5.9. Comparison of SISO grind (y_{ψ_m}) optimization with $y_{J_{T,sp}}$ for $t \leq 100$ hours and with u_{ϕ_c} for $t > 100$ hours. The initial conditions are indicated by □, the switchover occurring at $t = 50$ h is indicated by ◇, and the final time conditions are indicated by ○.

Table 5.6. SISO throughput (Q_{mso}) optimization results. $\overline{Q}^1_{mso}$ indicates the average peak reached with $y_{J_{T,sp}}$ and $\overline{Q}^2_{mso}$ indicates the average peak reached with u_{ϕ_c}.

Method	Average value	Convergence rate	Results
PESC	$\overline{Q}^1_{mso} = 120.31\ \mathrm{m}^3/\mathrm{h}$	$t = 18.0$ h	Fig. 5.8
	$\bar{y}^1_{J_{T,sp}} = 0.32\ (-)$		
	$\overline{Q}^2_{mso} = 155.62\ \mathrm{m}^3/\mathrm{h}$	$t = 14.3$ h	
	$\bar{u}^2_{\phi_c} = 0.75\ (-)$		
TESC	$\overline{Q}^1_{mso} = 120.47\ \mathrm{m}^3/\mathrm{h}$	$t = 19.0$ h	Fig. 5.8
	$\bar{y}^1_{J_{T,sp}} = 0.31\ (-)$		
	$\overline{Q}^2_{mso} = 154.38\ \mathrm{m}^3/\mathrm{h}$	$t = 15.1$ h	
	$\bar{u}^2_{\phi_c} = 0.75\ (-)$		
SESC	$\overline{Q}^1_{mso} = 120.48\ \mathrm{m}^3/\mathrm{h}$	$t = 26.2$ h	Fig. 5.8
	$\bar{y}^1_{J_{T,sp}} = 0.31\ (-)$		
	$\overline{Q}^2_{mso} = 154.24\ \mathrm{m}^3/\mathrm{h}$	$t = 3.8$ h	
	$\bar{u}^2_{\phi_c} = 0.75\ (-)$		

Table 5.7. SISO grind (y_{ψ_m}) optimization results. $\bar{y}^1_{\psi_m}$ indicates the average peak reached with $y_{J_{T,sp}}$ and $\bar{y}^2_{\psi_m}$ indicates the average peak reached with u_{ϕ_c}.

Method	Average value	Convergence rate	Results
PESC	$\bar{y}^1_{\psi_m} = 119.96\ (-)$	$t = 22.5$ h	Fig. 5.9
	$\bar{y}^1_{J_{T,sp}} = 0.34\ (-)$		
	$\bar{y}^2_{\psi_m} = 0.79\ (-)$	$t = 184.6$ h	
	$\bar{u}^2_{\phi_c} = 0.65\ (-)$		
TESC	$\bar{y}^1_{\psi_m} = 0.69\ (-)$	$t = 27.3$ h	Fig. 5.9
	$\bar{y}^1_{J_{T,sp}} = 0.37\ (-)$		
	$\bar{y}^2_{\psi_m} = 0.82\ (-)$	$t = 128.2$ h	
	$\bar{u}^2_{\phi_c} = 0.66\ (-)$		
SESC	$\bar{y}^1_{\psi_m} = 0.67\ (-)$	$t = 13.6$ h	Fig. 5.9
	$\bar{y}^1_{J_{T,sp}} = 0.30\ (-)$		
	$\bar{y}^2_{\psi_m} = 0.76\ (-)$	$t = 18.3$ h	
	$\bar{u}^2_{\phi_c} = 0.62\ (-)$		

5.3.4.2 ESC perturbing multiple variables (MISO)

In this section, $y_{J_{T,sp}}$ and u_{ϕ_c} are manipulated together (both switches A and B are closed in Fig. 5.1) to optimize either Q_{mso} or y_{ψ_m}. This configuration is referred to as multiple-input single-output (MISO) optimization.

For throughput (Q_{mso}) optimization (Fig. 5.10), all three ESCs behave relatively similarly and u_{ϕ_c} quickly converges to the maximum mill speed compared to y_{J_T}. There is a strong positive correlation between Q_{mso} and u_{ϕ_c}, where the throughput increases as the mill speed increases. However, the optimal y_{J_T} lies between $y_{J_T} \in [0.20, 0.45]$ for different values of u_{ϕ_c}. Therefore, y_{J_T} takes longer to settle within the neighbourhood of its optimal value.

For grind (y_{ψ_m}) optimization (Fig. 5.11), PESC converges to a different operating condition as compared to TESC and SESC. This is due to the difference in the optimization gains chosen for the tuning parameters for PESC (Table 5.9) and the effects of the hard constraints that prevent the ESC from exploring beyond the bound regions as described in Section 5.2.1. Due to the faster adaptation of u_{ϕ_c} with TESC and SESC, both ESC methods converge to the lower limit of u_{ϕ_c}. The mill speed is set to a constant value of $u_{\phi_c} = 0.60$ to constrain the ESC methods from exploring beyond the bound region. Therefore, TESC and SESC continue to only manipulate y_{J_T} and reach the neighbourhood of the local extremum along the y_{J_T} axis. However, PESC does not converge to any of the limits of u_{ϕ_c} or y_{J_T} and is steered toward the neighbourhood of the global extremum. Further, as the ESCs converge to $u_{\phi_c} \to 0.60$, the model response of y_{ψ_m} at higher values of y_{J_T} begins to flatten. The influence of noise is sufficient to prevent the ESCs from exploring further due to the insignificant increase in the measured y_{ψ_m} along the y_{J_T} axis. In all cases, the ESCs steered the process toward a higher y_{J_T} and lower u_{ϕ_c}, where the y_{ψ_m} peak is likely to be located.

Careful consideration has to be given to the parameters associated with the optimization speed used for each perturbed input. If the tuning parameters are poorly chosen for either of the inputs, the effects of the perturbed input will be negligible on the output relative to the other perturbed input. As a result, the ESC is likely to adapt one of the inputs over the other. For example, similar optimization gain values are used for PESC in the results shown in Fig. 5.10. However, PESC tends to adapt u_{ϕ_c} faster compared to y_{J_T}. The effects of this are not crucial for optimizing the process if there is only a global extremum, but the ESC could instead converge toward a local extremum if there are multiple. The results in Fig. 5.11 demonstrate that the TESC and SESC converge toward the neighbourhood of an

Table 5.8. MISO throughput (Q_{mso}) ESC tuning parameters.

Method	Variable	Tuning parameter values	Results
PESC	$y_{J_{T,sp}}$	$k = 15$, $a = 0.002$, $\omega_h = 1.4$ rad/h, $\omega = 1.6$ rad/h, $\omega_l = 0.05$ rad/h	Fig. 5.10
	u_{ϕ_c}	$k = 20$, $a = 0.002$, $\omega_h = 1.8$ rad/h, $\omega = 2$ rad/h, $\omega_l = 0.1$ rad/h	
TESC	$y_{J_{T,sp}}$	$k_T = 1$, $k_{\eta_1} = 0.25$, $k_{\eta_2} = 0.25$, $\sigma = 0.001$, $z_\theta = 1$, $a = 0.001$, $\omega = 1$ rad/h, $k = 0.01$	Fig. 5.10
	u_{ϕ_c}	$k_T = 2$, $k_{\eta_1} = 0.5$, $k_{\eta_2} = 0.5$, $\sigma = 0.001$, $z_\theta = 1$, $a = 0.001$, $\omega = 0.5$ rad/h, $k = 0.02$	
SESC	$y_{J_{T,sp}}$	$\rho = 0.8$, $\chi = 2$, $\gamma = 0.8$, $\sigma = 0.6$, $T_s = 2$ h	Fig. 5.10
	u_{ϕ_c}	$\rho = 0.8$, $\chi = 2$, $\gamma = 0.8$, $\sigma = 0.6$, $T_s = 2$ h	

unknown peak, but not the global extremum. The initial conditions and the tuning parameters are important to consider when applying ESC to optimize the grinding mill performance, as both these factors influence the convergence trajectory of the ESC.

Table 5.9. MISO grind (y_{ψ_m}) ESC tuning parameters.

Method	Variable	Tuning parameter values	Results
PESC	$y_{J_{T,sp}}$	$k = 2000$, $a = 0.002$, $\omega_h = 1.1$ rad/h, $\omega = 1.6$ rad/h, $\omega_l = 0.05$ rad/h	Fig. 5.11
	u_{ϕ_c}	$k = 500$, $a = 0.002$, $\omega_h = 1.8$ rad/h, $\omega = 2$ rad/h, $\omega_l = 0.1$ rad/h	
TESC	$y_{J_{T,sp}}$	$k_T = 0.75$, $k_{\eta_1} = 0.75$, $k_{\eta_2} = 0.75$, $\sigma = 1e-05$, $z_\theta = 1$, $a = 0.001$, $\omega = 0.5$ rad/h, $k = 0.01$	Fig. 5.11
	u_{ϕ_c}	$k_T = 1$, $k_{\eta_1} = 0.25$, $k_{\eta_2} = 0.25$, $\sigma = 1e-05$, $z_\theta = 1$, $a = 0.001$, $\omega = 1$ rad/h, $k = 0.01$	
SESC	$y_{J_{T,sp}}$	$\rho = 0.8$, $\chi = 2$, $\gamma = 0.5$, $\sigma = 0.5$, $T_s = 4$ h	Fig. 5.11
	u_{ϕ_c}	$\rho = 0.8$, $\chi = 2$, $\gamma = 0.5$, $\sigma = 0.5$, $T_s = 4$ h	

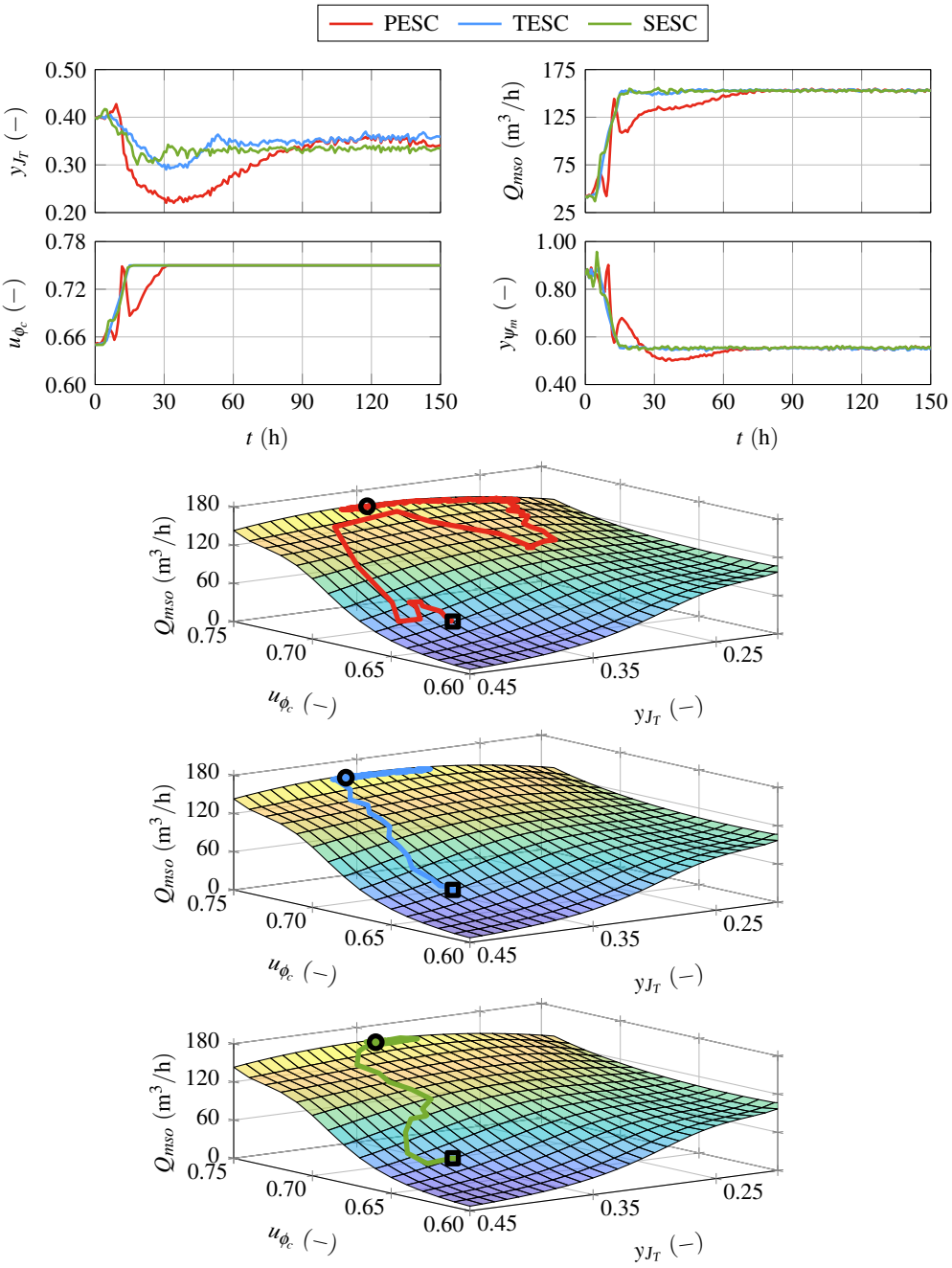

Figure 5.10. Comparison of MISO throughput (Q_{mso}) optimization with both $y_{J_{T,sp}}$ and u_{ϕ_c}. The initial conditions are indicated by □ and the final time conditions are indicated by ○.

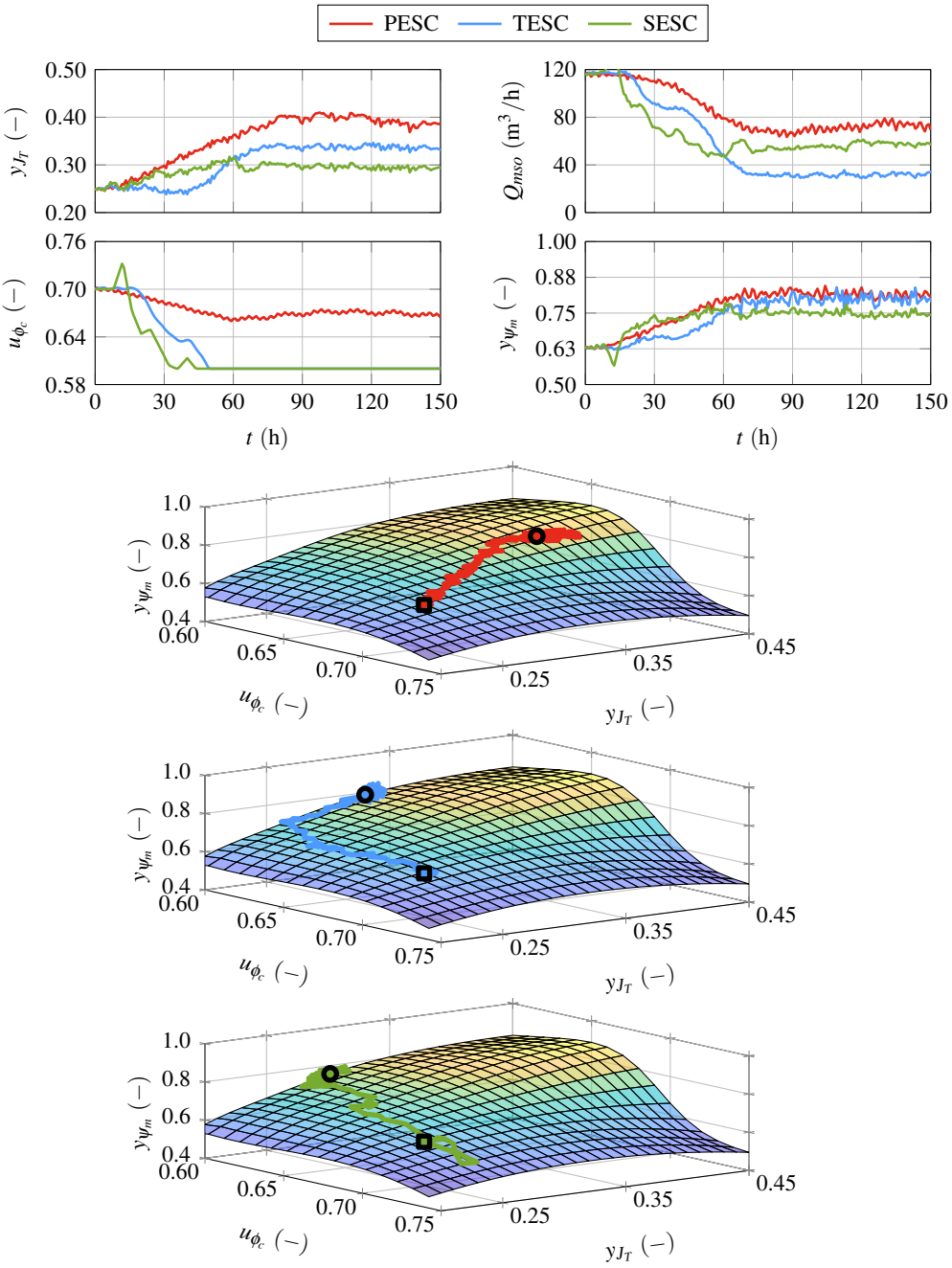

Figure 5.11. Comparison of MISO grind (y_{ψ_m}) optimization with both $y_{J_{T,sp}}$ and u_{ϕ_c}. The initial conditions are indicated by □ and the final time conditions are indicated by ○.

Table 5.10. MISO throughput (Q_{mso}) optimization results.

Method	Average value	Convergence rate	Results
PESC	$\overline{Q}_{mso} = 153.03\ \mathrm{m}^3/\mathrm{h}$	$t = 70.1$ h	Fig. 5.10
	$\bar{y}_{J_{T,sp}} = 0.34\ (-)$		
	$\bar{u}_{\phi_c} = 0.75\ (-)$		
TESC	$\overline{Q}_{mso} = 153.04\ \mathrm{m}^3/\mathrm{h}$	$t = 40.3$ h	Fig. 5.10
	$\bar{y}_{J_{T,sp}} = 0.36\ (-)$		
	$\bar{u}_{\phi_c} = 0.75\ (-)$		
SESC	$\overline{Q}_{mso} = 152.86\ \mathrm{m}^3/\mathrm{h}$	$t = 38.7$ h	Fig. 5.10
	$\bar{y}_{J_{T,sp}} = 0.33\ (-)$		
	$\bar{u}_{\phi_c} = 0.75\ (-)$		

Table 5.11. MISO grind (y_{ψ_m}) optimization results.

Method	Average value	Convergence rate	Results
PESC	$\bar{y}_{\psi_m} = 0.81\ (-)$	$t = 110.4$ h	Fig. 5.11
	$\bar{y}_{J_{T,sp}} = 0.39\ (-)$		
	$\bar{u}_{\phi_c} = 0.67\ (-)$		
TESC	$\bar{y}_{\psi_m} = 0.80\ (-)$	$t = 77.9$ h	Fig. 5.11
	$\bar{y}_{J_{T,sp}} = 0.33\ (-)$		
	$\bar{u}_{\phi_c} = 0.60\ (-)$		
SESC	$\bar{y}_{\psi_m} = 0.75\ (-)$	$t = 117.2$ h	Fig. 5.11
	$\bar{y}_{J_{T,sp}} = 0.29\ (-)$		
	$\bar{u}_{\phi_c} = 0.60\ (-)$		

The results in Fig. 5.11 show that if the ESC is poorly tuned for multiple inputs relative to one another, one of the ESC perturbed inputs can be quickly steered toward the constraints as seen in the ESC trajectory with TESC. If hard constraints are imposed on the ESC manipulated inputs and a constant value is then set to prevent the ESC from exploring beyond the constraints, the gradient-based ESCs such as PESC and TESC are unable to perturb and extract gradient information.

A penalty function term can be included in the ESC objective function to prevent the ESC from approaching the constraints. The aim of the penalty function is to penalize the ESC objective function as the ESC manipulated variable approaches a constraint. In this optimization scenario, the penalty function is expressed as a sigmoid function. The penalty term is formulated as,

$$\Pi(u) = \begin{cases} \dfrac{L}{1+e^{k(u-u_0)}}, & u < \text{ soft lower limit}, \\ 0, & \text{soft lower limit } \leq u \leq \text{ soft upper limit}, \\ \dfrac{L}{1+e^{-k(u-u_0)}}, & u > \text{ soft upper limit}. \end{cases} \tag{5.2}$$

where k is used to set the steepness of the curve, L is the maximum value of the penalty function, u_0 is the midpoint of the sigmoid curve and u is the value of the perturbed variable. The contribution of the penalty term should be scaled such that an increase in the optimized variable does not significantly outweigh the contribution of the penalty term. The contribution of the penalty term is at a maximum when the value of the manipulated variable is equal or beyond the physical hard constraints and it is at a minimum when the value of the manipulated variable is equal to the soft upper or lower limits as illustrated in Fig. 5.12. The sigmoid curve is used to represent physical actuator limitations. Therefore, the system should not exceed the constraints.

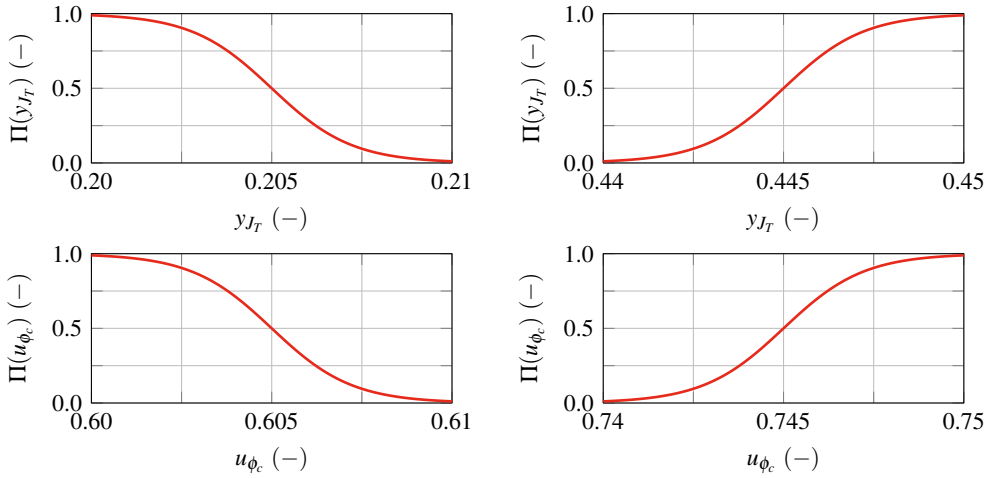

Figure 5.12. Penalty function contribution.

The ESC objective function with the penalty term is formulated as,

$$J = J(Q_{mso}, y_{\psi_m}) - \lambda_{y_{J_T}} \Pi(y_{J_T}) - \lambda_{u_{\phi_c}} \Pi(u_{\phi_c}) \tag{5.3}$$

where $\lambda_{y_{J_T}}$ and $\lambda_{u_{\phi_c}}$ are weightings used to scale the contribution of the penalty terms and the penalty terms, $\Pi(y_{J_T})$ and $\Pi(u_{\phi_c})$, are given in (5.4) and (5.5), respectively. The penalty term associated with

the mill load is,

$$\Pi(y_{J_T}) = \begin{cases} \dfrac{1}{1+e^{900\left(y_{J_T}-0.205\right)}}, & y_{J_T} < 0.21, \\ 0, & 0.21 \leq y_{J_T} \leq 0.44, \\ \dfrac{1}{1+e^{-900\left(y_{J_T}-0.445\right)}}, & y_{J_T} > 0.44, \end{cases} \tag{5.4}$$

The penalty term associated with the mill speed is,

$$\Pi(u_{\phi_c}) = \begin{cases} \dfrac{1}{1+e^{900\left(u_{\phi_c}-0.605\right)}}, & u_{\phi_c} < 0.61, \\ 0, & 0.61 \leq u_{\phi_c} \leq 0.74, \\ \dfrac{1}{1+e^{-900\left(u_{\phi_c}-0.745\right)}}, & u_{\phi_c} > 0.74. \end{cases} \tag{5.5}$$

An example of TESC optimizing y_{ψ_m} with the objective function described in (5.3) is shown in Fig. 5.13. A weighting of $\lambda_{y_{J_T}} = 30$ and $\lambda_{u_{\phi_c}} = 30$ was used to scale the contribution of the penalty terms. The addition of the penalty term results in the ESC steering away from the constraints as they are

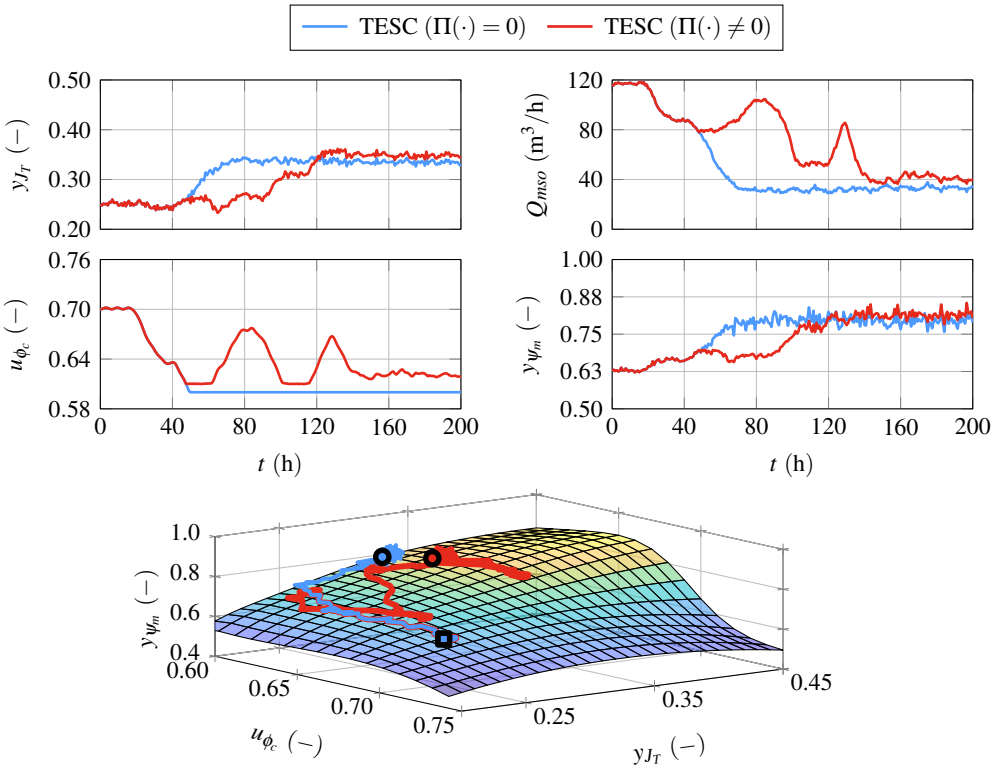

Figure 5.13. Comparison of TESC MISO grind (y_{ψ_m}) optimization with (red) and without (blue) the penalty terms. The initial and final time conditions are indicated by □ and ○, respectively.

approached and is driven nearer toward the global extremum. In Fig. 5.11, due to the faster adaptation of u_{ϕ_c} compared to y_{J_T}, the ESC tracked the local extremum along the constrained mill speed and converged to $y_{\psi_m} = 0.80$. However, in Fig. 5.13, with the addition of the penalty terms to the objective function, the ESC converged to $y_{\psi_m} = 0.82$.

The penalty function approach is specific to the gradient-based methods (PESC and TESC) to allow the ESC to explore the input-output map near the limits of the operating conditions. For SESC, a large constant value can be used instead as the penalty term as it would not upset the extremum seeking algorithm. Applying a penalty term can be useful if the objective is to prevent the ESC from exploring near the constraints of the process. However, this approach can be challenging to determine a balanced weighting for the penalty terms. If the weighting is too small relative to the contribution of the measured optimized variable, then the ESC could likely track a local extremum near the constraints rather than the global extremum if the ESC is poorly tuned as was observed in Fig. 5.11. If the weighting is too large, then an optimum located near the operating limits would not be reached as the ESC would steer away from the limits.

5.3.5 Multiple plant output optimization

The strategies mentioned thus far demonstrate that extremum seeking can operate the grinding mill at an extremum for either Q_{mso} or y_{ψ_m}. However, optimizing for one of the outputs leaves the other output at a suboptimum operating point.

From a practical perspective, optimizing y_{ψ_m} at the cost of significantly reducing Q_{mso} or vice-versa may not be practical to meet operational objectives. Depending on the market value of the valuable minerals produced, it could also be beneficial to maximize y_{ψ_m} while processing a sufficient amount of ore material (Q_{mso}). The inverse relationship that exists between Q_{mso} and y_{ψ_m} indicates that a balance between both outputs has to be considered to maximize profits (Bauer & Craig 2008). This section addresses how ESC can be applied to avoid the observed decreased performance shown in the single output optimization cases. In multiple-output optimization, both outputs are considered when optimizing the mill performance with ESC. The results are shown in Figs. 5.15–5.19. The convergence results and tuning parameters used are summarized in Tables 5.12–5.17.

5.3.5.1 ESC with a weighted objective function

In this section, an optimization strategy is proposed to optimize the mill performance with the use of a weighted objective function using the control configuration shown in Fig. 5.1 with switches A and

B closed (Fig. 5.1). Both Q_{mso} and y_{ψ_m} are scaled using min-max normalization to ensure that both outputs contribute relatively equally in magnitude to the ESC objective function across the range of y_{J_T} and u_{ϕ_c}. The ESC objective function is formulated as,

$$J(Q_{mso},\, y_{\psi_m}) = \lambda J_{Q_{mso}} + (1-\lambda) J_{y_{\psi_m}}, \tag{5.6a}$$

$$J_{Q_{mso}} = \frac{Q_{mso} - Q_{mso}^{min}}{Q_{mso}^{max} - Q_{mso}^{min}}, \tag{5.6b}$$

$$J_{y_{\psi m}} = \frac{y_{\psi_m} - y_{\psi_m}^{min}}{y_{\psi_m}^{max} - y_{\psi_m}^{min}}, \tag{5.6c}$$

where $Q_{mso}^{min} = 0\ \mathrm{m^3/h}$, $Q_{mso}^{max} = 160\ \mathrm{m^3/h}$, $y_{\psi_m}^{min} = 0.5$, and $y_{\psi_m}^{max} = 1.0$, which are chosen based on the theoretically smallest and largest values obtained from the grind curves (Fig. 2.5). These values could also be chosen based on the designed specifications of the grinding mill. The weighting factor is denoted by λ and is used to adjust the contribution of Q_{mso} or y_{ψ_m} to the objective function, J. To illustrate the contribution between $J_{Q_{mso}}$ or $J_{y_{\psi_m}}$ for an equal weighting of $\lambda = 0.5$, the 3-D surface of the objective function is shown in Fig. 5.14.

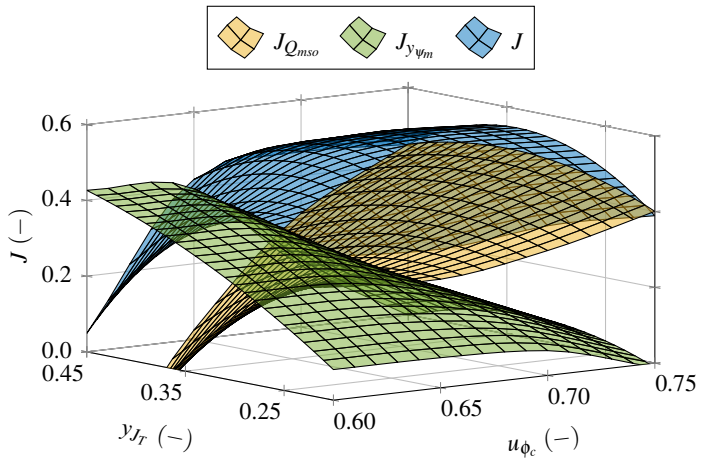

Figure 5.14. Contribution of $J_{Q_{mso}}$ and $J_{y_{\psi m}}$ to J with $\lambda = 0.5$.

The results of the weighted objective function optimization strategy are shown only for PESC in Fig. 5.15 and summarized in Table 5.13. The ESC perturbs only a single variable, $y_{J_{T,sp}}$, to maximize

Table 5.12. Single-input, weighted objective PESC tuning parameters.

Method	Variable	Tuning parameter values	Results
PESC	$y_{J_{T,sp}}$	$k = 2000$, $a = 0.001$, $\omega_h = 1.2\ \mathrm{rad/h}$, $\omega = 1.4\ \mathrm{rad/h}$, $\omega_l = 0.05\ \mathrm{rad/h}$	Fig. 5.15

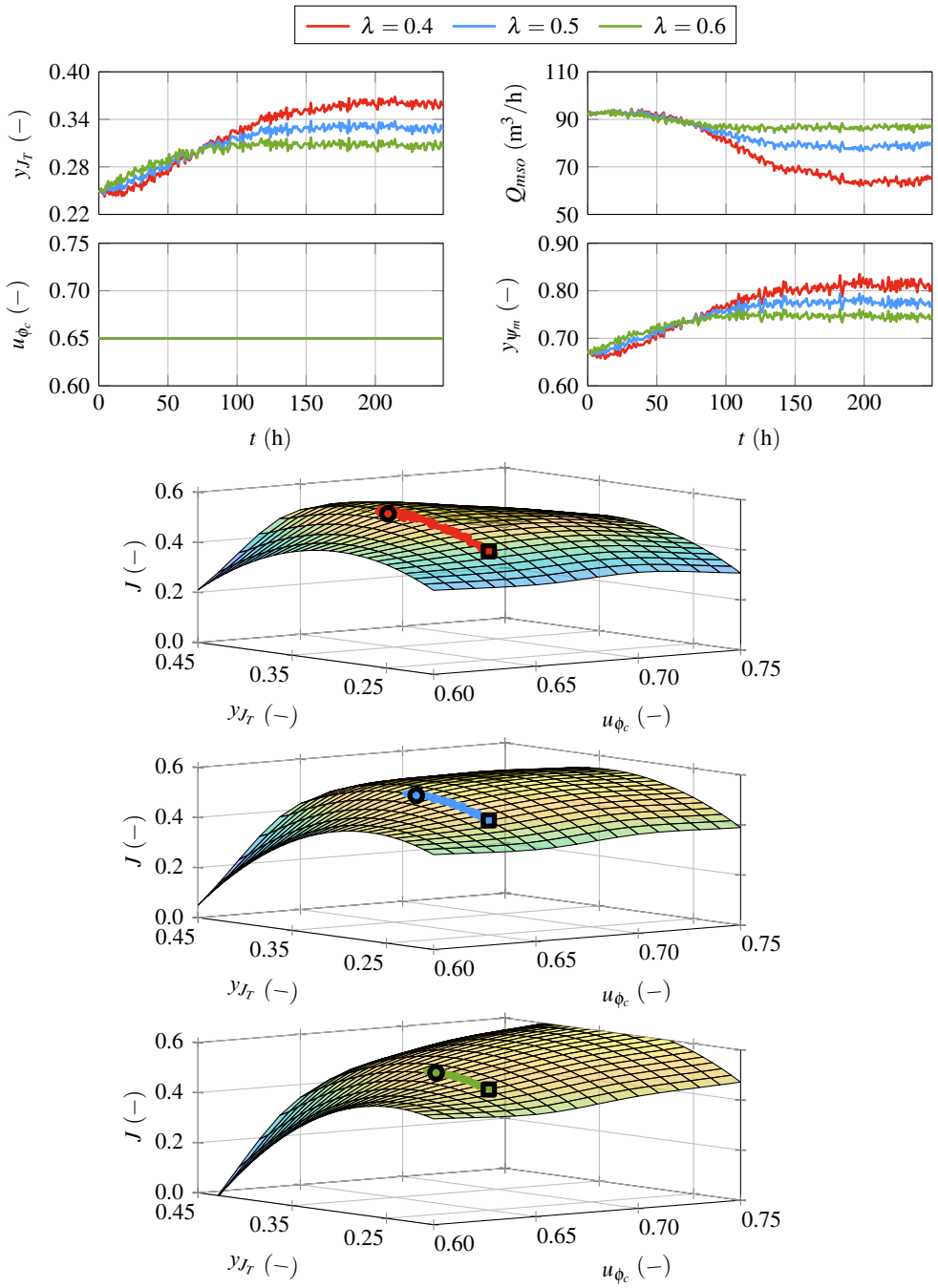

Figure 5.15. Single-input, weighted objective PESC optimization. The initial conditions are indicated by □ and the final time conditions are indicated by ○.

the weighted objective function. As the value of λ is increased, the 3-D surface maps of J vary and the optimum of the new surface map shifts from a higher Q_{mso} to a higher y_{ψ_m}. The advantage of employing a weighted objective function is that only a single variable is necessary for the ESC to achieve a balance between Q_{mso} and y_{ψ_m} and meet operational objectives. Using the weighted objective function to optimize a process with multiple outputs would be beneficial if there are fewer inputs than

Table 5.13. Single-input, weighted objective PESC optimization results.

λ	Average value	Convergence rate	Results
0.4	$\overline{Q}_{mso} = 65.36\ \mathrm{m}^3/\mathrm{h}$	$t = 122.4$ h	Fig. 5.15
	$\overline{y}_{\psi_m} = 0.81\ (-)$		
	$\overline{J} = 0.54\ (-)$		
	$\overline{y}_{J_{T,sp}} = 0.36\ (-)$		
0.5	$\overline{Q}_{mso} = 79.60\ \mathrm{m}^3/\mathrm{h}$	$t = 71.7$ h	Fig. 5.15
	$\overline{y}_{\psi_m} = 0.77\ (-)$		
	$\overline{J} = 0.52\ (-)$		
	$\overline{y}_{J_{T,sp}} = 0.33\ (-)$		
0.6	$\overline{Q}_{mso} = 86.96\ \mathrm{m}^3/\mathrm{h}$	$t = 36.2$ h	Fig. 5.15
	$\overline{y}_{\psi_m} = 0.74\ (-)$		
	$\overline{J} = 0.52\ (-)$		
	$\overline{y}_{J_{T,sp}} = 0.31\ (-)$		

there are outputs. This would be the case if, for example, the grinding mill is not equipped with a variable speed drive to vary u_{ϕ_c}. In this case, y_{J_T} is used to optimize for both Q_{mso} and y_{ψ_m}, but with the inverse relationship between the outputs, the plant operator would have to consider a trade-off between Q_{mso} and y_{ψ_m}.

Employing the weighted objective function would mean that the performance of Q_{mso} or y_{ψ_m} performance does not drastically decrease, as is seen in the single-output optimization results. Instead, λ is used as a parameter to reach an acceptable Q_{mso} or y_{ψ_m}, and the ESC would track the extremum of the objective function. However, to effectively balance between Q_{mso} and y_{ψ_m}, some prior knowledge of the unknown grind curves would be necessary to choose a suitable value for λ. For example, the plant operator cannot explicitly choose the value of Q_{mso} or y_{ψ_m} that the grinding mill will operate at by choosing λ. The relationship between λ and J is non-linear as can be seen in Fig. 5.15 and Table 5.13. The measured Q_{mso} and y_{ψ_m} do not scale proportionally with λ. Further, since the grind curves are time-varying, the contribution of $J_{Q_{mso}}$ and $J_{y_{\psi_m}}$ could also vary over time and λ would need to be adjusted.

5.3.5.2 ESC with paired control

Paired multi-input multi-output (MIMO) control ensures that the operational objectives are satisfied while optimizing the process by utilizing the mill variables y_{J_T} and u_{ϕ_c} to optimize Q_{mso} or y_{ψ_m}. The strategy pairs an output to be optimized (Q_{mso} or y_{ψ_m}) with one of the manipulated variables ($y_{J_{T,sp}}$ or u_{ϕ_c}) to the ESC, while the other output is paired to the remaining manipulated variable and controlled to setpoint by a regulatory controller as shown in Figs. 5.16 and 5.17. This strategy is useful when

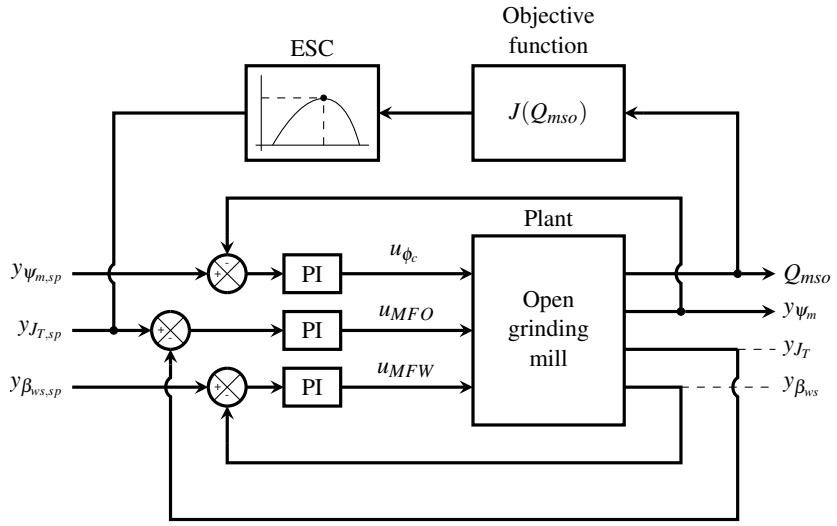

Figure 5.16. Control system diagram of the open grinding mill circuit optimized with ESC, Q_{mso} is optimized and y_{ψ_m} is controlled to setpoint.

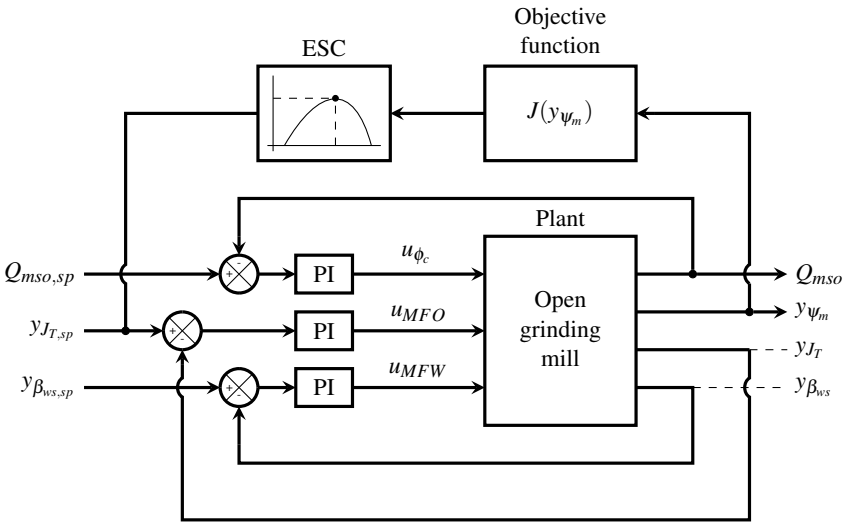

Figure 5.17. Control system diagram of the open grinding mill circuit optimized with ESC, y_{ψ_m} is optimized and Q_{mso} is controlled to setpoint.

Table 5.14. MIMO throughput (Q_{mso}) ESC tuning parameters.

Method	Variable	Tuning parameter values	Results
PESC	$y_{J_{T,sp}}$	$k = 20$, $a = 0.002$, $\omega_h = 1.8$ rad/h, $\omega = 2$ rad/h, $\omega_l = 0.1$ rad/h	Fig. 5.18
TESC	$y_{J_{T,sp}}$	$k_T = 2$, $k_{\eta_1} = 0.25$, $k_{\eta_2} = 0.25$, $\sigma = 0.001$, $z_\theta = 1$, $a = 0.0005$, $\omega = 0.5$ rad/h, $k = 0.01$	Fig. 5.18
SESC	$y_{J_{T,sp}}$	$\rho = 0.9$, $\chi = 2$, $\gamma = 0.6$, $\sigma = 0.5$, $T_s = 2$ h	Fig. 5.18

considering the environmental issues associated with the comminution stage. From an environmental perspective, there is a significant amount of valuable minerals that could be lost to the tailings in the separation process if the grind quality is poor. Most commonly, the mill is operated to maximize Q_{mso} while achieving the minimum acceptable y_{ψ_m}. Therefore, to reduce the waste of valuable minerals lost to waste or if the market demand leans toward a high-grade concentrate, it would be beneficial to achieve an increased y_{ψ_m} as opposed to maximizing Q_{mso}. The paired control strategy enables the processing plant to satisfy operational objectives for either Q_{mso} or y_{ψ_m} while maximizing the net economic benefit.

In Fig. 5.18, the ESC optimizes Q_{mso} by perturbing $y_{J_{T,sp}}$ and a regulatory controller controls y_{ψ_m} to setpoint by manipulating u_{ϕ_c} as illustrated in the block diagram in Fig. 5.16. The ESC tuning parameters are provided in Table 5.14 and the convergence results comparing the ESC methods are summarized in Table 5.16. The regulatory controller and the ESC operate together without significantly

Table 5.15. MIMO grind (y_{ψ_m}) ESC tuning parameters.

Method	Variable	Tuning parameter values	Results
PESC	$y_{J_{T,sp}}$	$k = 4000$, $a = 0.002$, $\omega_h = 1.8$ rad/h, $\omega = 2$ rad/h, $\omega_l = 0.1$ rad/h	Fig. 5.19
TESC	$y_{J_{T,sp}}$	$k_T = 3$, $k_{\eta_1} = 0.25$, $k_{\eta_2} = 0.25$, $\sigma = 1e-05$, $z_\theta = 1$, $a = 0.0001$, $\omega = 1$ rad/h, $k = 0.01$	Fig. 5.19
SESC	$y_{J_{T,sp}}$	$\rho = 0.7$, $\chi = 2$, $\gamma = 0.5$, $\sigma = 0.5$, $T_s = 2$ h	Fig. 5.19

hindering each other's performance. The regulatory controller is able to drive y_{ψ_m} to setpoint, while the ESC tracks the Q_{mso} extremum along the operating conditions given by the setpoint.

In Fig. 5.19, the ESC optimizes y_{ψ_m} by perturbing $y_{J_{T,sp}}$ and a regulatory controller controls Q_{mso} to setpoint by manipulating u_{ϕ_c} as illustrated in the block diagram in Fig. 5.17. The ESC tuning parameters are provided in Table 5.15 and the convergence results comparing the ESC methods are summarized in Table 5.17.

Table 5.16. MIMO throughput (Q_{mso}) optimization results.

Method	Average value	Convergence rate	Results
PESC	$\overline{Q}_{mso} = 113.06\ \mathrm{m}^3/\mathrm{h}$	$t = 78.0$ h	Fig. 5.18
	$\overline{y}_{J_{T,sp}} = 0.31\ (-)$		
TESC	$\overline{Q}_{mso} = 115.10\ \mathrm{m}^3/\mathrm{h}$	$t = 52.1$ h	Fig. 5.18
	$\overline{y}_{J_{T,sp}} = 0.32\ (-)$		
SESC	$\overline{Q}_{mso} = 116.67\ \mathrm{m}^3/\mathrm{h}$	$t = 48.2$ h	Fig. 5.18
	$\overline{y}_{J_{T,sp}} = 0.33\ (-)$		

Table 5.17. MIMO grind (y_{ψ_m}) optimization results.

Method	Average value	Convergence rate	Results
PESC	$\overline{y}_{\psi_m} = 0.74\ (-)$	$t = 54.5$ h	Fig. 5.19
	$\overline{y}_{J_{T,sp}} = 0.38\ (-)$		
TESC	$\overline{y}_{\psi_m} = 0.75\ (-)$	$t = 31.8$ h	Fig. 5.19
	$\overline{y}_{J_{T,sp}} = 0.37\ (-)$		
SESC	$\overline{y}_{\psi_m} = 0.75\ (-)$	$t = 14.5$ h	Fig. 5.19
	$\overline{y}_{J_{T,sp}} = 0.35\ (-)$		

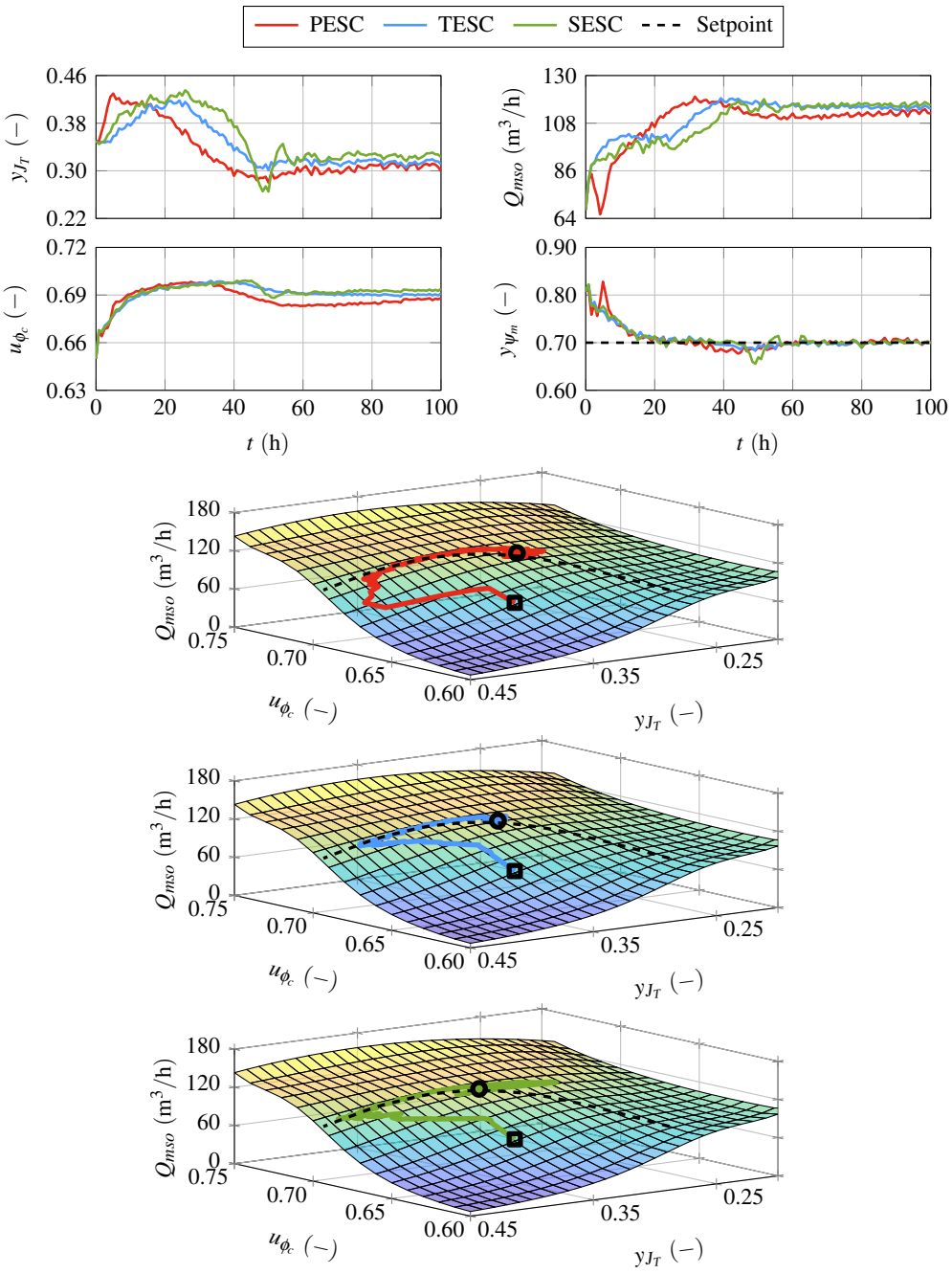

Figure 5.18. Comparison of MIMO throughput (Q_{mso}) optimization with $y_{J_{T,sp}}$ and y_{ψ_m} is controlled at setpoint ($y_{\psi_{m,sp}}$) with u_{ϕ_c}. The black dashed line on the 3-D surface maps indicates the operating conditions (y_{J_T} and u_{ϕ_c}) where $y_{\psi_m} = 0.70$. The initial conditions are indicated by □ and the final time conditions are indicated by ○.

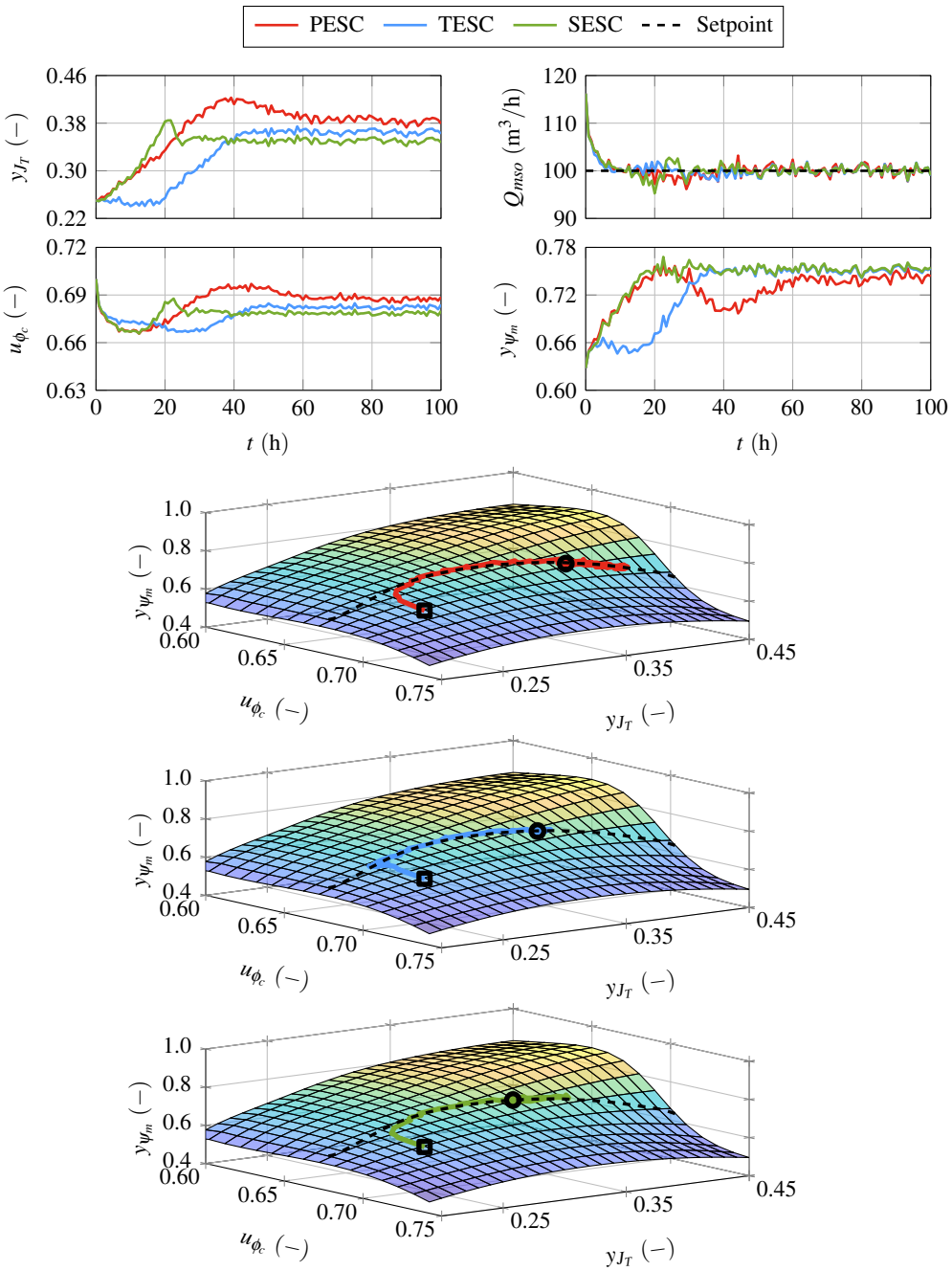

Figure 5.19. Comparison of MIMO grind (y_{ψ_m}) optimization with $y_{J_{T,sp}}$ and Q_{mso} is controlled at setpoint ($Q_{mso,sp}$) with u_{ϕ_c}. The black dashed line on the 3-D surface maps indicates the operating conditions (y_{J_T} and u_{ϕ_c}) where $Q_{mso} = 100$ m^3/h. The initial conditions are indicated by □ and the final time conditions are indicated by ○.

5.4 CHAPTER SUMMARY

In this chapter, the simulated dynamic step response of the grinding mill is compared to the grind curve data. The simulated response shows a good correlation to the measured data and is adequate to apply extremum seeking methods to explore the input-output map of the model. A dynamic response of the open grinding mill circuit is presented to demonstrate the interactions that exist between the manipulated and controlled process variables.

Several control strategies are simulated to demonstrate the application of the ESCs for optimizing grinding mill performance. The extremum seeking methods presented in Chapter 4 are applied to optimize the open grinding mill circuit described in Section 3.2 of Chapter 3. The ESC strategies are simulated to optimize the mill performance by either manipulating the mill load, mill speed or both as single-input or multiple-input cases. The optimization strategies include single-output and multiple-output optimization, where either the throughput, the grind, or a weighted combination of the measured throughput and grind are used as the ESC objective function. Additionally, the optimization strategies include the cases where the throughput or grind is optimized by the ESC and the remaining output is controlled to setpoint. The influence of disturbances, noise and constraints on the ESC performance are considered and briefly discussed.

CHAPTER 6 OPTIMIZING A SINGLE-STAGE CLOSED GRINDING CIRCUIT

6.1 CHAPTER OVERVIEW

In this chapter, the model of the closed grinding mill circuit with a screen (Section 3.4.1) and a hydrocyclone (Section 3.4.2), respectively, is simulated and optimized with the extremum seeking methods described in Chapter 4.

6.2 SIMULATIONS

Several strategies are simulated to demonstrate the application of the ESCs for optimizing the closed grinding mill circuit performance. The aim is not to determine the best extremum seeking method, but to investigate the application of the ESCs to optimize a closed grinding mill circuit considering the different interactions that exist between the controlled variables.

The closed grinding circuit is sensitive to changes in the mill speed as shown in the simulated dynamic step response for the closed grinding circuit equipped with a screen or hydrocyclone (Figs. 3.7 and 3.8). Therefore, due to the narrow operating range of the mill speed, the ESC optimization trajectories are not shown on the 3-D surface maps of the performance indicators as in Chapter 5.

6.2.1 Setup

The simulation environment (as shown in Figs. 6.1 and 6.7) is summarized as follows:

- A sampling period of 60 seconds is used for the simulations.
- White Gaussian noise with a noise level of -10 dB is added to the output Q_{csus}, and a noise level of -50 dB is added to the outputs y_{ψ_c}, y_{SVOL}, y_{CFD} to evaluate the performance of the ESCs subject to measurement noise.

- A PI controller is used to control the mill load to setpoint ($y_{J_{T,sp}}$) by manipulating u_{MFO} if the mill load is used as a perturbation variable by the ESC. The mill speed (u_{ϕ_c}) is directly perturbed by the ESC if it is used as a perturbation variable.
- A PI controller is used to regulate the mill discharge water to solids ratio at $y_{\beta_{ws,sp}} = 0.9$ by manipulating u_{MFW}.
- The ESCs are restricted to explore in a region that is defined by the grind curves, $y_{J_T} \in [0.20, 0.45]$ and $u_{\phi_c} \in [0.60, 0.75]$ by enforcing hard constraints on both y_{J_T} and u_{ϕ_c}.
- If the sump volume is controlled to setpoint ($y_{SVOL_{sp}}$), a PI controller is used to control y_{SVOL} to setpoint by manipulating u_{CFF}.
- If the classifier (screen or hydrocyclone) feed density is controlled to setpoint ($y_{CFD_{sp}}$), a PI controller is used to control y_{CFD} to setpoint by manipulating u_{SFW}. Fig. 6.1 and Fig. 6.7 illustrates that either $y_{J_{T,sp}}$ or u_{ϕ_c} can be separately manipulated while the other variable is kept constant, or both can be simultaneously manipulated by the ESC to steer the grinding mill circuit. If either of the manipulated variables are disconnected from the ESC by opening switch A or B, they are set to a constant value.
- The values of the parameters used for the screen and hydrocyclone modules are provided in Table 6.1 and Table 6.7, respectively.

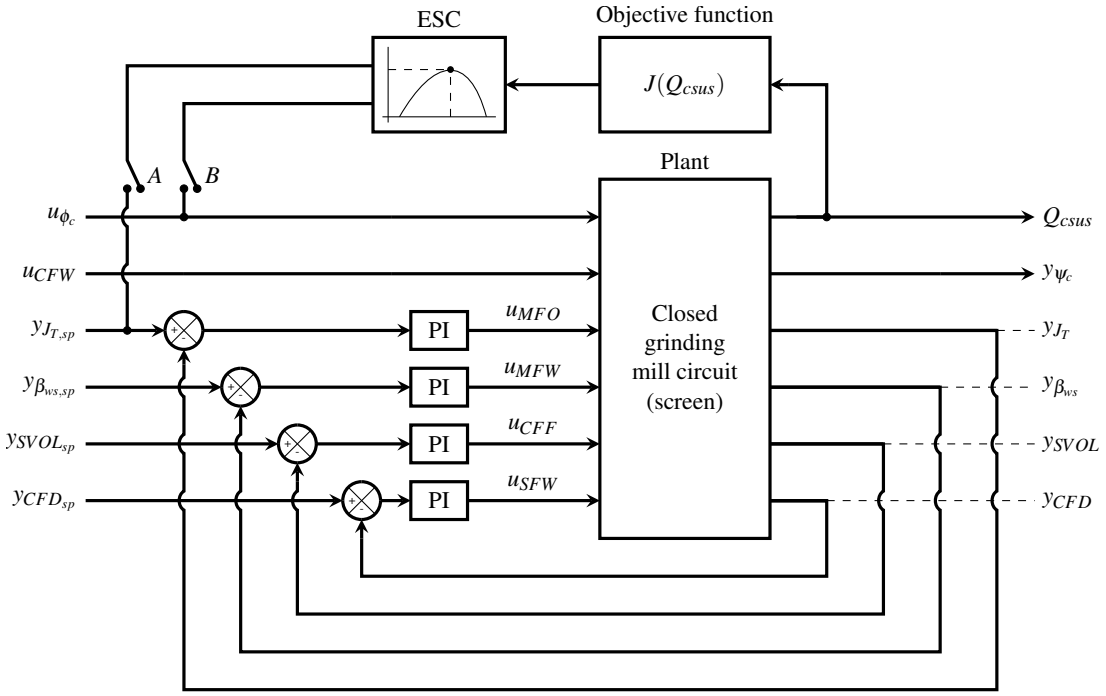

Figure 6.1. Control system diagram of the closed grinding circuit with a screen optimized with ESC.

Table 6.1. Screen model parameter values.

Variable	Value	Unit	Description
D_1	0.10	$(-)$	Fraction of the water flow-rate that forms part of the circulating load carrying the solids parameter
D_2	0.15	$(-)$	Fraction of solids in the slurry that are larger than the target specification size and form part of the circulating load parameter
D_3	1.10	$(-)$	Final product particle size fitting parameter

6.2.1.1 Objective function

The configuration of the closed grinding mill circuit with ESC is illustrated by the block diagrams in Fig. 6.1 and Fig. 6.7. The objective function for the ESC is to maximize the circuit throughput,

$$J(Q_{csus}) = Q_{csus}. \tag{6.1}$$

6.2.2 Closed grinding mill circuit with a screen

6.2.2.1 Dynamic step response

A stepped sweep response of the simulated closed grinding mill circuit with a screen is shown in Fig. 6.2, where y_{J_T} is incrementally swept. At $y_{J_T} = 0.20$, the initial conditions of x_{mr} is negative, therefore, y_{J_T} is swept in the range $y_{J_T} \in [0.25, 0.45]$. Two simulated scenarios are shown in Fig. 6.2. In both scenarios, the PI control loops of Fig. 6.1 for y_{J_T}, $y_{\beta_{ws}}$ and y_{SVOL} are active during the sweep. The blue plotted data shows the response of the closed grinding mill circuit with y_{CFD} controlled to setpoint and the red plotted data shows the response when y_{CFD} is left uncontrolled, i.e. the PI control loop for y_{CFD} is inactive.

The step response is used to show the effect of manipulating y_{J_T} which propagates to Q_{csus}. Since Q_{csus} is measured by the volume of solids in the under size stream, Q_{csus} is directly coupled to y_{CFD} as seen in Fig. 6.2. As in the open grinding mill simulations, it is expected that there is a peak throughput (Q_{csus}) for a specific value of y_{J_T} and u_{ϕ_c}. However, the step response of sweeping the mill speed (u_{ϕ_c}) is not shown since the peak exists beyond the range of $u_{\phi_c} \in [0.60, 0.75]$.

For ESC optimization, y_{CFD} should be left uncontrolled for the perturbations in y_{J_T} and u_{ϕ_c} to be observed in Q_{csus}. If u_{SFW} is kept constant, the change in the discharge rate of the solids from the

grinding mill due to the perturbed mill load or speed can then be observed in the measured Q_{csus}. Therefore, y_{SVOL} should be controlled to setpoint, which is achieved by manipulating u_{CFF}. The stepped sweep response also demonstrates the inverse relationship that exists between Q_{csus} and y_{ψ_c}, when Q_{csus} is at its maximum then y_{ψ_c} is near its minimum. Further, maximum throughput is achieved below the peak power consumption as observed in Craig et al. (1992).

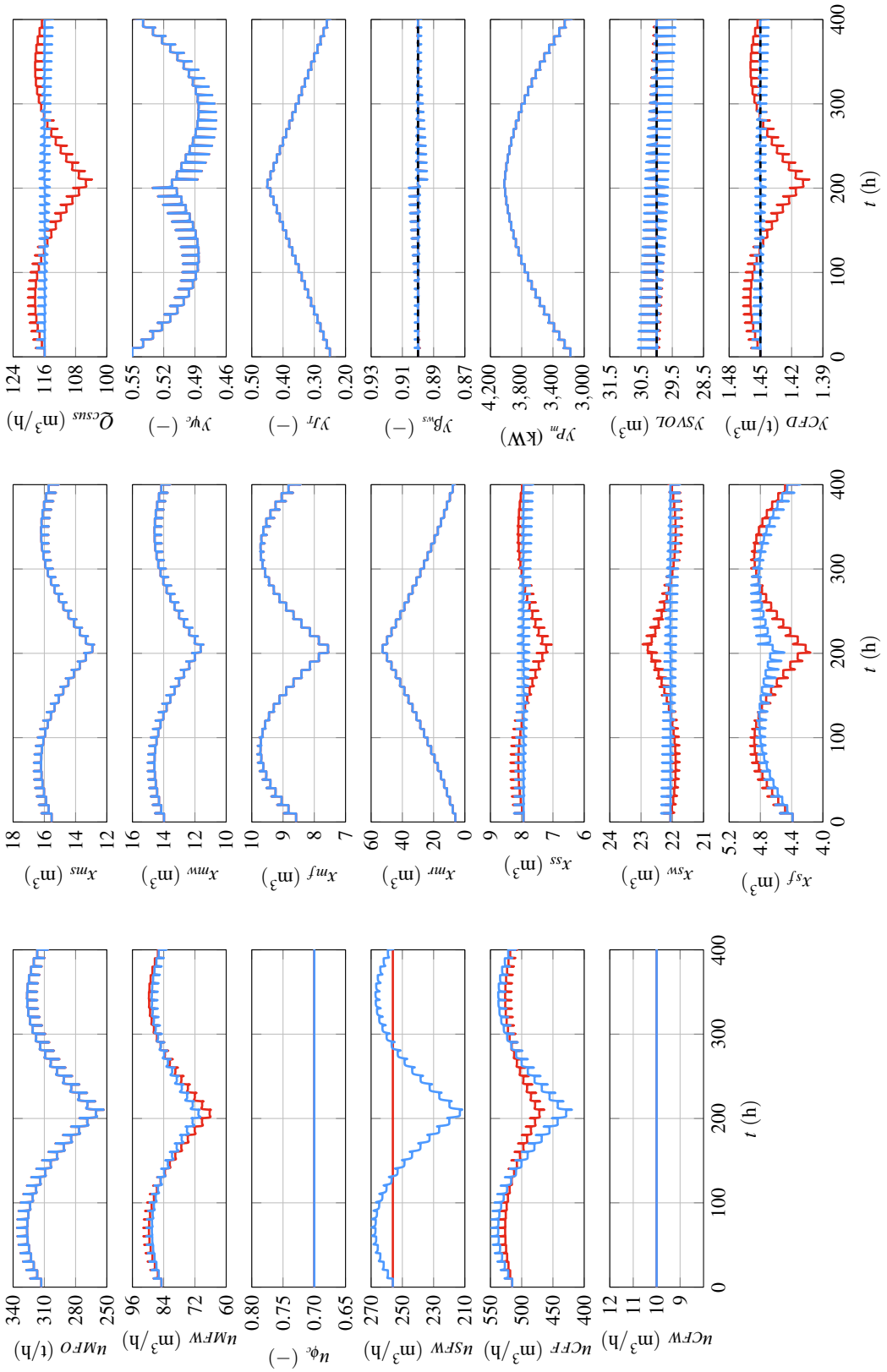

Figure 6.2. Comparison of the dynamic step response of the closed circuit model with a screen classifier. y_{SVOL} is controlled to setpoint, $y_{SVOL_{sp}} = 30\ \mathrm{m}^3$. The red plotted data shows the circuit with y_{CFD} uncontrolled and the blue plotted data shows the circuit with y_{CFD} controlled to setpoint, $y_{CFD_{sp}} = 1.45\ \mathrm{t/m}^3$. $y_{J_{T,sp}}$ is stepped from $y_{J_{T,sp}} = 0.25$ to $y_{J_{T,sp}} = 0.45$. The black dashed line indicates the setpoint.

6.2.2.2 Throughput optimization with mill load

In Fig. 6.3, the ESC optimizes grinding mill circuit throughput (Q_{csus}) by perturbing $y_{J_{T,sp}}$ (i.e., only switch A is closed in Fig. 6.1). The ESC tuning parameters are provided in Table 6.2 and the convergence results comparing the ESC methods are summarized in Table 6.3.

During the initial search for the Q_{csus} peak, y_{SVOL} oscillates for the TESC and SESC methods, which attenuate as the ESC converges toward the extremum. Since, PESC converges at a slower rate, the observed variations in y_{SVOL} are significantly smaller relative to TESC and SESC. Both TESC and SESC converge toward the optimum y_{J_T} and a higher Q_{csus} compared to PESC (Table 6.3). The step response in Fig. 6.2 shows that the throughput peak of $Q_{csus} = 118.4\ (\mathrm{m}^3/\mathrm{h})$ is located at $y_{J_T} = 0.31$. The poorer performance of PESC, which converges to $y_{J_T} = 0.34$, can be attributed to the tuning parameters used. This highlights that the extremum seeking methods do require that the tuning parameters are carefully chosen and one cannot simply apply the extremum seeking to find the optimum without going through the tuning process.

Table 6.2. Closed grinding mill circuit with screen throughput (Q_{csus}) optimization ESC tuning parameters.

Method	Variable	Tuning parameter values	Results
PESC	$y_{J_{T,sp}}$	$k = 15$, $a = 0.002$, $\omega_h = 1.4$ rad/h, $\omega = 1.6$ rad/h, $\omega_l = 0.05$ rad/h	Figs. 6.3 and 6.5
	u_{ϕ_c}	$k = 20$, $a = 0.002$, $\omega_h = 1.8$ rad/h, $\omega = 2$ rad/h, $\omega_l = 0.1$ rad/h	Figs. 6.4 and 6.5
TESC	$y_{J_{T,sp}}$	$k_T = 1$, $k_{\eta_1} = 0.25$, $k_{\eta_2} = 0.25$, $\sigma = 0.001$, $z_\theta = 1$, $a = 0.001$, $\omega = 1$ rad/h, $k = 0.01$	Figs. 6.3 and 6.5
	u_{ϕ_c}	$k_T = 2$, $k_{\eta_1} = 0.5$, $k_{\eta_2} = 0.5$, $\sigma = 0.001$, $z_\theta = 1$, $a = 0.001$, $\omega = 0.5$ rad/h, $k = 0.02$	Figs. 6.4 and 6.5
SESC	$y_{J_{T,sp}}$	$\rho = 0.6$, $\chi = 2$, $\gamma = 0.7$, $\sigma = 0.7$, $T_s = 3$ h	Figs. 6.3 and 6.5
	u_{ϕ_c}	$\rho = 0.6$, $\chi = 2$, $\gamma = 0.7$, $\sigma = 0.7$, $T_s = 3$ h	Figs. 6.4 and 6.5

6.2.2.3 Throughput optimization with mill speed

In Fig. 6.4, the ESC optimizes grinding mill circuit throughput (Q_{csus}) by perturbing u_{ϕ_c} (i.e., only switch B is closed in Fig. 6.1). The results comparing the ESC methods are summarized in Table 6.4 and the ESC tuning parameters are provided in Table 6.2.

Similarly, as in the previous simulation, there are large variations in y_{SVOL} for the TESC and SESC methods, which attenuate as the ESC converges toward the extremum. All three ESC methods converge toward the hard constrained upper mill speed value, $u_{\phi_c} = 0.75$. In this simulation, the grinding mill circuit achieves a higher throughput performance when the ESC manipulates u_{ϕ_c} compared to using y_{J_T} (Fig. 6.3). In both cases, the large variations in y_{SVOL} do not significantly influence the ESC performance to track the extremum. One additional aspect to consider is that the sump volume is not constrained in the simulated results. Although not considered in this work, a supervisory controller or a simple PI override controller can be implemented to limit u_{CFF} such that the sump will not overflow or run dry (Olivier & Craig 2017*a*).

6.2.2.4 Throughput optimization with mill load and speed

In Fig. 6.5, the ESC optimizes grinding mill circuit throughput (Q_{csus}) by perturbing both $y_{J_{T,sp}}$ and u_{ϕ_c} (switch A and B are closed in Fig. 6.1). The results comparing the ESC methods are summarized in Table 6.5 and the ESC tuning parameters are provided in Table 6.2.

Each ESC method converges toward the hard constrained upper mill speed value, $u_{\phi_c} = 0.75$. The large increase in Q_{csus} (Fig. 6.4) is due to u_{ϕ_c} being driven toward a higher value, but there is also an increase in Q_{csus} due to y_{J_T}, although a minor increase relative to u_{ϕ_c} as indicated by the convergence results in Table 6.5.

6.2.2.5 Comparison of throughput optimization strategies (PESC)

In Fig. 6.6, the optimization results from Figs. 6.3–6.5 with PESC are compared and the results are summarized in Table 6.6. Using both $y_{J_{T,sp}}$ and u_{ϕ_c} to optimize the grinding mill circuit throughput performance achieves the highest Q_{csus}. Q_{csus} and y_{ψ_c} are significantly more sensitive to changes in u_{ϕ_c} than in $y_{J_{T,sp}}$. Typically, the u_{ϕ_c} is kept constant while the $y_{J_{T,sp}}$ is used to maximize Q_{csus} to avoid the large variation in y_{ψ_c}. Fig. 6.5 also shows the influence of u_{ϕ_c} on y_{SVOL}, which can quickly cause the sump to overfill. Additionally, the ESC is able to track the optimum Q_{csus} from a lower ($y_{J_T} = 0.25$) or a higher ($y_{J_T} = 0.40$) initial condition as shown in Fig. 6.3 and Fig. 6.6, respectively.

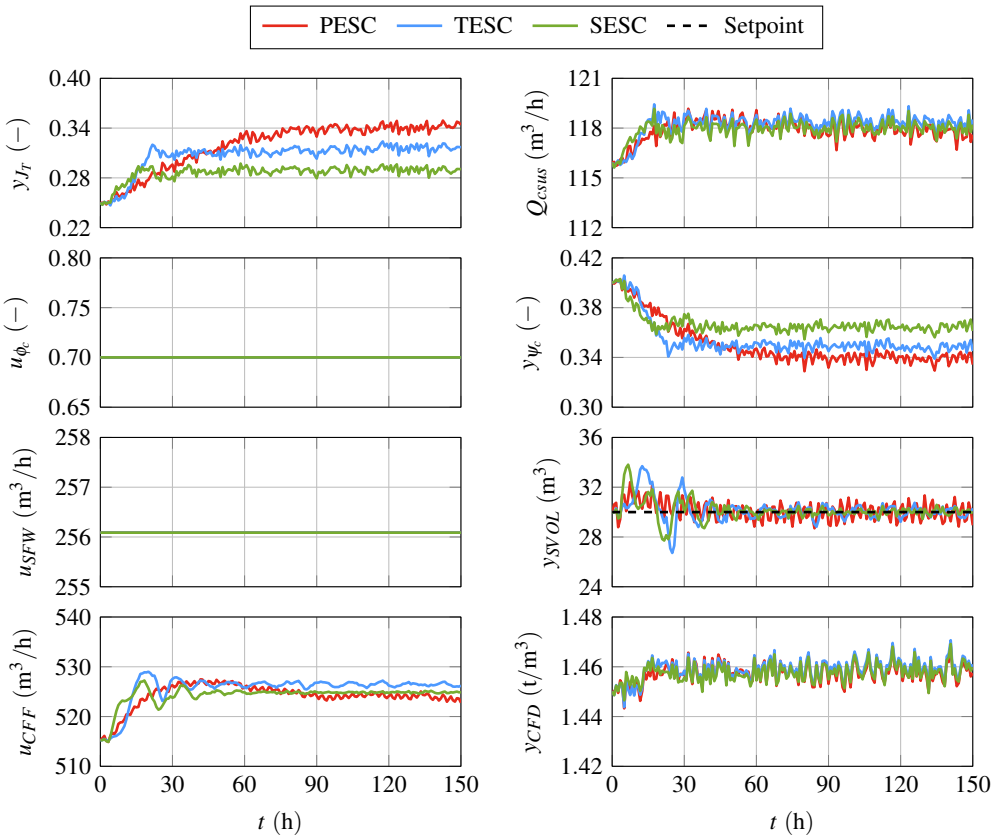

Figure 6.3. Comparison of throughput (Q_{csus}) optimization with $y_{J_{T,sp}}$.

Table 6.3. Throughput (Q_{csus}) optimization results with $y_{J_{T,sp}}$ perturbed.

Method	Average value	Convergence rate	Results
PESC	$\overline{Q}_{csus} = 117.66$ m^3/h	$t = 57.1$ h	Fig. 6.3
	$\bar{y}_{J_{T,sp}} = 0.34$ (−)		
TESC	$\overline{Q}_{csus} = 118.31$ m^3/h	$t = 28.9$ h	Fig. 6.3
	$\bar{y}_{J_{T,sp}} = 0.32$ (−)		
SESC	$\overline{Q}_{csus} = 118.02$ m^3/h	$t = 27.3$ h	Fig. 6.3
	$\bar{y}_{J_{T,sp}} = 0.29$ (−)		

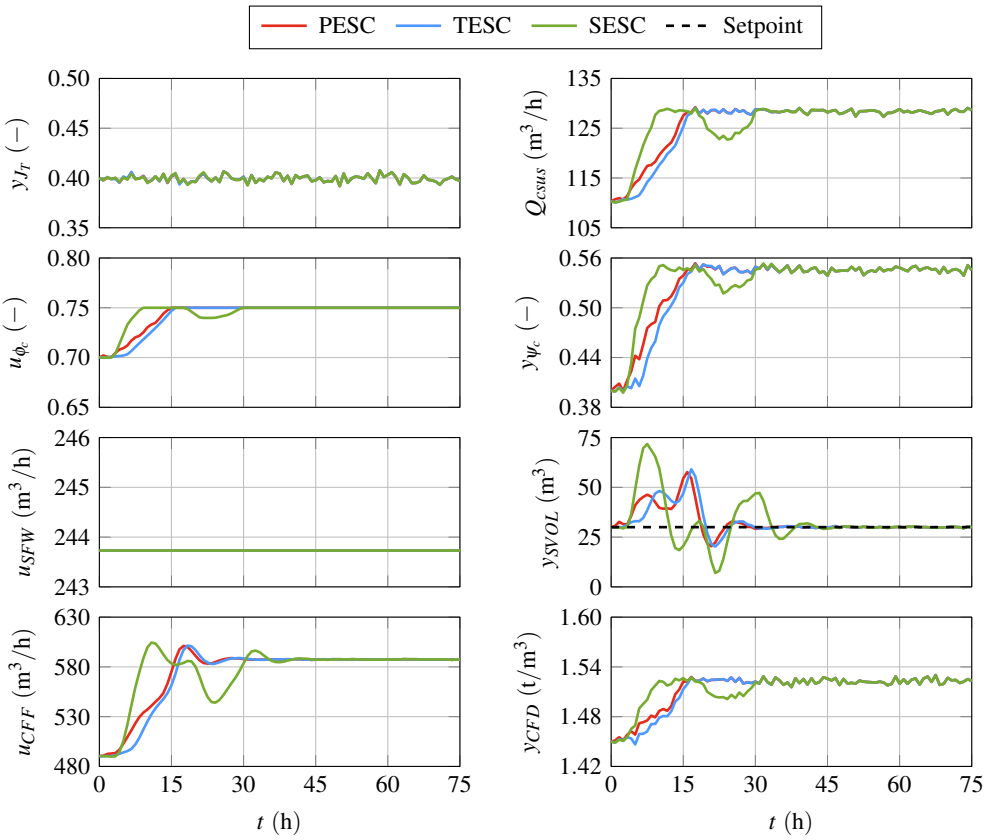

Figure 6.4. Comparison of throughput (Q_{csus}) optimization with u_{ϕ_c}.

Table 6.4. Throughput (Q_{csus}) optimization results with u_{ϕ_c} perturbed.

Method	Average value	Convergence rate	Results
PESC	$\overline{Q}_{csus} = 128.25$ m^3/h	$t = 14.7$ h	Fig. 6.4
	$\overline{u}_{\phi_c} = 0.75$ (−)		
TESC	$\overline{Q}_{csus} = 128.34$ m^3/h	$t = 15.6$ h	Fig. 6.4
	$\overline{u}_{\phi_c} = 0.75$ (−)		
SESC	$\overline{Q}_{csus} = 128.29$ m^3/h	$t = 28.9$ h	Fig. 6.4
	$\overline{u}_{\phi_c} = 0.75$ (−)		

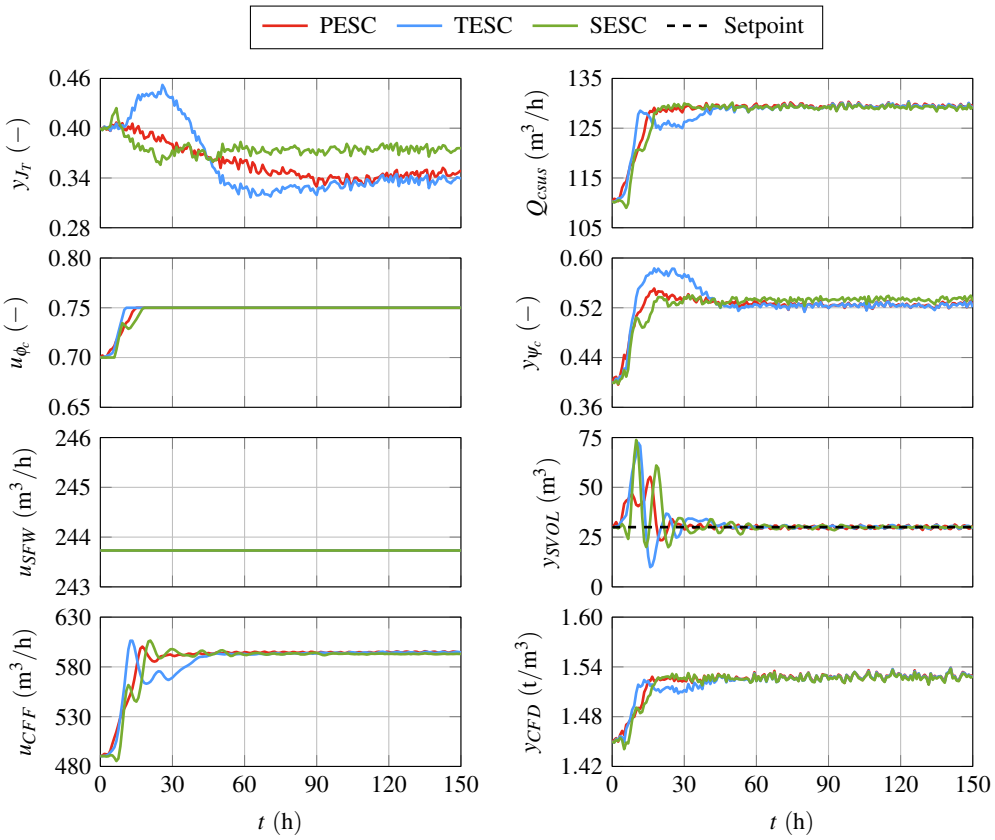

Figure 6.5. Comparison of throughput (Q_{csus}) optimization with $y_{J_{T,sp}}$ and u_{ϕ_c}.

Table 6.5. Throughput (Q_{csus}) optimization results with $y_{J_{T,sp}}$ and u_{ϕ_c} perturbed.

Method	Average value	Convergence rate	Results
PESC	$\overline{Q}_{csus} = 129.50\ \mathrm{m}^3/\mathrm{h}$	$t = 15.0$ h	Fig. 6.5
	$\overline{y}_{J_{T,sp}} = 0.35\ (-)$		
	$\overline{u}_{\phi_c} = 0.75\ (-)$		
TESC	$\overline{Q}_{csus} = 129.44\ \mathrm{m}^3/\mathrm{h}$	$t = 37.5$ h	Fig. 6.5
	$\overline{y}_{J_{T,sp}} = 0.34\ (-)$		
	$\overline{u}_{\phi_c} = 0.75\ (-)$		
SESC	$\overline{Q}_{csus} = 129.42\ \mathrm{m}^3/\mathrm{h}$	$t = 17.5$ h	Fig. 6.5
	$\overline{y}_{J_{T,sp}} = 0.37\ (-)$		
	$\overline{u}_{\phi_c} = 0.75\ (-)$		

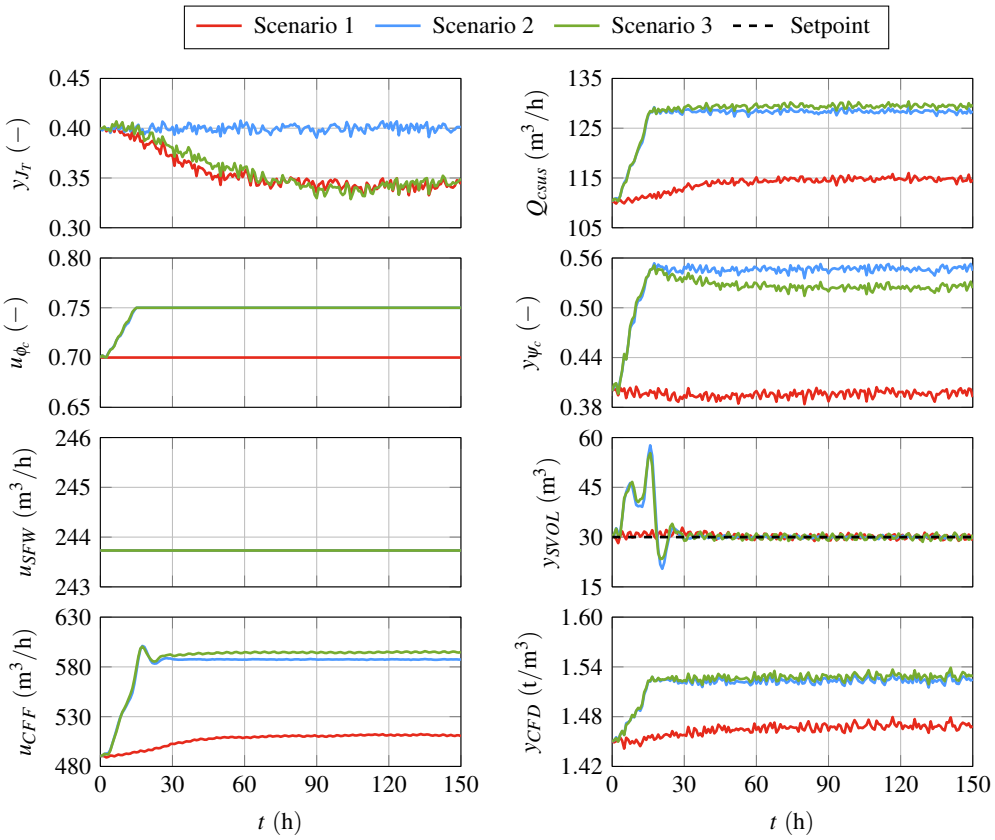

Figure 6.6. PESC throughput (Q_{csus}) optimization with $y_{J_{T,sp}}$ (Scenario 1), with u_{ϕ_c} (Scenario 2), with both $y_{J_{T,sp}}$ and u_{ϕ_c} (Scenario 3).

Table 6.6. Comparison of PESC throughput (Q_{csus}) optimization results with perturbing $y_{J_{T,sp}}$ (Scenario 1), with u_{ϕ_c} (Scenario 2), and, with $y_{J_{T,sp}}$ and u_{ϕ_c} (Scenario 3).

Scenario	Average value	Convergence rate	Results
1	$\overline{Q}_{csus} = 114.68$ m³/h	$t = 27.8$ h	Fig. 6.6
	$\overline{y}_{J_{T,sp}} = 0.34$ (−)		
	$\overline{u}_{\phi_c} = 0.70$ (−)		
2	$\overline{Q}_{csus} = 128.25$ m³/h	$t = 14.7$ h	Fig. 6.6
	$\overline{y}_{J_{T,sp}} = 0.40$ (−)		
	$\overline{u}_{\phi_c} = 0.75$ (−)		
3	$\overline{Q}_{csus} = 129.50$ m³/h	$t = 15.0$ h	Fig. 6.6
	$\overline{y}_{J_{T,sp}} = 0.35$ (−)		
	$\overline{u}_{\phi_c} = 0.75$ (−)		

6.2.3 Closed grinding mill circuit with a hydrocyclone

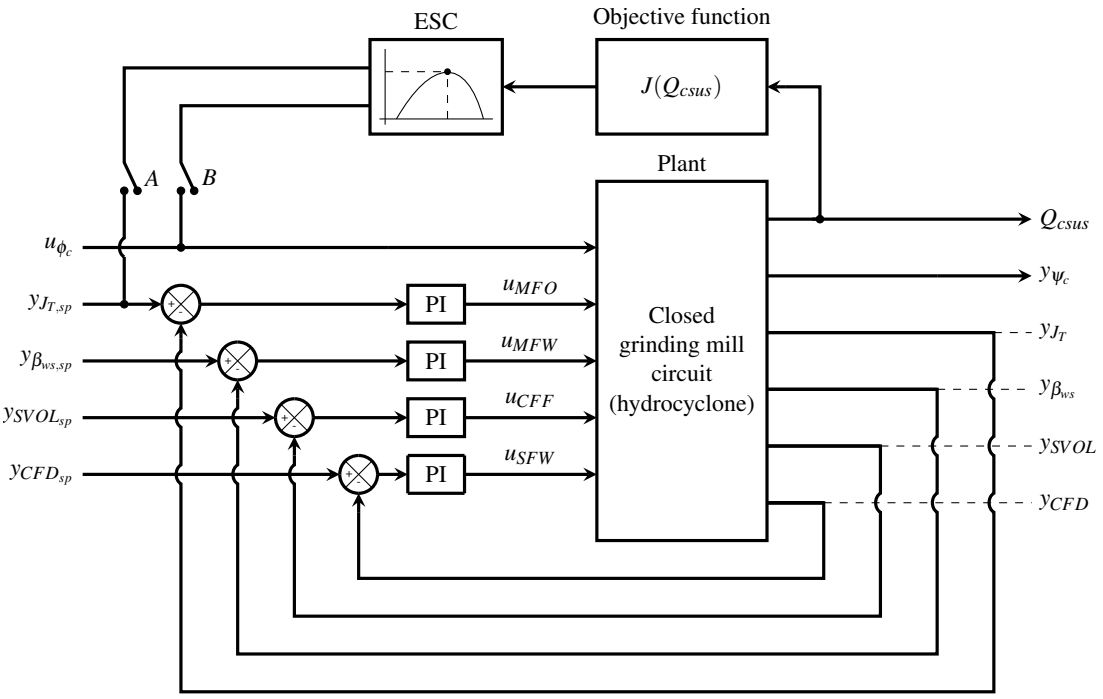

Figure 6.7. Control system diagram of the closed grinding circuit with a hydrocyclone optimized with ESC.

6.2.3.1 Dynamic step response

A stepped sweep response of the simulated closed grinding mill circuit with a hydrocyclone is shown in Fig. 6.8, where y_{J_T} is incrementally swept. Similarly, as in the stepped sweep response of the grinding mill circuit with a screen (Fig. 6.2), at $y_{J_T} = 0.20$, the initial conditions of x_{mr} is negative, therefore,

Table 6.7. Hydrocyclone model parameter values.

Variable	Value	Unit	Description
α_{su}	0.87	$(-)$	Fraction of solids in the underflow parameter
ε_c	129	$(\mathrm{m}^3/\mathrm{h})$	Coarse split parameter
C_1	0.6	$(-)$	Fitting parameter
C_2	0.7	$(-)$	Fitting parameter
C_3	2.0	$(-)$	Fitting parameter
C_4	1.1	$(-)$	Fitting parameter
C_5	1.1	$(-)$	Fitting parameter

y_{J_T} is swept in the range $y_{J_T} \in [0.30, 0.45]$. The closed grinding mill circuit with a hydrocyclone is sensitive to changes in u_{ϕ_c}. A 2% step change in the mill speed rapidly drives the mill rock state x_{mf} toward zero as seen in Fig. 3.8. Therefore, this section does not consider using u_{ϕ_c} to explore and find the optimal mill speed.

Two simulated scenarios are shown in Fig. 6.8. In both scenarios, the PI control loops of Fig. 6.7 for y_{J_T}, $y_{\beta_{ws}}$ and y_{SVOL} are active during the sweep. The blue plotted data shows the response of the closed grinding mill circuit with y_{CFD} controlled to setpoint and the red plotted data shows the response when y_{CFD} is left uncontrolled, i.e. the PI control loop for y_{CFD} is inactive.

The step response is used to show the effect of manipulating y_{J_T} being propagated to the throughput (Q_{csus}) when y_{CFD} is uncontrolled or controlled to setpoint. In both cases, the step response shows a peak in Q_{csus}. However, when y_{CFD} is not controlled, the peak Q_{csus} is lower and shifted compared to when y_{CFD} is controlled to setpoint. Therefore, to maximize the throughput of the grinding mill circuit closed with a hydrocyclone, y_{CFD} should be controlled to setpoint.

6.2.3.2 Throughput optimization with mill load

In Fig. 6.9, the ESC optimizes grinding mill circuit throughput (Q_{csus}) by perturbing $y_{J_{T,sp}}$, while y_{SVOL} and y_{CFD} are controlled to setpoint by regulatory controllers. The ESC tuning parameters are provided in Table 6.8 and the convergence results comparing the ESC methods are summarized in Table 6.10.

Table 6.8. Closed grinding mill circuit with hydrocyclone throughput (Q_{csus}) optimization ESC tuning parameters.

Method	Variable	Tuning parameter values	Results
PESC	$y_{J_{T,sp}}$	$k = 25$, $a = 0.002$, $\omega_h = 2.5$ rad/h, $\omega = 4$ rad/h, $\omega_l = 0.1$ rad/h	Figs. 6.9 and 6.10
TESC	$y_{J_{T,sp}}$	$k_T = 2$, $k_{\eta_1} = 0.5$, $k_{\eta_2} = 0.5$, $\sigma = 0.001$, $z_\theta = 1$, $a = 0.0005$, $\omega = 0.5$ rad/h, $k = 0.01$	Figs. 6.9 and 6.10
SESC	$y_{J_{T,sp}}$	$\rho = 0.8$, $\chi = 2$, $\gamma = 0.8$, $\sigma = 0.8$, $T_s = 5$ h	Figs. 6.9 and 6.10

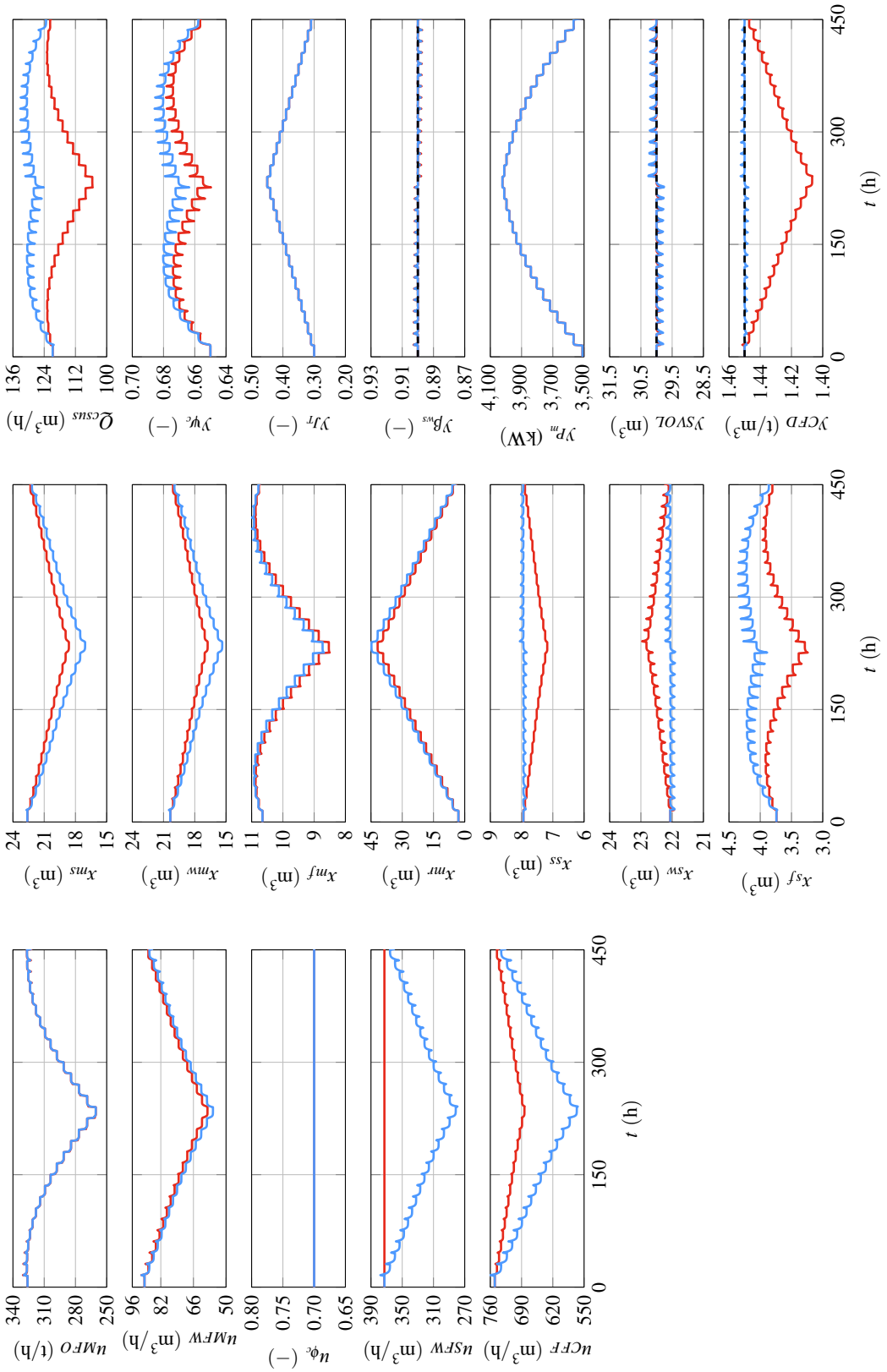

Figure 6.8. Comparison of the dynamic step response of the closed circuit model with a hydrocyclone classifier. y_{SVOL} is controlled to setpoint, $y_{SVOL_{sp}} = 30$ m^3. The red plotted data shows the circuit with y_{CFD} uncontrolled and the blue plotted data shows the circuit with y_{CFD} controlled to setpoint, $y_{CFD_{sp}} = 1.45$ t/m^3. $y_{J_{T,sp}}$ is stepped from $y_{J_{T,sp}} = 0.30$ to $y_{J_{T,sp}} = 0.45$. The black dashed line indicates the setpoint.

The step response in Fig. 6.8 shows that the throughput peak of $Q_{csus} = 130.5$ (m^3/h) is located at $y_{J_{T,sp}} = 0.37$. Interestingly, all three ESC methods converge to slightly below the optimum mill load. PESC and SESC converged to $y_{J_{T,sp}} = 0.35$, whereas, TESC converged toward $y_{J_{T,sp}} = 0.34$. The largest difference between the lowest ESC throughput (TESC) and the optimum throughput is 2.2 (m^3/h), which can be attributed to influence of noise.

In Fig. 6.10, the ESC optimizes grinding mill circuit throughput (Q_{csus}) by perturbing $y_{J_{T,sp}}$, y_{SVOL} is controlled to setpoint by a regulatory controller and y_{CFD} is left uncontrolled. The ESC tuning parameters are provided in Table 6.8 and the convergence results comparing the ESC methods are summarized in Table 6.11.

It can be seen that the ESC tracks the peak throughput seen in Fig. 6.8 indicated by the red plots. The step response in Fig. 6.8 shows that the throughput peak of $Q_{csus} = 122.9$ (m^3/h) is located at $y_{J_{T,sp}} = 0.34$. In this scenario, TESC and SESC converged toward the optimum mill load of $y_{J_{T,sp}} = 0.34$, whereas, PESC converged slightly above the optimum, $y_{J_{T,sp}} = 0.35$. However, the difference in the final converged values of Q_{csus} is insignificant.

6.2.3.3 Effects of tuning parameters

One of the downsides of ESC is that a poorly tuned controller can result in sub-optimal performance. However, in the context of a model-free optimization method searching for the unknown optimum, it can be challenging to determine the best tuning ESC settings. The tuning process would require that most unknown disturbances are mitigated to ensure that any increase or decrease in the performance is due to the ESC tuning and not an external factor. Tuning the controller online can prove to be tedious and time-consuming, especially for a process with slow dynamics such as a grinding mill circuit. Therefore, a model of the plant could be useful to determine an initial set of tuning parameters

Table 6.9. Comparison of PESC tuning parameters.

Tuning set	Variable	Tuning parameter values	Results
1	$y_{J_{T,sp}}$	$k = 25$, $a = 0.002$, $\omega_h = 2.5$ rad/h, $\omega = 4$ rad/h, $\omega_l = 0.1$ rad/h	Fig. 6.11
2	$y_{J_{T,sp}}$	$k = 25$, $a = 0.002$, $\omega_h = 1.8$ rad/h, $\omega = 2$ rad/h, $\omega_l = 0.1$ rad/h	Fig. 6.11

in a simulation environment, which could be further fine-tuned online. Tuning the ESC parameters is largely a trial-and-error approach and without a suitable simulation environment, it is recommended to choose tuning parameters that are conservative such as low optimization gains and a slow perturbation frequency.

An example of the significance of tuning the ESC controller is illustrated in Fig. 6.11. The two PESC tuning parameter sets which are compared are provided in Table 6.9 and the results are summarized in Table 6.12. The first tuning parameter set achieved an increase of $Q_{csus} = 3.24$ m^3/h compared to the second tuning parameter set. Tuning the ESC parameters is not trivial, especially in the context of searching for an unknown optimum. Fig. 6.11 demonstrates that PESC with the second tuning parameter set will steer the process toward an unknown extremum. However, it is not guaranteed to reach the global extremum. Therefore, additional effort is required to determine where the global extremum is located to ensure that the ESC performance is satisfactory and tuned correctly.

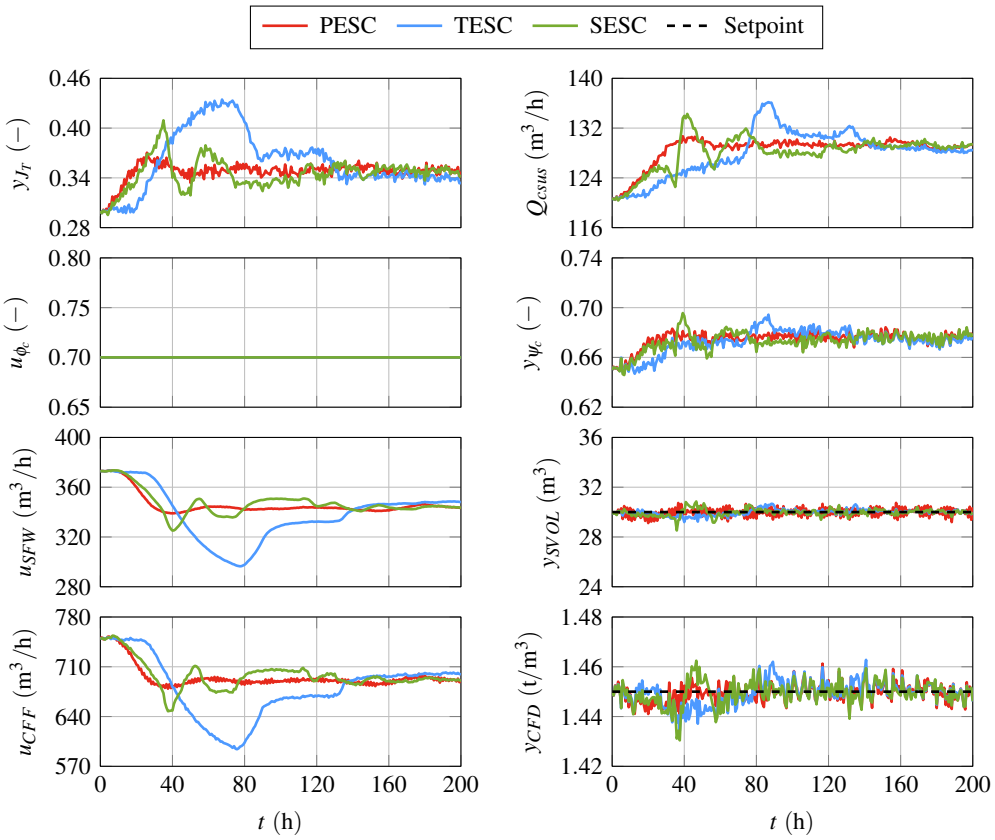

Figure 6.9. Comparison of throughput (Q_{csus}) optimization with $y_{J_{T,sp}}$, y_{SVOL} and y_{CFD} are controlled to setpoint.

Table 6.10. Throughput (Q_{csus}) optimization results with $y_{J_{T,sp}}$ perturbed.

Method	Average value	Convergence rate	Results
PESC	$\overline{Q}_{csus} = 129.20\ \mathrm{m}^3/\mathrm{h}$	$t = 46.0$ h	Fig. 6.9
	$\overline{y}_{J_{T,sp}} = 0.35\ (-)$		
TESC	$\overline{Q}_{csus} = 128.32\ \mathrm{m}^3/\mathrm{h}$	$t = 143.9$ h	Fig. 6.9
	$\overline{y}_{J_{T,sp}} = 0.34\ (-)$		
SESC	$\overline{Q}_{csus} = 129.25\ \mathrm{m}^3/\mathrm{h}$	$t = 116.3$ h	Fig. 6.9
	$\overline{y}_{J_{T,sp}} = 0.35\ (-)$		

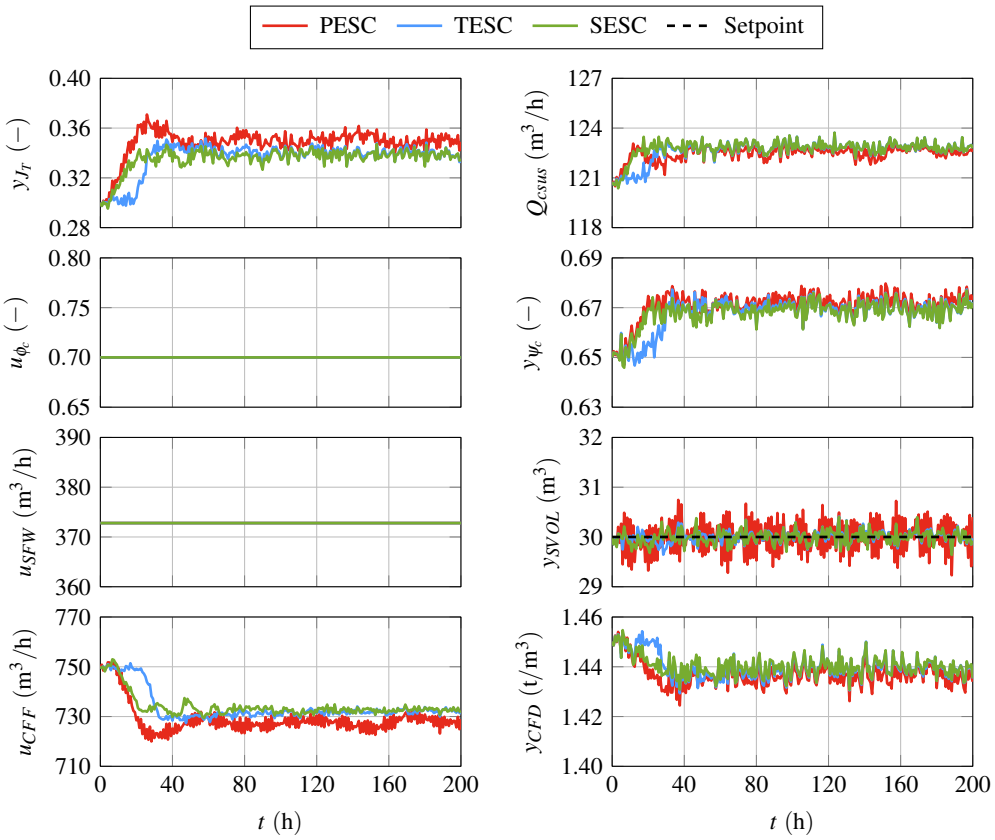

Figure 6.10. Comparison of throughput (Q_{csus}) optimization with $y_{J_{T,sp}}$, y_{SVOL} is controlled to setpoint and y_{CFD} is left uncontrolled.

Table 6.11. Throughput (Q_{csus}) optimization results with $y_{J_{T,sp}}$ perturbed.

Method	Average value	Convergence rate	Results
PESC	$\overline{Q}_{csus} = 122.59\ \mathrm{m}^3/\mathrm{h}$	$t = 6.3$ h	Fig. 6.10
	$\overline{y}_{J_{T,sp}} = 0.35\ (-)$		
TESC	$\overline{Q}_{csus} = 122.86\ \mathrm{m}^3/\mathrm{h}$	$t = 21.0$ h	Fig. 6.10
	$\overline{y}_{J_{T,sp}} = 0.34\ (-)$		
SESC	$\overline{Q}_{csus} = 122.85\ \mathrm{m}^3/\mathrm{h}$	$t = 8.4$ h	Fig. 6.10
	$\overline{y}_{J_{T,sp}} = 0.34\ (-)$		

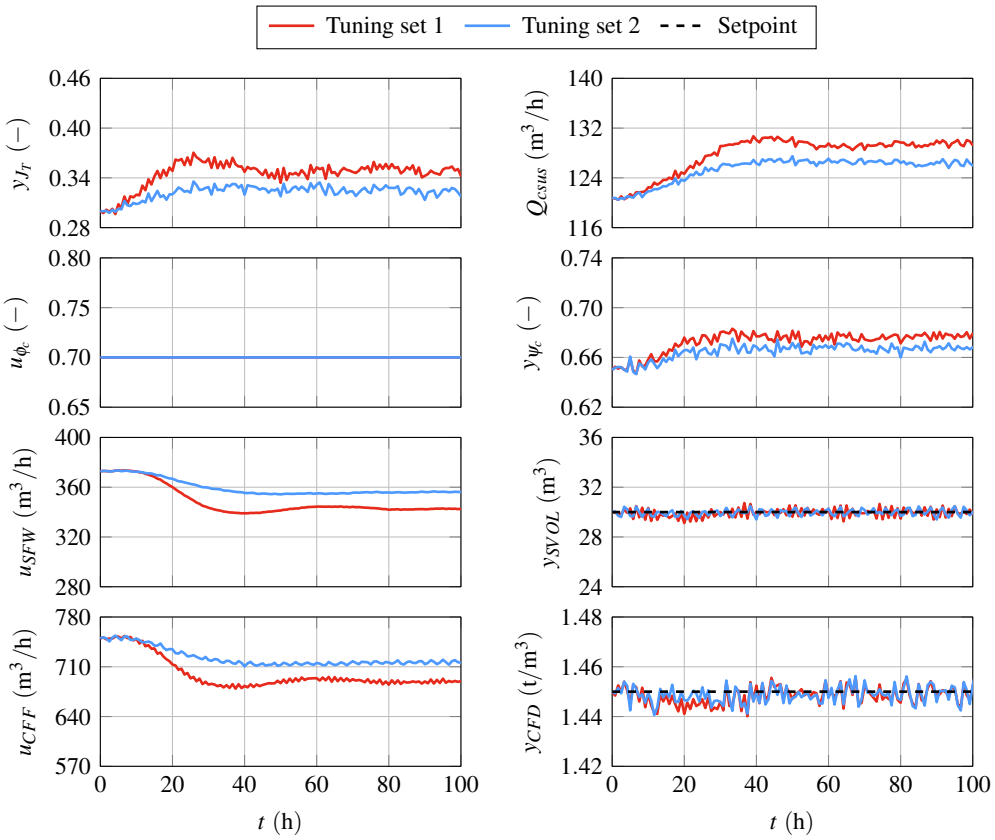

Figure 6.11. Comparison of throughput (Q_{csus}) optimization with $y_{J_{T,sp}}$ with different PESC tuning parameters, y_{SVOL} and y_{CFD} are controlled to setpoint.

Table 6.12. Comparison of throughput (Q_{csus}) optimization results with $y_{J_{T,sp}}$ perturbed and different PESC tuning parameters.

Tuning set	Average value	Convergence rate	Results
1	$\overline{Q}_{csus} = 129.20\ \mathrm{m}^3/\mathrm{h}$	$t = 46.0$ h	Fig. 6.11
	$\overline{y}_{J_{T,sp}} = 0.35\ (-)$		
2	$\overline{Q}_{csus} = 125.96\ \mathrm{m}^3/\mathrm{h}$	$t = 24.3$ h	Fig. 6.11
	$\overline{y}_{J_{T,sp}} = 0.33\ (-)$		

6.3 CHAPTER SUMMARY

In this chapter, several strategies demonstrate the application of the ESCs for optimizing the throughput of a grinding mill circuit closed with a screen or a hydrocyclone classifier. The extremum seeking methods presented in Chapter 4 are applied to optimize the closed grinding mill circuit described in Section 3.5.

A stepped sweep response of mill load is shown to locate the peak of the throughput of the circuit that will be optimized. Additionally, the response is used to identify the key process variables that should be controlled to maintain process stability without hindering the ESCs ability to extract the input-output information.

The ESC optimizes the throughput of the closed grinding mill circuit with a screen classifier by manipulating the mill load, mill speed or both. The different optimization strategies are compared and the results show the improved throughput performance that can be achieved when either the mill speed, mill load or both are used. In the closed grinding mill circuit with a hydrocyclone classifier, the throughput is optimized with the mill load and the mill speed is kept constant. The throughput performance is improved with the ESC optimization, however, a higher throughput performance can be achieved when the hydrocyclone feed density is regulated at setpoint compared to when the hydrocyclone feed density is not uncontrolled. Additionally, the significance of the tuning parameters on optimizing the grinding mill circuit performance are also considered and briefly discussed.

CHAPTER 7 CONCLUSION

Grind curves established for a grinding mill circuit show that there exists an extremum for each of the performance indicators, i.e. throughput, grind quality and power consumption, which can be useful to a plant operator. The parabolic characteristics of grind curves motivates the idea of applying extremum seeking methods to locate and track the unknown extremum.

This dissertation investigates several optimization strategies to improve grinding mill performance with ESC by manipulating the mill load or speed. The single output optimization results show that ESC is useful in steering the process towards an extremum for a single output. However, this results in poor performance for the other outputs that are not controlled due to the inverse relationship that exists between the throughput and grind. Alternatively, a weighted objective function and a paired control strategy are proposed that show that ESC can be useful to not only steer the process toward an optimum, but also satisfy the operational objectives for a grinding mill.

ESC was also applied to optimize the throughput performance of a closed grinding mill circuit, either with a screen or hydrocyclone classifier. Extremum seeking is effective if there is a strong relationship that exists between the perturbed variable and the optimized variable. The multivariate nature of the grinding mill circuit requires key process variables pairs to be identified and controlled to allow the ESC perturbations to effectively propagate to the optimized process variable. Extremum seeking can be useful if one can identify and isolate the interactions from the critical variables that drive the process to optimal conditions and regulate the remaining variables at setpoint, especially if the controlled process is inherently multivariable and exhibits strong coupling between the key variables.

Although the grind curves are not time-varying in the simulations shown in this work, they are time-varying in practice due to feed ore variations. ESCs are beneficial as they can automatically and

continuously track extremums and maintain process performance near optimal operating conditions. However, this is only achieved through gradient-based methods (PESC and TESC) that can adapt based on the changes measured in the objective function. SESC is only able to track an extremum for the initial period until it converges, after which the method maintains its current operating conditions and does not adjust them accordingly in the event of disturbances. In that case, the operating conditions are no longer optimal, and an operator needs to reinitialize the SESC.

The simulation results given in this work showed that the ESCs have relatively long convergence times. This is acceptable if the feed ore characteristics do not frequently change. The convergence times depend on a number of factors, including the initial conditions chosen, disturbances, the dynamics of the process and the tuning parameters of the ESC. A plant operator can reduce the convergence time by initially choosing a good set of operating conditions based on prior knowledge. The focus of this dissertation was, however, not on the convergence times of the ESCs, but rather on their ability to steer the process toward an unknown optimum from different initial conditions. Additionally, the dissertation investigated possible optimization strategies to adopt extremum seeking on the optimization layer.

Applying ESC is largely a trial and error approach, which can be even more challenging to effectively implement when searching for an unknown peak. The tuning parameters influence the controller performance and can result in sub-optimal grinding performance. The advantage of the extremum seeking methods is their model-free nature, but there are benefits of utilizing a model of the process during the initial implementation stages of ESC. A model of the process to be optimized can be used to quickly simulate different optimization strategies and determine tuning parameters that can be fined tuned online.

7.1 CHOOSING AN ESC

Choosing an ESC to optimize the grinding mill performance is based on several factors such as speed of convergence, accuracy, and ease of tuning. PESC is simple to tune. However, the convergence performance of PESC is limited to the dynamics of the plant. Furthermore, the dither signal amplitude should overpower the effects of noise, but it should also not be too large to minimize the variations observed in the measured output.

TESC is favourable as a dither-based extremum seeking method due to the smaller dither signal that

can be used. For most of the simulated results, the amplitude of the dither signal used for TESC was an order of magnitude smaller than the amplitude for the dither signal used in PESC. Additionally, TESC does not have tuning parameters that are necessarily limited to the dynamics of the process, but it does have the most tuning parameters, 8, when compared to PESC (5) and SESC (4). The TESC method can be more difficult to tune as it has more parameters and requires a better fundamental understanding of the ESC method than the PESC and SESC methods. Furthermore, if the ESC perturbs multiple variables, the number of tuning parameters increases by a factor of the number of perturbed variables.

SESC is favourable as a dither-free extremum seeking method due to the lack of perturbations. However, the lack of gradient information indicates that the controller will not operate near optimal conditions if the extremum is time-varying. The SESC method also requires basic knowledge of the plant dynamics to ensure sufficient time for the plant to settle after each iteration. If the settling time chosen is too long, the plant will unnecessarily operate sub-optimally until it reaches the extremum. However, if the settling time is too short, the method will not be able to effectively steer the plant toward the extremum. Furthermore, SESC is robust to measurement noise since the method operates on the functional value of the objective function rather than the gradient information. Additionally, if the SESC tuning parameters are not conservatively chosen, it can cause the ESC to require large step changes pushing the system close to or beyond the acceptable operating boundaries.

7.2 FUTURE WORK

The investigation of applying extremum seeking to optimize grinding mill circuits has shown the potential of ESC as an optimizer to track the optimal steady-state operating points. However, the slow convergence rate of the extremum seeking methods is one of major drawbacks of ESC. There are some interesting approaches to consider that could extend on the work investigated in this dissertation to improve the ESC performance in optimizing grinding mills.

In the current work, only the measurements of the optimized variable are used to steer the process towards an extremum. However, the parabolic nature of grind curves could be used to improve extremum seeking convergence performance. A parameter estimation technique could be investigated to estimate the coefficients of the polynomial functions that describe the grind curves as the ESC explores the input-output map. Extremum seeking methods that exploit the model knowledge could be used to significantly improve the convergence performance based on the continuously updated grind

curve model.

The work covered in this dissertation implements a basic framework for ESC to operate on the optimization layer and simple regulatory controller to maintain key process variables at setpoint. Future work, could consider a multivariable supervisory controller to complement the ESC to reject undesired disturbances that would influence the ESC performance as well as to enforce process constraints.

REFERENCES

Aguila-Camacho, N., Duarte-Mermoud, M. A. & Orchard, M. E. (2020), 'Fractional order controllers for throughput and product quality control in a grinding mill circuit', *European Journal of Control* **51**, 122–134.

Aguila-Camacho, N., le Roux, J. D., Duarte-Mermoud, M. A. & Orchard, M. E. (2017), 'Control of a grinding mill circuit using fractional order controllers', *Journal of Process Control* **53**, 80–94.

Åström, K. & Wittenmark, B. (2013), *Adaptive Control*, Dover Books on Electrical Engineering, 2nd edn, Dover Publications.

Ballantyne, G. R., Powell, M. S. & Tiang, M. (2012), 'Proportion of energy attributable to comminution', *Proceedings of 11th Mill Operators' Conference,* pp. 25–30.

Bauer, M. & Craig, I. K. (2008), 'Economic assessment of advanced process control – A survey and framework', *Journal of Process Control* **18**, 2–18.

Benosman, M. (2016), *Learning-based Adaptive Control: An Extremum Seeking Approach - Theory and Applications*, Butterworth-Heinemann, Oxford.

Botha, S., le Roux, J. D. & Craig, I. K. (2018), 'Hybrid non-linear model predictive control of a run-of-mine ore grinding mill circuit', *Minerals Engineering* **123**, 49–62.

Bouffard, S. C. (2015), 'Benefits of process control systems in mineral processing grinding circuits', *Minerals Engineering* **79**, 139–142.

Chen, X., Zhai, J., Li, Q. & Fei, S. (2007), 'Fuzzy logic based on-line efficiency optimization control of a ball mill grinding circuit', *Fourth International Conference on Fuzzy Systems and Knowledge Discovery (FSKD 2007)* **2**, 575–580.

Chen, X., Zhai, J., Li, S. & Li, Q. (2007), 'Application of model predictive control in ball mill grinding circuit', *Minerals Engineering* **20**(11), 1099–1108.

Chioua, M., Srinivasan, B., Guay, M. & Perrier, M. (2016), 'Performance improvement of extremum seeking control using recursive least square estimation with forgetting factor', *IFAC-PapersOnLine* **49**(7), 424–429.

Coetzee, L. C., Craig, I. K. & Kerrigan, E. C. (2010), 'Robust nonlinear model predictive control of a run-of-mine ore milling circuit', *IEEE Transactions on Control Systems Technology* **18**(1), 222–229.

Cortinovis, A., Mercangöz, M., Mathur, T., Poland, J. & Blaumann, M. (2013), 'Nonlinear coal mill modeling and its application to model predictive control', *Control Engineering Practice* **21**, 308–320.

Craig, I. K., Hulbert, D. G., Metzner, G. & Moult, S. P. (1992), 'Optimized multivariable control of an industrial run-of-mine milling circuit', *Journal of the Southern African Institute of Mining and Metallurgy* **92**, 169–176.

Craig, I. K. & MacLeod, I. M. (1995), 'Specification framework for robust control of a run-of-mine ore milling circuit', *Control Engineering Practice* **3**(5), 621–630.

Cramer, L. A. (2008), 'What is your PGM concentrate worth?', *Third International Platinum Conference 'Platinum in Transformation',* pp. 387–394.

Curry, J. A., Ismay, M. J. L. & Jameson, G. J. (2014), 'Mine operating costs and the potential impacts of energy and grinding', *Minerals Engineering* **56**, 70–80.

Frausto, J. J., Ballantyne, G. R., Runge, K., Powell, M. S., Wightman, E. M., Evans, C. L., Gonzalez, P. & Gomez, S. (2021), 'The effect of screen versus cyclone classification on the mineral liberation properties of a polymetallic ore', *Minerals Engineering* **169**, 106930.

Fu, L. & Ümit Özgüner (2011), 'Extremum seeking with sliding mode gradient estimation and asymptotic regulation for a class of nonlinear systems', *Automatica* **47**(12), 2595–2603.

Ghaffari, A., Krstić, M. & Nešić, D. (2012), 'Multivariable Newton-based extremum seeking', *Automatica* **48**(8), 1759–1767.

Guay, M. & Dochain, D. (2015), 'A time-varying extremum-seeking control approach', *Automatica* **51**, 356–363.

Guay, M. & Dochain, D. (2017), 'A proportional-integral extremum-seeking controller design technique', *Automatica* **77**, 61–67.

Guay, M., Moshkar, E. & Dochain, D. (2015), 'A constrained extremum-seeking control approach', *International Journal of Robust and Nonlinear Control* **25**, 3132–3153.

Gupta, A. & Yan, D. S. (2016), *Mineral Processing Design and Operation: An Introduction*, Elsevier, Oxford.

Hadizadeh, M., Farzanegan, A. & Noaparast, M. (2017), 'Supervisory fuzzy expert controller for SAG mill grinding circuits: Sungun copper concentrator', *Mineral Processing and Extractive Metallurgy Review* **38**(3), 168–179.

Herbst, J. A. & Lo, Y. C. (1996), 'Financial implications of comminution system optimization', *International Journal of Mineral Processing* **44-45**, 209–221.

Hodouin, D. (2011), 'Methods for automatic control, observation, and optimization in mineral processing plants', *Journal of Process Control* **21**, 211–225.

Hodouin, D., Jämsä-Jounela, S. L., Carvalho, M. T. & Bergh, L. (2001), 'State of the art and challenges in mineral processing control', *Control Engineering Practice* **9**, 995–1005.

Hulbert, D. G., Craig, I. K., Coetzee, M. L. & Tudor, D. (1990), 'Multivariable control of a run-of-mine milling circuit', *Journal of the Southern African Institute of Mining and Metallurgy* **90**, 173–181.

Hunnekens, B. G. B., Haring, M. A. M., van de Wouw, N. & Nijmeijer, H. (2014), 'A dither-free extremum-seeking control approach using 1st-order least-squares fits for gradient estimation', *53rd IEEE Conference on Decision and Control,* pp. 2679–2684.

Korovin, S. K. & Utkin, V. I. (1974), 'Using sliding modes in static optimization and nonlinear programming', *Automatica* **10**(5), 525–532.

Krstić, M. & Wang, H. (1997), 'Design and stability analysis of extremum seeking feedback for general nonlinear systems', *Proceedings of the 36th IEEE Conference on Decision and Control,* pp. 1743–1748.

Lagarias, J., Reeds, J., Wright, M. & Wright, P. (1998), 'Convergence properties of the Nelder–Mead simplex method in low dimensions', *SIAM Journal on Optimization* **9**, 112–147.

Laiji, H., Bo, X. & Ping, Z. (2012), 'Fuzzy logic based multivariable supervisory control of a complicated industrial process', *Proceedings of the 31st Chinese Control Conference,* pp. 7598–7602.

le Roux, J. D. & Craig, I. K. (2019), 'Plant-wide control framework for a grinding mill circuit', *Industrial and Engineering Chemistry Research* **58**, 11585–11600.

le Roux, J. D., Craig, I. K., Hulbert, D. G. & Hinde, A. L. (2013), 'Analysis and validation of a run-of-mine ore grinding mill circuit model', *Minerals Engineering* **43-44**, 121–134.

le Roux, J. D., Craig, I. K. & Padhi, R. (2013), 'State and parameter estimation for a grinding mill circuit from operational input-output data', *IFAC Proceedings Volumes* **46**(32), 178–183.

le Roux, J. D., Olivier, L. E., Naidoo, M. A. & Craig, I. K. (2016), 'Throughput and product quality control for a grinding mill circuit using non-linear MPC', *Journal of Process Control* **42**, 35–50.

le Roux, J. D., Padhi, R. & Craig, I. K. (2014), 'Optimal control of grinding mill circuit using model predictive static programming: A new nonlinear MPC paradigm', *Journal of Process Control* **24**, 29–40.

le Roux, J. D., Steinboeck, A., Kugi, A. & Craig, I. K. (2020), 'Steady-state and dynamic simulation of a grinding mill using grind curves', *Minerals Engineering* **152, 106208**.

Liu, S. & Krstić, M. (2016), 'Stochastic averaging in discrete time and its applications to extremum seeking', *IEEE Transactions on Automatic Control* **61**, 90–102.

Lu, X., Krstić, M., Chai, T. & Fu, J. (2021), 'Hardware-in-the-loop multiobjective extremum-seeking control of mineral grinding', *IEEE Transactions on Control Systems Technology* **29**, 961–971.

Manzie, C. & Krstić, M. (2007), 'Discrete time extremum seeking using stochastic perturbations', *2007 46th IEEE Conference on Decision and Control,* pp. 3096–3101.

Maritz, M. G., le Roux, J. D. & Craig, I. K. (2019), 'Feed size distribution feedforward control for a grinding mill circuit', *IFAC-PapersOnLine* **52**, 7–12.

Matthews, B. & Craig, I. K. (2013), 'Demand side management of a run-of-mine ore milling circuit', *Control Engineering Practice* **21**(6), 759–768.

Meyer, E. & Craig, I. (2010), 'The development of dynamic models for a dense medium separation circuit in coal beneficiation', *Minerals Engineering* **23**(10), 791–805.

Moase, W. H., Manzie, C. & Brear, M. J. (2009), 'Newton-like extremum-seeking part I: Theory', *Proceedings of the 48th IEEE Conference on Decision and Control (CDC) held jointly with 2009 28th Chinese Control Conference,* pp. 3839–3844.

Moema, J. S., Papo, M. J., Slabbert, G. A. & Zimba, J. R. (2009), 'Grinding media quality assurance for the comminution of gold ores', *Proceedings of the World Gold Conference,* pp. 27–33.

Morrell, S., Finch, W. M., Kojovic, T. & Delboni Jr., H. (1996), 'Modelling and simulation of large diameter autogeneous and semi-autogeneous mills', *International Journal of Mineral Processing* **44-45**, 289–300.

Musa, F. & Morrison, R. (2009), 'A more sustainable approach to assessing comminution efficiency', *Minerals Engineering* **22**(7), 593–601.

Nadolski, S., Klein, B., Kumar, A. & Davaanyam, Z. (2014), 'An energy benchmarking model for mineral comminution', *Minerals Engineering* **65**, 178–186.

Napier-Munn, T. J., Morrell, S., Morrison, R. D. & Kojovic, T. (2005), *Mineral Communition Circuits: Their Operation and Optimisation*, 3rd edn, Julius Kruttschnitt Mineral Research Centre, Isles Road, Indooroopilly, Queensland 4068, Australia.

Nešić, D., Tan, Y. & Mareels, I. (2006), 'On the Choice of Dither in Extremum Seeking Systems: a Case Study', *Proceedings of the 45th IEEE Conference on Decision and Control* **44**, 2789–2794.

Nelder, J. A. & Mead, R. (1965), 'A simplex method for function minimization', *Computer Journal* **7**, 308–313.

Olivier, L. & Craig, I. K. (2017*a*), 'Should I shut down my processing plant? An analysis in the presence of faults', *Journal of Process Control* **56**, 35–47.

Olivier, L. E. & Craig, I. K. (2015), 'Development and application of a model-plant mismatch expression for linear time-invariant systems', *Journal of Process Control* **32**, 77–86.

Olivier, L. E. & Craig, I. K. (2017*b*), 'A survey on the degree of automation in the mineral processing industry', *2017 IEEE AFRICON,* pp. 404–409.

Pan, Y., Ümit Özgüner & Acarman, T. (2003), 'Stability and performance improvement of extremum seeking control with sliding mode', *International Journal of Control* **76**(9-10), 968–985.

Pauw, O. G., King, R. P., Garner, K. C. & van Aswegen, P. C. (1985), 'The control of pebble mills at Buffelsfontein Gold Mine by use of a multivariable peak-seeking controller', *Journal of the Southern African Institute of Mining and Metallurgy* **85**, 89–96.

Pomerleau, A., Hodouin, D., Desbiens, A. & Éric Gagnon (2000), 'A survey of grinding circuit control methods: from decentralized PID controllers to multivariable predictive controllers', *Powder Technology* **108**(2), 103–115.

Powell, M. & Mainza, A. (2006), 'Extended grinding curves are essential to the comparison of milling performance', *Minerals Engineering* **19**(15), 1487–1494.

Powell, M. S., Morrell, S. & Latchireddi, S. (2001), 'Developments in the understanding of South African style SAG mills', *Minerals Engineering* **14**, 1143–1153.

Powell, M. S., van der Westhuizen, A. P. & Mainza, A. N. (2009), 'Applying grindcurves to mill operation and optimisation', *Minerals Engineering* **22**, 625–632.

Qin, S. J. & Badgwell, T. A. (2003), 'A survey of industrial model predictive control technology', *Control Engineering Practice* **11**(7), 733–764.

Ramasamy, M., Narayanan, S. S. & Rao, C. D. P. (2005), 'Control of ball mill grinding circuit using model predictive control scheme', *Journal of Process Control* **15**(3), 273–283.

Rawlings, J. B. (2000), 'Tutorial overview of model predictive control', *IEEE Control Systems Magazine* **20**(3), 38–52.

Salazar, J. L., Magne, L., Acuña, G. & Cubillos, F. (2009), 'Dynamic modelling and simulation of semi-autogenous mills', *Minerals Engineering* **22**, 70–77.

Skogestad, S. (2004), 'Control structure design for complete chemical plants', *Computers & Chemical Engineering* **28**, 219–234.

Steyn, C. W. & Sandrock, C. (2013), 'Benefits of optimisation and model predictive control on a fully autogenous mill with variable speed', *Minerals Engineering* **53**, 113–123.

Tan, Y., Moase, W., Manzie, C., Nešić, D. & Mareels, I. (2010), 'Extremum seeking from 1922 to 2010', *Proceedings of the 29th Chinese Control Conference,* pp. 14–26.

Tao, G. (2014), 'Multivariable adaptive control: A survey', *Automatica* **50**(11), 2737–2764.

Tessier, J., Duchesne, C. & Bartolacci, G. (2007), 'A machine vision approach to on-line estimation of run-of-mine ore composition on conveyor belts', *Minerals Engineering* **20**, 1129–1144.

van der Westhuizen, A. P. & Powell, M. S. (2006), 'Milling curves as a tool for characterising SAG mill performance', *Proceedings of the International Conference on Autogenous and Semi-Autogenous Grinding Technology,* pp. 217–232.

Viklund, T., Albertsson, J., Burstedt, J., Isaksson, M. & Söderlund, J. (2006), 'Evolution of AG mill control system at Boliden Mineral AB', *Proceedings of the International Conference on Autogenous and Semi-Autogenous Grinding Technology,* pp. 311–325.

Wang, C., Nadolski, S., Mejia, O., Drozdiak, J. & Klein, B. (2013), 'Energy and cost comparisons of hpgr-based circuits: Engineering, geology, mineralogy, metallurgy, chemistry, etc', *Engineering and Mining Journal* **214**(12), 102–108.

Wei, D. & Craig, I. K. (2009*a*), 'Economic performance assessment of two rom ore milling circuit controllers', *Minerals Engineering* **22**(9), 826–839.

Wei, D. & Craig, I. K. (2009*b*), 'Grinding mill circuits - A survey of control and economic concerns', *International Journal of Mineral Processing* **90**, 56–66.

Wills, B. A. & Finch, J. A. (2015), *Wills' Mineral Processing Technology: An Introduction to the Practical Aspects of Ore Treatment and Mineral Recovery*, 8th edn, Butterworth-Heinemann, Oxford.

Xiong, Q. & Jutan, A. (2003), 'Continuous optimization using a dynamic simplex method', *Chemical Engineering Science* **56**, 3817–3828.

Zhang, C. & Ordóñez, R. (2012), *Extremum-seeking Control and Applications: A Numerical Optimization-Based Approach*, Springer-Verlag London, London.

Zhou, P., Lu, S., Yuan, M. & Chai, T. (2016), 'Survey on higher-level advanced control for grinding circuits operation', *Powder Technology* **288**, 324–338.